



universität
wien

MASTERARBEIT / MASTER'S THESIS

Titel der Masterarbeit / Title of the Master's Thesis

„Enzymatic Cascades in *Escherichia Coli* based on the
Equilibration of Reactive Aldehyde Intermediates“

verfasst von / submitted by

Lydia Suchy, BSc MSc

angestrebter akademischer Grad / in partial fulfilment of the requirements for the degree of
Master of Science (MSc)

Wien, 2021 / Vienna, 2021

Studienkennzahl lt. Studienblatt /
degree programme code as it appears on
the student record sheet:

UA 066 877

Studienrichtung lt. Studienblatt /
degree programme as it appears on
the student record sheet:

Masterstudium
Genetik und Entwicklungsbiologie

Betreut von / Supervisor:

Assoc. Prof. Priv. Doz. Dr. Florian Rudroff

Acknowledgements

First, I would like to thank Florian Rudroff for receiving me in the working group and giving me the chance to realise my master thesis under his supervision in the Bioorganic Synthetic Chemistry working group at the Institute for Applied Synthetic Chemistry, TU Vienna. I am truly grateful for this opportunity which helped me to find new interests and combine them with old ones.

Furthermore, I would like to thank Marko D. Mihovilovic, Michael Schnürch and Christian Stanetty for their input and the nice and welcoming atmosphere in the working group.

I would like to thank Dörte Rother, Nicholas Turner and Uwe T. Bornscheuer for donating the plasmids harbouring the respective enzyme-encoding genes.

Next, I want to thank the “BioHub”, my fellow Bio-colleagues in the working group for all the support and help. A special thanks goes to Julia for welcoming me and for introducing me to the research done in the working group in my first internship. Consequently, a big “thank you” also later on to Julia and Tom for their friendship and for advising and helping me whenever I needed help. Moreover, I would like to thank Hamid for his help and humour...and especially, for his chair. I want to thank all the other “BioHubs”: Richard, who somehow is the one always keeping things in order and operating in the biolab, Stefan for always being so honest and funny, Freddy for talking about scientific and world (war) problems, Heci for seeing the potential in my facial expressions, Astrid for always being so nice to me, Hubert for telling me that everything is going to be fine and Clemens for always being cool and for the nice cooperation.

Then, I would like to thank the whole research group (as well as former colleagues). I really appreciate the super nice working environment and the kindness of everyone: Blanca, Christoph, David, Dominik, Drasi, Eleni, Farooq, Jakob, Johanna, Kathi S., Kathi O., Laszlo, Nic, Nina, Rafaela, Raheleh, Resi, Simon, Tobi and Viktor.

Moreover, I would like to thank all the other personnel at the institute, who are essential for keeping up the research.

Furthermore, a big thank you goes to all my friends and my family who have always been so supporting and encouraging and were always there for me in good and in difficult times.

Lastly, I want to thank my partner who has been my biggest cheerleader throughout all my studies and has always supported me and all my ideas.

Table of Contents

1	Abbreviations	6
2	Abstract	8
3	Deutsche Zusammenfassung	9
4	Compound library	10
4.1	Substrates and Intermediates of Biocatalytic Cascades	10
4.2	Products of Biocatalytic Cascades	11
5	Introduction	12
5.1	Biocatalysis	12
5.1.1	Biocatalytic Cascade Reactions.....	12
5.2	Biocatalytic Cascades <i>in Vivo</i> compared to <i>in Vitro</i> Approaches	12
5.3	Pathway Design of Synthetic Enzyme Cascades	13
5.3.1	Challenges of Multiple Recombinant Protein Expression.....	14
5.4	Aldehydes as Intermediates in Biocatalytic Cascade Reactions	16
5.4.1	Inhibition or Reversal of Byproduct Formation	16
5.5	Biocatalytic Carbonylation, Transamination and Reductive Amination	18
6	Research Question	21
7	Results and Discussion	22
7.1	Correction of a Mutation in the <i>alkJ</i> Gene by Q5 Site Directed Mutagenesis	22
7.2	Verification of Redox Activity of the Enzymes Alcohol Dehydrogenase (<i>AlkJ</i>) and Carboxylic Acid Reductase (<i>CAR_{Ni}</i>)	23
7.2.1	Discussion	27
7.3	Biocatalyst Selection for Reaction with the Aldehyde Species	27
7.3.1	Pyruvate Decarboxylase <i>PDC_{Ap}</i> and Mutant <i>PDC_{Ap}_mutant</i>	27
7.3.2	ω -Transaminases <i>VfIH6</i> , <i>AspFum</i> and <i>AspTer</i>	28
7.3.3	Reductive Aminase <i>AspRedAm</i> and Imine Reductases <i>PIR13</i> and <i>PIR23</i>	29
7.3.4	Discussion	31
7.4	Construction of Vectors for the Co-expression of Selected Biocatalysts with <i>alkJ</i>	32
7.5	Co-Expression of GOI and <i>alkJ</i> from the Assembled Constructs and Validation of Biocatalytic Mini-Pathway	33
7.5.1	<i>AlkJ</i> and <i>PDC_{Ap}</i> /Mutant <i>PDC_{Ap}_mutant</i>	33
7.5.2	<i>AlkJ</i> and <i>VfIH6</i> / <i>AspFum</i> / <i>AspTer</i>	35
7.5.3	<i>AlkJ</i> and <i>AspRedAm</i> / <i>PIR13</i> / <i>PIR23</i>	38
7.5.4	Discussion	40
7.6	Co-Transformation of two Plasmids for Co-Production of all Cascade Enzymes and Validation of Biocatalytic Maxi-Pathway	41
7.6.1	<i>AlkJ</i> , Mutant <i>PDC_{Ap}_mutant</i> and <i>CAR_{Ni}</i>	41
7.6.2	<i>AlkJ</i> , <i>VfIH6</i> / <i>AspFum</i> / <i>AspTer</i> and <i>CAR_{Ni}</i>	43
7.6.3	<i>AlkJ</i> , <i>PIR23</i> and <i>CAR_{Ni}</i>	47
7.6.4	Discussion	50
8	Conclusion	52
9	Material and Methods - General Preparations	53
9.1	General Stock Solutions	53

9.2	Standard Media and Buffer.....	54
10	Material and Methods - General Procedures	57
10.1	Cultivation of Bacteria	57
10.1.1	Overnight Culture	57
10.1.2	Preparation of Cryostocks	57
10.1.3	Cultivation on LB-agar Plates (Recovery of Bacteria from Cryostock)	57
10.2	Preparation Chemically Competent <i>E. coli</i> Cells	57
10.3	Transformation of Chemically Competent Cells.....	58
10.4	Plasmid DNA Isolation and Quantification	58
10.4.1	Verification of DNA by Sequencing (Plasmid Template).....	58
10.5	Dilution of Primers.....	58
10.6	Colony PCR	58
10.7	Gel Electrophoresis.....	59
10.8	NEBuilder® HiFi DNA Assembly	60
10.8.1	Primer Design	60
10.8.2	PCR Amplification of Target DNA Fragments	60
10.8.3	Gel Purification of PCR Amplified DNA Fragments	61
10.8.4	Assembly	61
10.8.5	Chemical Transformation	62
10.8.6	Verification by Colony PCR	62
10.8.7	Plasmid DNA isolation and Verification by Sequencing.....	62
10.9	Enzyme Expression in <i>E. coli</i>.....	62
10.9.1	Cultivation in LB-Miller and TB Media for Conventional Induction	62
10.9.2	Cultivation in Autoinduction Media	62
10.9.3	Preparation of <i>E. coli</i> Cell-free Extracts (CFEs)	62
10.9.4	Preparation of <i>E. coli</i> Resting Cells (RCs)	62
10.10	Bradford Assay for Determination of Protein Concentration.....	63
10.11	Sodium Dodecylsulfate Polyacrylamide Gel Electrophoresis (SDS-PAGE).....	63
10.12	Biotransformations	64
10.12.1	Standard Reaction Conditions for Biotransformations employing CFEs	64
10.12.2	Standard Reaction Conditions for Biotransformations using RCs	65
10.12.3	Analysis of Product Formation with Calibrated Gas Chromatography (GC).....	65
10.12.4	Sample Preparation for Calibration by GC/FID.....	65
11	Experimental	66
11.1	Enzyme Library	66
11.2	Preliminary Verification of Correct Enzyme Sequences	69
11.3	Correction of Mutation in <i>AlkJ</i> by Q5® Site-directed Mutagenesis.....	69
11.4	Characterizations of Single Enzymes	71
11.4.1	Characterization of Carboxylic Acid Reductase <i>CAR_{Ni}</i> for Reduction of Carboxylic Acids to Aldehydes.....	72
11.4.2	Characterization of Alcohol Dehydrogenase <i>AlkJ</i> for Oxidation of Primary Alcohols to Aldehydes.....	72
11.4.3	Characterization of Alcohol Dehydrogenase <i>AlkJ-short</i> for Oxidation of Primary Alcohols to Aldehydes	73
11.4.4	Characterization of Pyruvate Decarboxylase <i>PDC_{Ap}</i> for C–C Bond Formation.....	74
11.4.5	Characterization of Pyruvate Decarboxylase <i>PDC_{Ap}-mutant</i> for C–C Bond Formation	74
11.4.6	Characterization of Different ω -Transaminases for C-N Formation (by Transamination).....	75
11.4.7	Characterization of Reductive Aminase <i>AspRedAm</i> for C-N Formation (by Reductive Amination)	76
11.4.8	Characterization of Imine Reductases <i>PIR13</i> & <i>PIR23</i> for C-N Formation (by Reductive Amination)	77
11.5	Construction of Vectors for the Co-expression of Pathway Enzymes	78

11.5.1	Generation of Backbone1 for Assembly of	
pKA1_alkj::pdc _{Ap} /pdc _{Ap} _mutant/vflh6/aspfum/aspredam/pir13/pir23.....		78
11.5.2	Successful Assembly of pKA1_alkj::pdc _{Ap} by NEBuilder® HiFi DNA Assembly.....	79
11.5.3	Successful Assembly of pKA1_alkj::pdc _{Ap} _mutant by NEBuilder® HiFi DNA Assembly.....	81
11.5.4	Successful Assembly of pKA1_alkj::vflh6 by NEBuilder® HiFi DNA Assembly.....	82
11.5.5	Successful Assembly of pKA1_alkj::aspfum by NEBuilder® HiFi DNA Assembly.....	83
11.5.6	Successful Assembly of pKA1_alkj::aspredam by NEBuilder® HiFi DNA Assembly.....	85
11.5.7	Successful Assembly of pKA1_alkj::pir13 by NEBuilder® HiFi DNA Assembly.....	86
11.5.8	Successful Assembly of pKA1_alkj::pir23 by NEBuilder® HiFi DNA Assembly.....	87
11.5.9	Generation of Backbone2 for Assembly of pKA1_alkj::aspter.....	89
11.5.10	Successful Assembly of pKA1_alkj::aspter by NEBuilder® HiFi DNA Assembly.....	89
11.6	Validation of Vector Functionality by Protein Production Analysis and Biotransformation (Mini-Pathway).....	91
11.6.1	Co-Expression Study of <i>AlkJ</i> and <i>PDC_{Ap}</i>	91
11.6.2	Co-Expression Study of <i>AlkJ</i> and <i>PDC_{Ap}_mutant</i> and Mini-Pathway Validation.....	91
11.6.3	Co-Expression Study of <i>AlkJ</i> and <i>VflH6/AspFum/AspTer</i> and Mini-Pathway Validation.....	92
11.6.4	Co-Expression Study of <i>AlkJ</i> and <i>AspRedAm</i>	93
11.6.5	Co-Expression Study of <i>AlkJ</i> and <i>PIR13/PIR23</i> and Mini-Pathway Validation.....	93
11.7	Expression of all Pathway Enzymes in a Single Host Cell and Validation by Biotransformation (Maxi-Pathway).....	93
11.7.1	Co-Production of <i>AlkJ</i> , <i>PDC_{Ap}_mutant</i> , <i>CAR_{Ni}</i> and <i>Pptase_{Ec}</i> and Maxi-Pathway Validation.....	93
11.7.2	Co-Production of <i>AlkJ</i> , <i>VflH6/AspFum/AspTer</i> , <i>CAR_{Ni}</i> and <i>Pptase_{Ec}</i> and Maxi-Pathway Validation.....	95
11.7.3	Co-Production of <i>AlkJ</i> , <i>PIR23</i> , <i>CAR_{Ni}</i> and <i>Pptase_{Ec}</i> and Maxi-Pathway Validation.....	96
12	Appendix.....	98
12.1	Gene Sequences.....	98
12.2	List of Primers.....	105
13	References.....	107

1 Abbreviations

abs.	absolute
ACN	acetonitrile
ADH	alcohol dehydrogenase
AIM	autoinduction medium
amp	ampicillin
ATP	adenosine triphosphate
bp	base pair
br	broad signal
CAR	carboxylic acid reductase
cam	chloramphenicol
CFE	cell free extract
DMSO	dimethyl sulfoxide
DNA	deoxyribonucleic acid
dH ₂ O	deionised water
dNTP mix	deoxyribonucleotide triphosphate mix
EDTA	ethylene-diamineteraacetic acid
<i>ee</i>	enantiomeric excess
<i>et al.</i>	“et alii” (and others)
<i>etc.</i>	“et cetera” (and so forth)
EtOAc	ethyl acetate
EtOH	ethanol
<i>E. coli</i>	<i>Escherichia coli</i>
<i>e.g.</i>	“exempli gratia” (for example)
FID	flame ionization detector
<i>fwd</i>	forward
<i>g</i>	gram
x g	relative centrifugal force
GC	gas chromatography
<i>GDH</i>	glucose dehydrogenase
GOI	gene of interest
h	hours
His	histidine
IPTG	isopropyl β-D-1-thiogalactopyranoside
IRED	imine reductase
IS	internal standard
Kan	kanamycin
kDa	kilodalton
Lac	lactose
LB	lysogeny broth
<i>LDH</i>	lactate dehydrogenase
m	multiplet
mg	milligram
MHz	megahertz
min	minutes
ml	millilitre
mmol	millimole
mM	millimolar

MS	mass spectrometry
NAD ⁺ (NADH)	nicotinamide adenine dinucleotide (reduced)
NADP ⁺ (NADPH)	nicotinamide adenine dinucleotide phosphate (reduced)
N-free	nitrogen-free
ng	nanogram
nm	nanometre
NMR	nuclear magnetic resonance
n.a.	not applicable/not available
<i>N. iowensis</i>	<i>Nocardia iowensis</i>
OD ₅₉₀	optical density at 590 nm
PAGE	polyacrylamide gel electrophoresis
PCR	polymerase chain reaction
PDC	pyruvate decarboxylase
pH	potential of hydrogen
PLP	pyridoxal phosphate
<i>P. putida</i>	<i>Pseudomonas putida</i>
R	organic residue
RBS	ribosome binding site
RCs	resting cells
RCM	resting cell medium
<i>rev</i>	reverse
Rhm	rhamnose
rpm	revolutions per minute
rt	room temperature
s	singlet
SDS	sodium dodecyl sulfate
SOC medium	super optimal broth medium with catabolite repression
TA	transaminase
TB	terrific broth
T _a	annealing temperature
T _m	melting temperature
ThDP	thiamine diphosphate
UV	ultraviolet
v	volume
w	weight
YT medium	yeast extract tryptone medium
μg	microgram
μl	microlitre
μM	micromolar

2 Abstract

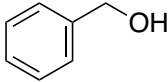
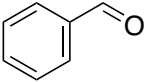
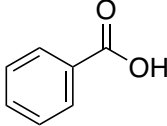
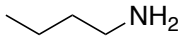
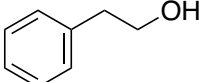
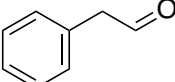
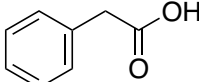
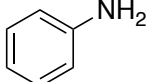
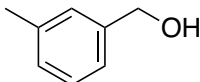
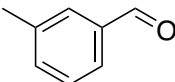
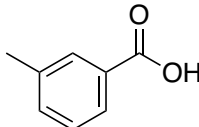
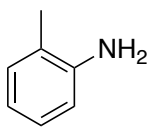
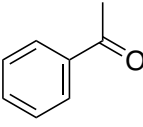
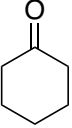
Synthetic enzyme cascades in living cells offer a great possibility for the production of valuable chemicals. Hereby, aldehydes represent important intermediates and precursors for numerous chemical compounds. However, highly reactive aldehyde species are toxic to the organism. Host cell responses compensate for cellular toxicity forming undesired byproducts (the respective alcohols and carboxylic acids) by endogenous enzyme activities. Previous research has shown that the carbon flux can be redirected from the byproducts to the target aldehyde intermediate by the enzymes alcohol dehydrogenase (*AlkJ*, *P. putida*) and carboxylic acid reductase (*CAR_{Ni}*, *N. iowensis*), leading to an equilibration between alcohols, aldehydes, and carboxylic acids in *E. coli* resting cells. At the same time, the aldehyde is freely available for further reaction. So far, aldolase (*Fsa1-A129S*, *E. coli*) has been the only enzyme applied in combination with this biocatalytic equilibrium. To expand this concept and prove that it can be applied to synthesise a wide range of compounds, new enzyme classes were incorporated into the cascade in place of the aldolase: pyruvate decarboxylase (*PDC_{Ap}_mutant*, *A. pasteurianus*), ω -transaminases (*VflH6*, *V. fluvialis*) and imine reductase (*PIR23*, *C. ferrugineus*). A two-plasmid approach was used for the co-expression of all enzymes. Therefore, the respective genes were subcloned into the plasmid containing the gene *alkj* and co-transformed with the plasmid harbouring *car_{Ni}* in *E. coli*. After confirmation of successful co-production of all enzymes, the three new biocatalytic pathways were tested. In this way, the biocatalytic concept was expanded successfully to yield α -hydroxy ketones, primary and secondary amines.

3 Deutsche Zusammenfassung

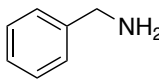
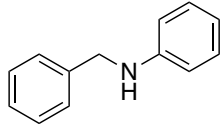
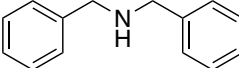
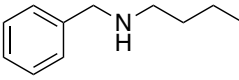
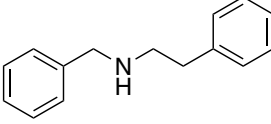
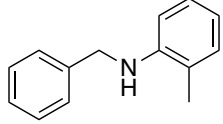
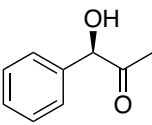
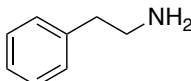
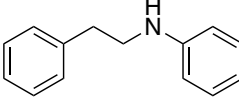
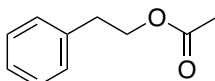
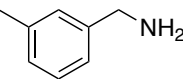
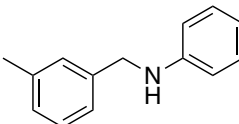
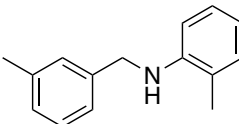
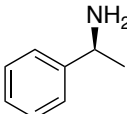
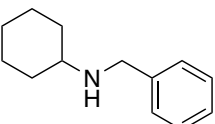
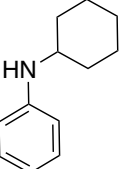
Synthetische Enzymkaskaden in lebenden Zellen bieten eine bedeutende Möglichkeit zur Herstellung wertvoller Chemikalien. Dabei stellen Aldehyde wichtige Zwischen- und Vorstufen für zahlreiche chemische Verbindungen dar. Hochreaktive Aldehydspezies sind jedoch für den Organismus toxisch. Mechanismen in der Wirtszelle kompensieren die Zelltoxizität, indem unerwünschte Nebenprodukte (die entsprechenden Alkohole und Carbonsäuren) durch endogene Enzymaktivitäten gebildet werden. Frühere Studien haben gezeigt, dass in ruhenden *E. coli*-Zellen primäre Alkohole und Carbonsäuren durch eine Alkoholdehydrogenase (*AlkJ*, *P. putida*) bzw. Carbonsäurereduktase (*CAR_{Ni}*, *N. iowensis*) in Aldehyde umgewandelt werden können. Dadurch wird der Kohlenstofffluss von den Nebenprodukten zum Aldehyd-Zwischenprodukt umgeleitet, was zu einem Gleichgewicht zwischen Alkoholen, Aldehyden und Carbonsäuren führt. Gleichzeitig steht der Aldehyd für die weitere Umsetzung frei zur Verfügung. Bisher wurde Aldolase (*Fsa1-A129S*, *E. coli*) als einziges Enzym mit diesem biokatalytischen Gleichgewicht kombiniert. Um das Spektrum dieses Konzepts zu erweitern und seine Anwendbarkeit für die Synthese verschiedener Verbindungen nachzuweisen, wurden anstelle der Aldolase neue Enzymklassen in die Kaskade eingebaut: Pyruvat-Decarboxylase (*PDC_{AP} mutant*, *A. pasteurianus*), ω -Transaminase (*VfIH6*, *V. fluvialis*) und Imin-Reduktase (*PIR23*, *C. ferrugineus*). Für die Co-expression aller Enzyme wurde ein Zwei-Plasmid-Ansatz verwendet. Dafür wurden die entsprechenden Gene in das Plasmid, welches das Gen *alkj* enthielt, subkloniert und mit dem Plasmid, welches das Gen *car_{Ni}* enthielt, in *E. coli* co-transformiert. Nach Bestätigung der erfolgreichen Co-produktion aller Enzyme, wurden die drei neuen biokatalytischen Kaskaden getestet. Auf diese Weise wurde das biokatalytische Konzept erfolgreich auf die Produktion von α -Hydroxyketonen, primären und sekundären Aminen erweitert.

4 Compound library

4.1 Substrates and Intermediates of Biocatalytic Cascades

Alcohols	Aldehydes/Ketones	Carboxylic Acids	Amine Reactants
1a 	1b 	1c 	6 
2a 	2b 	2c 	7 
3a 	3b 	3c 	8 
	4a 		
	5a 		

4.2 Products of Biocatalytic Cascades

Primary amines (transamination)	Secondary amines (reductive amination)	α -Hydroxy ketones (carbonylation)	Byproducts
1d 	1e  1f  1h  1i  1j 	1g 	
2d 	2e 		2f 
3d 	3e  3f 		
4b 	5b  5c 		

5 Introduction

5.1 Biocatalysis

A biocatalyst can be defined as a nontoxic, biodegradable natural catalyst (most commonly an enzyme) produced from renewable sources. Biocatalysts can be used to catalyse chemical reactions in industrial processes, including the production of chemicals with importance in many aspects of life, such as drug substances, flavors, fragrances, electronic chemicals, and polymers [1]. This is of great importance as pharmaceuticals and food industry products do not tolerate contamination of even traces of any catalyst metals [2]. The most relevant factors for the development of new catalysts are efficiency and sustainability. Thus, compared to conventional catalysis for organic syntheses, biocatalysis represents a “greener” technology because it allows milder reaction conditions [3, 4]. Organic solvents can be avoided, and no pressure or high temperature has to be applied. Thereby, it reduces pollution and cost and creates greater sustainability [5]. Additionally, many synthetic transformations yet unknown by chemical means become possible. The main advantage of a biocatalyst is that it is chemo-, regio- and stereoselective. However, chemoselectivity may also be considered a negative aspect as enzymes tend to have a limited substrate scope [6]. Biocatalysis often allows for the shortening of synthetic routes by avoiding protecting group manipulations, chiral resolutions, by-product formation *etc.* [6, 7]. Another positive aspect is that there is an immense diversity in enzymes. Advances in DNA manipulation technologies and in bioinformatics (*e.g.* DNA synthesis and high-throughput screenings) has led to the discovery of new enzymes and the redesign of biocatalysts [8]. Therefore, many limitations of using enzymes as catalysts can be overcome by the development of engineering methods [9].

5.1.1 Biocatalytic Cascade Reactions

Shortening of synthetic routes by application of multistep reactions improves the efficiency of a synthetic process. Developments in biocatalysis have led to the advancement from single-step reactions of simple molecules to multi-enzyme cascades enabling the direct transformation of low-value chemicals into a variety of highly valuable products (*e.g.* chiral compounds) [10, 11]. Therefore, biocatalytic reactions that are metabolically unrelated in Nature are combined in a one-pot fashion. Advantages are the reduction of time because reaction intermediates do not have to be isolated and purified and consequently also the reduction of waste as the use of organic solvents can be minimized. This ultimately results in decreased production costs [12]. In practice, either isolated enzymes can be used to realise a biocatalytic cascade reaction (*in vitro*) or a microorganism that overproduces the desired enzymes can be used as host cell (*in vivo*). Additionally, both approaches can be combined in a cascade type reaction, or a chemical reaction step can be added [13].

5.2 Biocatalytic Cascades *in Vivo* compared to *in Vitro* Approaches

Living organisms use enzymatic cascade-type transformations for the building up of highly complex molecules. Taking Nature as a model, either an organism's metabolic network can be engineered (metabolic engineering), or multiple heterologous enzymes are incorporated and expressed in a single host organism (*in vivo* biotransformation). In a biotransformation, the introduced substrate is only used for the desired product synthesis and has no other role in the cell [14]. On the other hand, the host organism can be used only for the production of the desired enzyme, and the biocatalytic reaction can be performed with the purified enzyme (*in vitro* biotransformation, see Figure 1).

In vitro systems require the laborious preparation of the enzymes, which involves the (heterologous) expression, isolation, and purification from host cells. Moreover, many biocatalysts require cofactors, which have to be added in stoichiometric amounts or complemented with a suitable recycling system

[15]. As the enzyme is not in its natural environment, it is strongly affected by solvent, pH and temperature, and thereby its stability or activity can be diminished. Whole-cell/*in vivo* biocatalysis bypasses these preparation steps, and cells can be cultivated at low cost. Moreover, the microbial host metabolism supplies and recycles expensive coenzymes/cofactors (*e.g.*, NADP⁺/NADPH), and the biocatalyst proves to be more stable as the host cellular environment protects the enzymes from harsh reaction conditions.

In cell-free/*in vitro* systems, reaction conditions can be manipulated and changed faster. It is easier to balance enzyme activities simply by adjusting the amount of added enzyme. As a result, they often yield higher productivity through a higher concentration of biocatalyst. Product purification is simpler and the application of purified enzymes avoids any complications that arise from the complex metabolic pathways operating in living whole-cells [5, 16]. In the whole-cell, the balancing of enzyme activities is more difficult than adjusting protein amounts in a cell free system. Promoters or expression systems have to be altered on the genetic level. Another problematic topic arises due to the toxicity of the cascade substrate, intermediate or product. This can lead to side reactions and thereby lower productivity of the cascade. Besides, unwanted interactions with the host background can occur due to competing reactions in the native metabolism. Even though the cellular environment and the cell membrane stabilize and protect the enzyme from potentially harmful reaction conditions, it can also act as a mass transport barrier making product isolation cumbersome. As a result of the mentioned complications, the scale-up *in vivo* can be difficult compared to *in vitro* systems.

All in all, *in vivo* biocatalysis is more cost-effective but requires much longer lead times. Therefore, in most cases it seems to have no advantage when considering one-step biotransformations. While *in vitro* systems seem to be easier to manipulate and offer the highest flexibility and immediate control, whole-cell systems offer some benefits when multiple enzymes are combined in a cascade type reaction, as the whole-cell puts the reactants into closer proximity [13, 15].

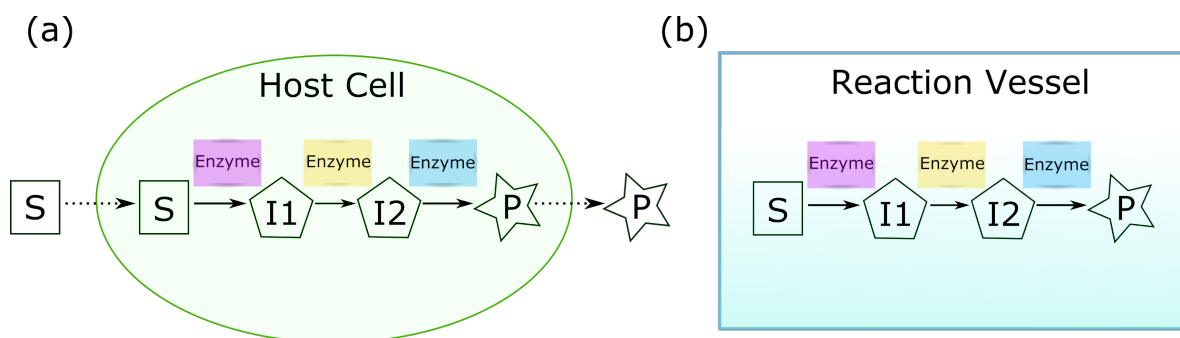


Figure 1: Schematic representation of (a) *in vivo* and (b) *in vitro* enzyme cascades. Substrate S is converted by different enzyme biocatalysts to product P via the intermediates I1 and I2.

5.3 Pathway Design of Synthetic Enzyme Cascades

Many factors have to be considered during the implementation of a biocatalytic cascade in the whole-cell [11]. Apart from the design of the cascade pathway itself, either by a retrosynthetic approach or by a “forward design” starting from an initial substrate, the thermodynamic feasibility of the overall cascade and especially the last reaction step has to be considered. The next aspect to consider is the host for the realization of the *in vivo* cascade reaction. The most prominent organisms of choice, which is “easy-to-use” is the bacterium *Escherichia coli* (*E. coli*) because of its rapid growth on inexpensive nutrients and its well-researched genetics [17]. The strain for the co-production of the desired enzymes is designed by genetic engineering. Usually, expression vectors are constructed using advanced cloning techniques as

e.g. Gibson assembly, Golden Gate/Modular Cloning (MoClo) or sequence-and ligation-independent cloning (SLIC) [18, 19]. The respective genes can be constructed as polycistronic operon (with a single promoter and terminator for all co-expressed genes), as multiple monocistronic operons (with individual promoters and terminators) or in a pseudo-operon configuration (with individual promoters for each gene but just one common terminator). Moreover, genes can be knocked out or integrated into the genome of the host *e.g.* by using the CRISPR technology [20]. Usually, resting cells that are metabolically active, but non-growing are used for the realization of biotransformations *in vivo*. This offers several advantages: Since the cells are washed, undesired growth metabolites and nutrients are removed. Moreover, carbon and energy sources are not used for growth anymore, enabling higher productivity of the artificial reaction pathway [14].

5.3.1 Challenges of Multiple Recombinant Protein Expression

In the following, challenges for the implementation of enzymatic cascades *in vivo* are summarized (see Figure 2).

First of all, potential cross-reactivity of the implemented enzymes and problems in the compatibility of the biocatalysts and their preferred reaction conditions (due to differences in activity and stability) can complicate the search for suitable biocatalysts/reaction conditions. After the selection of suitable biocatalysts, probably the most prominent problem is an insufficient expression of the pathway enzymes. The target enzymes for a *de novo* pathway must be individually produced or co-expressed in the host in active form and in sufficient amounts balanced for individual activities. If the enzyme stoichiometry is unbalanced, (toxic) cascade intermediates can accumulate, and the overall flux through the cascade is reduced [21]. In this regard, balancing enzyme stoichiometry is of great importance for the success of a synthetic enzyme cascade *in vivo*. Either the transcription or translation of the enzymes can be modulated by the implementation of different regulatory elements *e.g.* by altering the sequences of promoter or ribosome binding sites (as an example, tools can be based on the BioBricks principles [22, 23]). Apart from promoter and ribosome binding sites, nearby sequences also can influence target gene expression, which is referred to as context dependency [24]. A second option to balance expression levels is the adjustment of the copy number of the genes, either by using plasmids with different copy numbers or by gene duplication [11]. A third option would be the containment of the components of the enzymatic cascade within distinct whole-cells in a mixed-culture approach [25]. This can facilitate control over the expression of the individual enzymes and reduce the metabolic burden on the respective cells, but on the other hand, mass transfer limitations are enhanced due to the additional cell membrane barriers [16].

Another relevant aspect is the availability of essential pathway components as cofactors/coenzymes. The addition of glucose to the reaction medium to stimulate the metabolism of the host can be sufficient for cofactor generation. However, metabolic enzymes compete with pathway enzymes for these cofactors. Many whole-cell enzymatic cascades employing redox enzymes are performed under resting-cell conditions. On the one hand, coenzymes are not produced in a sufficient amount any more, leading to a loss of productivity [7]. On the other hand, the cell does not have to invest the energy (*e.g.* ATP) and metabolic resources (*e.g.* NAD(P)H) for the production of biomass. In order to overcome resulting limitations in cofactor availability, recycling *in vivo* could be important for the scale-up of a process [26]. Moreover, knock-out of reactions, which compete for the same cofactors can be applied. The development of self-sufficient redox systems, in which oxidising and reducing reactions are coupled, offer an elegant alternative [27]. An example of a self-sufficient redox conversion of alcohols to the corresponding amines was given by Klatte *et al.* [28, 29].

Subsequently, one main challenge of recombinant protein expression is that the introduction of metabolically nonrelated enzymes might interfere with the metabolic host network (resulting in dead-end

metabolites), which on the other hand might affect the production of the recombinant proteins themselves [15, 30, 31]. The expression of multiple recombinant proteins from individual plasmids can lead to a high metabolic load/burden, which induces stress responses in the host leading to a reduction of productivity in the synthetic pathway [21]. Additionally, enzymes in the host can react to the artificially introduced ones, leading to cross-inhibition, cross-linking of protein domains, mutagenesis, damaging of other enzymes, *etc* [7]. Moreover, the reactivity/toxicity of reaction substrates, intermediates or products (*e.g.* activated alkenes with a conjugated carbonyl group or aldehydes) complicate the implantation of an enzymatic cascade *in vivo*. Unbalanced heterologous enzyme production or different enzyme kinetics can lead to the leaking or accumulation of potentially reactive/toxic pathway intermediates. The metabolic background of the host responds to accumulated toxic intermediates that can lead to side reactions and the formation of byproducts [32, 33]. Therefore, an optimal carbon flux through the cascade is of high importance.

When considering cellular stress in general, there are repair mechanisms, which play a role in the survival of stressed cells and therefore could be useful for the optimization of cascades in living cells [34, 35]. Moreover, the metabolic background can be reduced by creating so-called “minimal genomes”, which include only the genes essential for life [36]. In order to have a maximum flow through the cascade, side reactions of reactive intermediates need to be avoided [37]. Low productivity represents a big issue for the realization of industrially convenient processes. Flux balance analysis in combination with metabolic flux analysis helps to create “whole-cell biocatalysts by design” by predicting the carbon flow and identification of putative bottlenecks [27]. Redirecting the carbon flux through the synthetic cascade and thereby eliminating unwanted background reactions can be done by strain engineering (*e.g.* by rational knock-out of genes), incorporation of additional enzymes or reaction engineering [21, 32, 33, 38]. The spatial organization represents another possibility to decrease side-reactions of unstable/toxic intermediates, as proximity of the pathway enzymes can enhance the flux through the cascade by reducing the diffusion of intermediates [39]. This can offer a possibility to increase productivity. Enzymes can be co-localized inside a cell by linkers, protein scaffolds or by separation from the cellular environment into microcompartments such as cellular organelles (*e.g.* peroxisomes, carboxysomes, mitochondria, *etc.*) or artificial compartments [11, 40-42].

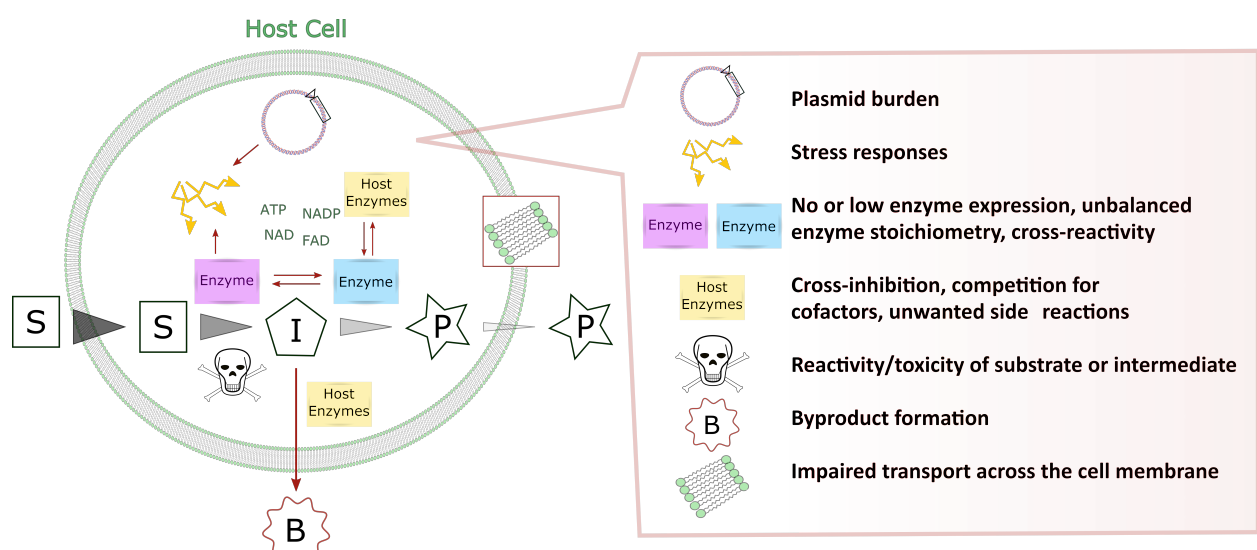


Figure 2: Challenges in a whole-cell biocatalytic cascade. Substrate S is converted via intermediate I to product P or byproduct B.

5.4 Aldehydes as Intermediates in Biocatalytic Cascade Reactions

Aldehydes are valuable products (*e.g.* for flavors and fragrances), but more importantly, they are intermediates and precursors for many pharmaceuticals. In this regard, microbial aldehyde synthesis has recently gained importance. Aldehydes can be enzymatically derived from alcohols or carboxylic acids or they can be converted to these by reduction or oxidation, respectively. Furthermore, aldehydes serve as intermediates for biocatalytic production of *e.g.* amines or several chiral carboligation products as *e.g.* cyanohydrins or aldols (see Figure 3) [43-47].

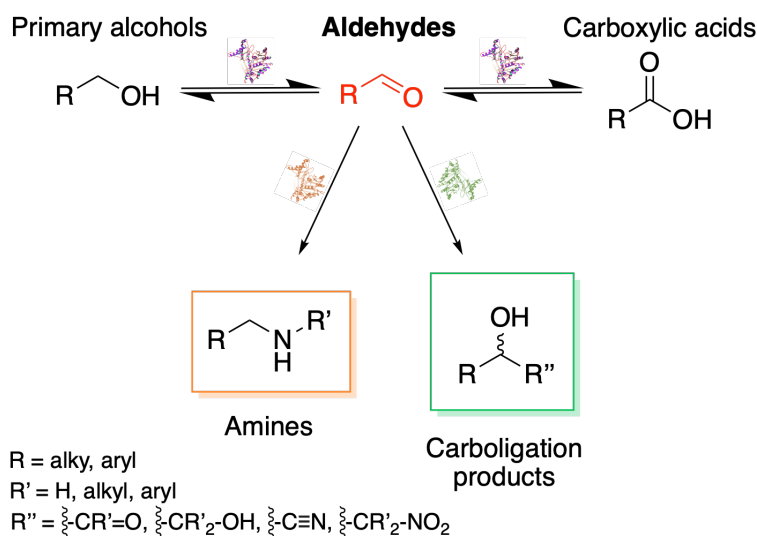


Figure 3: Examples for biocatalytic conversion of aldehydes. Aldehydes (red) can be derived from and converted to primary alcohols and carboxylic acids and are important intermediates in the synthesis of amines and carboligation products [43].

However, in living organisms, the high reactivity of aldehydes contributes to cellular toxicity, and thus, most host strains cannot accumulate them. This represents a significant problem in aldehyde production *in vivo* and consequently in many biosynthetic routes, as that they get reduced to the corresponding alcohols and partially the corresponding carboxylic acid rapidly by endogenous enzymes [32, 44]. Former methods for the biocatalytic production of aldehydes applied *in situ* extraction or reaction of the aldehyde with a “scavenger” molecule [43].

5.4.1 Inhibition or Reversal of Byproduct Formation

With increasing knowledge about metabolic networks in *E. coli* and other host organisms, strategies have been developed to avoid this cellular toxicity of aldehydes by removing target genes from the genome in order to inhibit unwanted side reactions (*e.g.* by rational knock-out of genes) [21]. As an example served an engineered *E. coli* strain, which tolerated the accumulation of aromatic aldehydes through the knockout of six ketoreductases, engineered by Kunjapur *et al.* [32]. The strain showed reduced aldehyde reduction (RARE) activity which was used for the reduction of vanillic acid to vanillin by the expression of carboxylic acid reductase from *Nocardia iowensis*. Thereby the side reaction to vanillyl alcohol by endogenous alcohol dehydrogenases was not observed. Moreover, by combining the enzymes carboxylic acid reductase and a mutant pyruvate decarboxylase, the chiral pharmaceutical intermediate (*R*)-phenylacetyl carbinol could be synthesized with 10-fold increased productivity [21, 32]. Alternatively, carbon fluxes can be rerouted by the introduction of a reversing enzymatic activity. Thus, unwanted background reactions can be eliminated, and byproducts are transformed into desired cascade intermediates (see Figure 4).

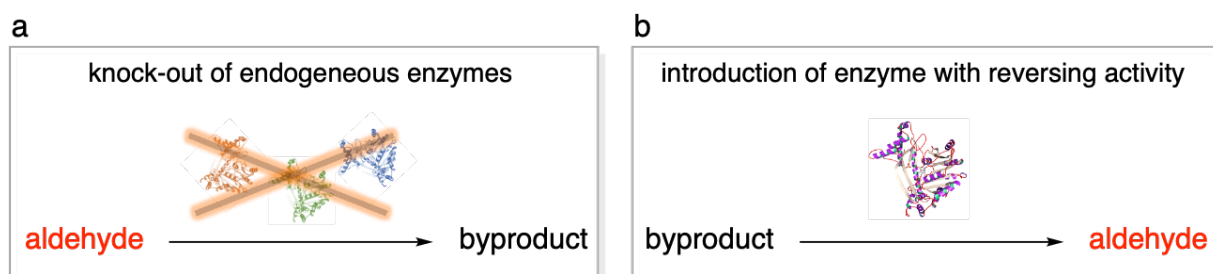


Figure 4: Inhibition or reversal of byproduct formation. Side reactions by endogeneous enzymes can be inhibited by rational knock-out (a), or byproducts can be transformed back into the desired aldehyde by introduction of enzymes with reversing activity (b).

An example was given by Bayer *et al.* by the equilibration of the formation of toxic aldehyde species using enzymes with opposing functional group transformation activity [33, 43]. The membrane-associated enzyme alcohol dehydrogenase (ADH) *AlkJ* from *P. putida* [48], which catalyses the oxidation of the alcohol, and the enzyme carboxylic acid reductase *CAR_{Ni}* from *Nocardia iowensis* [49, 50], which catalyses the reduction of the carboxylic acid to the reactive aldehyde species were combined. The combination of both enzymes antagonized the respective reduction and oxidation of the reactive aldehyde species by the host background or overoxidation by *AlkJ* itself. This “hidden reservoir of reactive aldehyde species” was combined with another biocatalytic step employing an aldolase for the coupling between an aldehyde acceptor and a carbonyl compound. D-fructose 6-phosphate aldolase *Fsa1-A129S* from *E. coli* [51] was used for the coupling of 2-phenylacetaldehyde with dihydroxyacetone yielding chiral polyhydroxylated compounds that are of special interest for the pharmaceutical industry (see Figure 5).

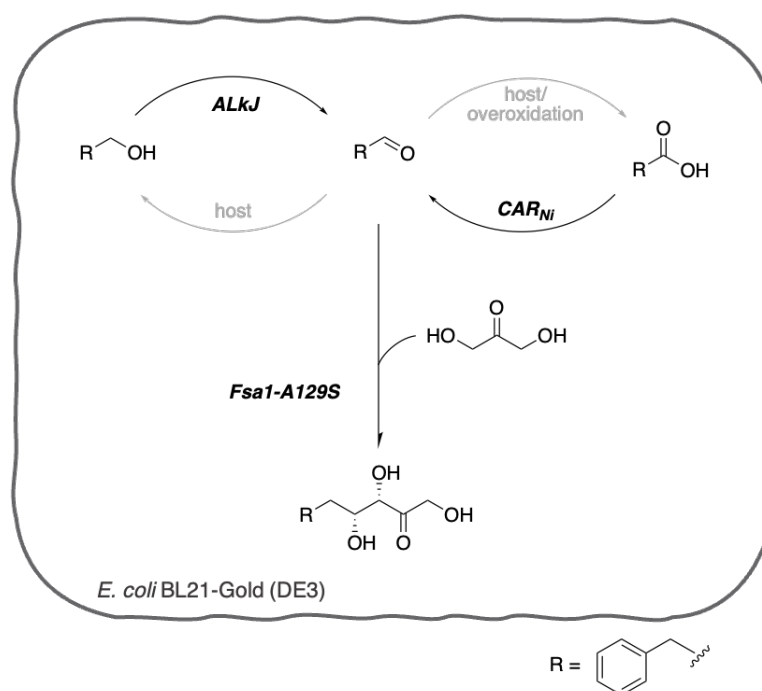


Figure 5: Enzymatic Pathway developed by Bayer *et al.* [33, 43]. Redox-equilibration of the formation of the reactive aldehyde species by the enzymes *CAR_{Ni}* and *AlkJ* and subsequent aldol reaction with dihydroxyacetone catalysed by *Fsa1-A129S* yielding chiral polyhydroxylated compounds.

5.5 Biocatalytic Carboligation, Transamination and Reductive Amination

As already mentioned earlier, aldehydes can be converted to other substance classes by various biocatalysts (see Figure 3). One example is the class of enzymes catalysing carboligation reactions. They show great potential for application in organic synthesis because of the high demand for stereoselective catalysts for C-C coupling reactions. This reaction type is fundamental for the synthesis of target compounds from smaller precursor molecules [52]. In a living organism, C-C bond forming enzymes are involved in the biosynthetic formation of carbohydrates. In this regard, it can be mainly distinguished between enzymes, which catalyse the formation of α -hydroxy ketones (ketolases) or the formation of β -hydroxy ketones (aldolases) [53]. There has been reported the combination of the previously described *in vivo* redox-equilibrium with an aldolase for the synthesis of polyhydroxylated compounds (see Chapter 5.4.1). Alternatively, pyruvate decarboxylases (PDCs, EC 4.1.1.1) offer the possibility to access α -hydroxy ketones. They belong to the family of carboxy-lyases (ketolases). Naturally, PDCs catalyse the decarboxylation of pyruvate to acetaldehyde and carbon dioxide (see Figure 6a). They are dependent on thiamine diphosphate (ThDP) as their prosthetic group and the cofactor Mg^{2+} . However, apart from the decarboxylation of pyruvate, several PDCs are known to catalyse carboligation reaction of an aldehyde (mostly acetaldehyde after decarboxylation of pyruvate, but also other aldehydes have been reported) with a second aldehyde, resulting in α -hydroxy ketones (see Figure 6b and c). Industrial processes for the production of (*R*)-phenylacetylcarbinol, an important drug intermediate, by fermentation of yeast have been described for many years [54]. Furthermore, some prokaryotic PDCs with carboligating activity have been characterized [55-57].

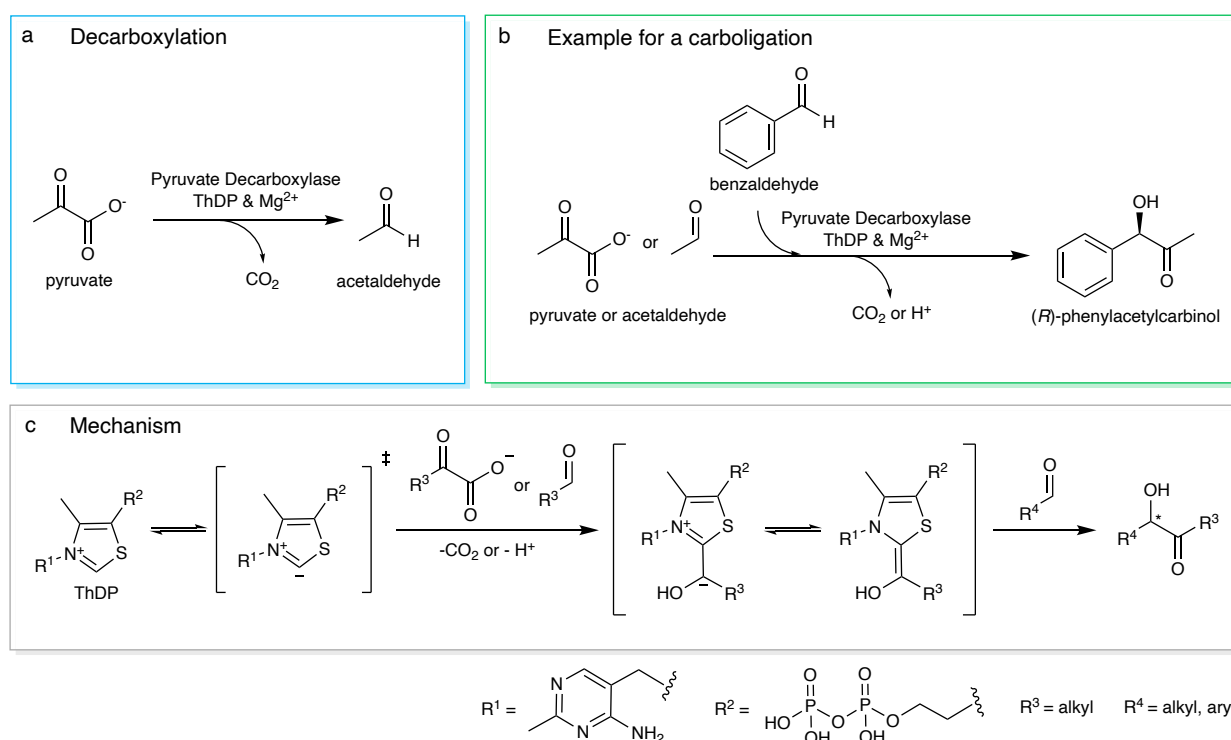


Figure 6: Decarboxylating and carboligating activity of pyruvate decarboxylase. a) Naturally, PDC catalyses the decarboxylation of pyruvate to acetaldehyde and carbon dioxide; b) several PDCs also show carboligating activity, here the formation of (*R*)-phenylacetylcarbinol is shown as an example; c) reaction mechanism of thiamine diphosphate (ThDP) dependent carboligation [58].

Alternative to the transformation of aldehydes to hydroxy ketones by carbonylation, the conversion of ketones or aldehydes to amines (C-N bond formation) represents another interesting biocatalytic possibility [59, 60]. Especially chiral amines are important for the synthesis of many drug molecules. One way to access amines from ketones/aldehydes is the use of transaminases (TAs) [61]. They catalyse the transfer of an amino group from an amine donor (originally between an amino acid and an α -keto acid) to an amine acceptor (carbonyl compound). Thereby prochiral ketones can be converted to corresponding (*S*)- or (*R*)-amines [62, 63]. Transaminases use the cofactor pyridoxal phosphate (PLP, see Figure 7), which serves as an intermediate amine acceptor transferring the amino group from one molecule to the other. α -transaminases only accept α -amino acids and α -keto acids as substrates. ω -transaminases (or amine transaminases, EC 2.6.1.18), on the other hand, accept any ketone or aldehyde and any primary amine (see Figure 7) [63, 64]. Since the discovery of ω -transaminases, they have been studied to a great extent [65, 66]. A limitation to the use of transaminases is the reversibility of the reaction. As the amination/deamination is reversible, all reactants and products exist in equilibrium with each other. Thus, usually, the equilibrium has to be pushed toward the product side by reaction engineering or follow-up reactions [63, 64].

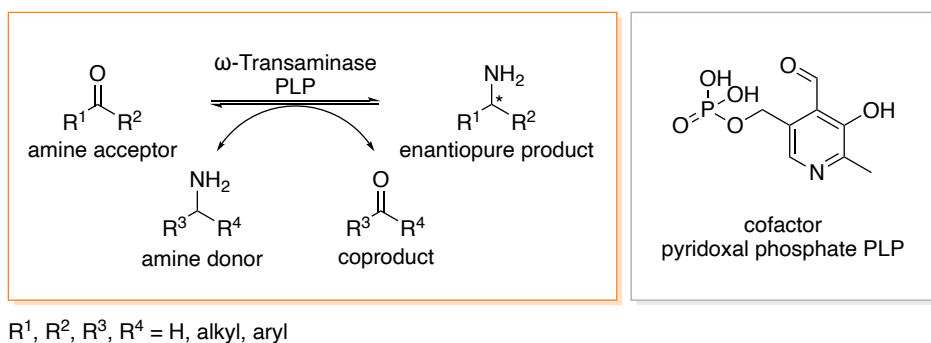
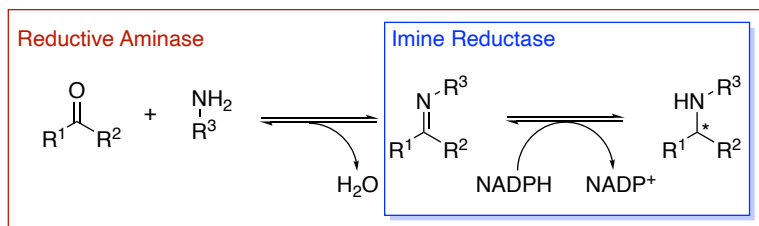


Figure 7: Enantioselective transamination reaction catalysed by an ω -transaminase. Synthesis of chiral amines by the ω -transaminase catalysed transfer of an amino group from an amine donor to an amine acceptor. Cofactor pyridoxal phosphate plays a crucial role in the transfer of the amino group.

Another possibility to access amines from a ketone/aldehyde starting material represents the use of imine reductases (EC 1.5.1.48) or reductive aminases. They are NADPH dependent and catalyse the enantioselective reductive coupling of a ketone/aldehyde with a primary amine. Thus, in comparison to the catalysis by ω -transaminases enabling the synthesis of primary amines, imine reductases/reductive aminases represent an effective possibility for the production of secondary amines. Imine reductases catalyse the reduction of preformed imines. Therefore, their activity depends on the efficiency of the imine formation and often, large excesses of amine are required for a quantitative conversion [67]. In comparison, reductive aminases (explored by Turner *et al.* [68, 69]) have the ability to catalyse both imine formation and reduction in the reaction. The imine is formed in the enzyme's active site, and subsequently reduced to the corresponding secondary amine. As a result, higher catalytic efficiencies can be achieved while employing a smaller excess of amine (see Figure 8).



R¹, R², R³ = H, alkyl, aryl

Figure 8: Reductive amination catalysed by imine reductases or reductive aminases. While imine reductases catalyse only the second step of the reductive amination, namely the reduction of a preformed imine, reductive aminases have been proven to take part also in the first step, the formation of the imine intermediate. The figure was adapted from Turner *et al.* [68].

Other examples for enzyme families which catalyse reductive amination of carbonyl compounds would be octopine dehydrogenases (OctDHs) for the coupling of α -amino acids with α -keto acids, amino acid dehydrogenases (AADHs) or amine dehydrogenases (AmDHs) for the conversion of α -keto acids or aldehydes/ketones respectively into primary amines [69].

6 Research Question

The purpose of this research is to expand the applicability of the previously developed biocatalytic redox-equilibrium created by the combination of the enzymes alcohol dehydrogenase (*AlkJ*, *P. putida*) and carboxylic acid reductase (*CAR_{Ni}*, *N. iowensis*) in *E. coli* resting cells (RCs) [33, 43]. This redox equilibrium, which creates a “reservoir of reactive aldehyde species” is going to be combined with three new enzyme classes in place of the previously described dihydroxyacetone-dependent aldolase (*Fsa1-A129S*, *E. coli*). A pyruvate decarboxylase (*PDC*), ω -transaminase (ω -*TA*), and imine reductase (*IRED*) will be tested for their ability to transform the aldehyde species into the respective value-added product (see Figure 9). The aim is to see if it is possible to express these other enzyme classes likewise in the bacterial host. Then, the applicability of this biocatalytic model will be tested after the incorporation of the new enzymes as biocatalysts for the final cascade step. If cloning and expression of the pathway enzymes is successful, the biocatalytic cascade employing all co-expressed enzymes will be tested and if possible, screened with different substrates to demonstrate the range of application.

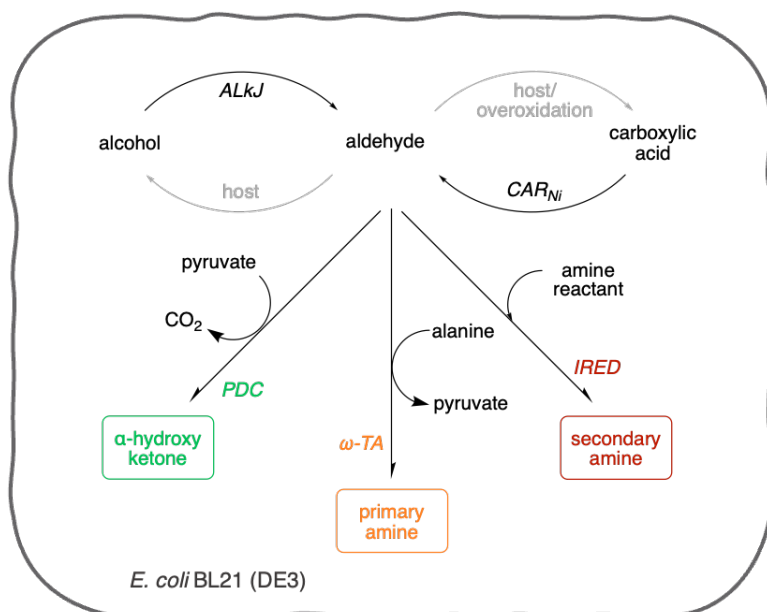


Figure 9: Overview of the proposed synthetic pathways in *E. coli* RCs. Formation of the biocatalytic aldehyde reservoir by *AlkJ* and *CAR_{Ni}* and subsequent incorporation of pyruvate decarboxylase (*PDC*), ω -transaminase (ω -*TA*) or imine reductase (*IRED*).

7 Results and Discussion

A major part of the realization of an enzymatic cascade *in vivo* consists of evaluating single enzyme activity and planning a strategy for co-expression of the respective enzymes. First, biocatalytic activity of all cascade enzymes had to be confirmed. Then, constructs for the co-expression of selected enzymes were designed *in silico* followed by assembly *in vitro* and subsequent co-expression studies and implementation of the biocatalytic cascade reaction *in vivo*. However, prior to the analysis of biocatalytic activity and molecular cloning, gene sequences of selected genes of interest were verified by sequencing.

7.1 Correction of a Mutation in the *alkj* Gene by Q5 Site Directed Mutagenesis

A point mutation (deletion) in the *alkj* gene (see Figure 10) in the template plasmid pKA1_alkj led to a premature stop codon by a frameshift and therefore, to a shorter version of the gene, hereinafter referred to as *alkj-short*.



Figure 10: Section of the sequence of *alkj* and *alkj-short*. The end of the gene sequences of *alkj* (a) and *alkj-short* (b) and the corresponding amino acid sequence is shown. The deletion in (b) led to a frameshift and a premature stop codon, resulting in a shortened gene sequence.

The mutation in *alkj* was corrected by Q5[®] site-directed mutagenesis (Q5[®] Site-Directed Mutagenesis Kit, New England Biolabs Inc.). It consists of three steps: PCR (exponential amplification), KLD reaction (intramolecular ligation and template removal) and transformation directly in *E. coli* BL21 (DE3). Gel electrophoresis of PCR (pKA1_alkj_mutag2) showed a band at approximately 7000 bp (see figure xy). For the assembly of pKA1_alkj::aspter, the mutation in *alkj* had to be corrected in a 2nd template plasmid pPOP (=pKA1_alkj::fsa1-A129S) [43], in order to keep the sequence of the T7 promoter upstream of the gene *aspter*. In this case, gel electrophoresis after PCR (pPOP_mutag) showed two bands, the expected band at approximately 8000 bp and an unexpected band at approximately 1700 bp (see Figure 11).

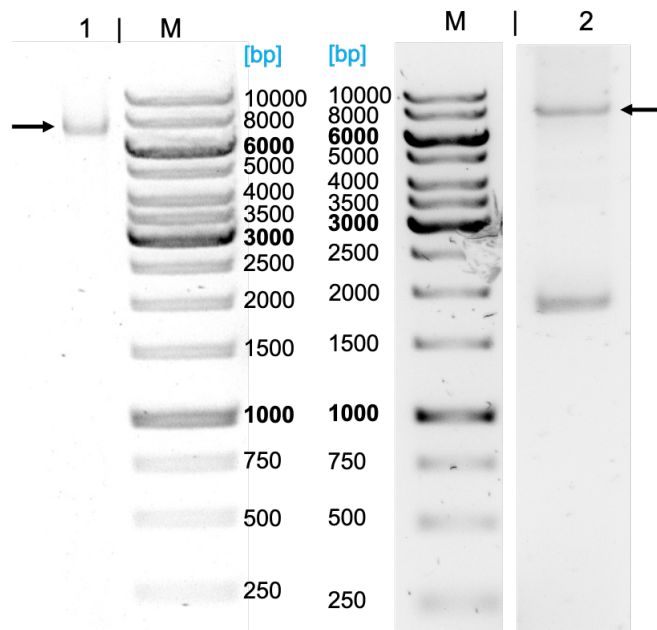


Figure 11: Gel electrophoresis of PCR reactions pKA1_alkj_mutag2 (1) and pPOP_mutag (2). For pKA1_alkj_mutag2 (1) there is a band visible at approximately 7000 bp, as expected. For pPOP_mutag (2) there are two bands visible, one at the expected 8000 bp and the other one at approximately 1700 bp.

After KLD reaction and transformation in *E. coli* BL21 (DE3), colonies were picked for the preparation of overnight cultures and subsequent plasmid isolation. Sequencing showed correct alignment and confirmed successful correction of the mutation in both template plasmids (pKA1_alkj and pPOP).

7.2 Verification of Redox Activity of the Enzymes Alcohol Dehydrogenase (*AlkJ*) and Carboxylic Acid Reductase (*CAR_{Ni}*)

Previously reported oxidising/reducing activity of the enzymes *CAR_{Ni}* and *AlkJ* needed to be confirmed in order to proceed with the implementation of the biocatalytic cascades *in vivo*. Therefore, the *E. coli* strain harbouring the plasmid with the respective gene (pETDuet1_aptase_{Ec}::*car_{Ni}* or pKA1_alkj) was cultivated, and optimized enzyme production was performed according to Table 27 in Chapter 11.1. RCs were prepared as described in Chapter 10.9.4 and standard reaction conditions for biotransformations using RCs are described in Chapter 10.12.2.

The reducing activity of the enzyme *CAR_{Ni}* was verified in RCs by the conversion of acid **1c** (as described in Chapter 11.4.1). The acid **1c** was converted to the reactive aldehyde **1b**, which in turn was converted to the corresponding alcohol **1a** by the *E. coli* enzymatic background (see Figure 12). Full conversion to the alcohol could be observed after 2 hours reaction time (see Figure 13).

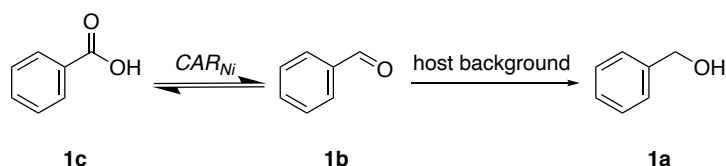


Figure 12: Model reduction reaction catalysed by *CAR_{Ni}*. Benzoic acid **1c** was converted to benzaldehyde **1b** by *CAR_{Ni}*. Subsequently, reduction to benzyl alcohol **1a** by the *E. coli* enzymatic background was observed.

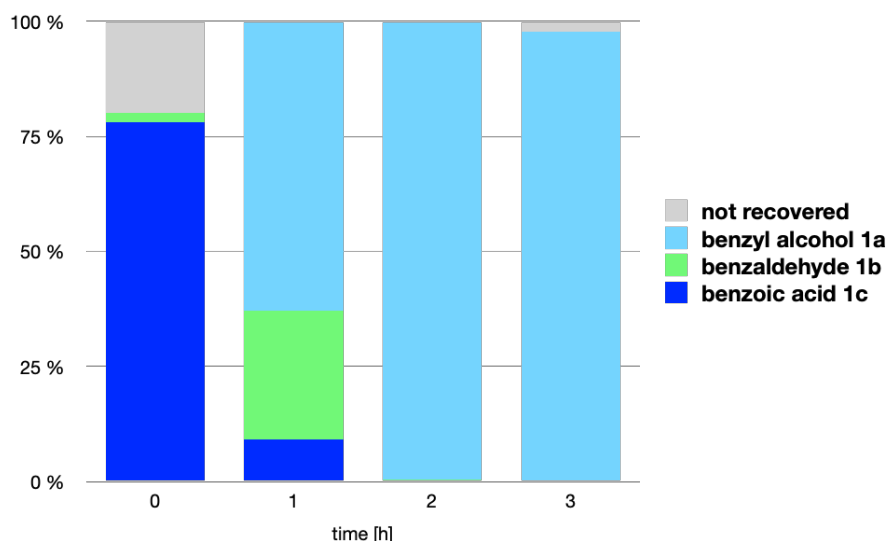


Figure 13: Reduction of benzoic acid 1c by CAR_{Ni}. Mean values of biological duplicates were analysed by calibrated GC/FID. The relative concentration of components over time is shown.

Subsequently, the oxidising activity of the enzyme *AlkJ* was verified in RCs (as described in Chapter 11.4.2). The substrate scope was tested with primary alcohols **1a-3a** (see Figure 14). Conversion to the aldehydes and, in the case of **1a** and **3a**, overoxidation to the carboxylic acids **1c** and **3c** was observed (see Figure 15). The mass loss could be explained by the volatility of cascade intermediates or by **1b** binding to/reacting with biomolecules such as proteins [70].

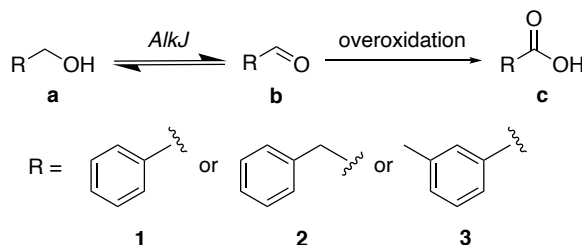


Figure 14: Model oxidation reactions catalysed by AlkJ. Alcohols **1-3a** were converted to aldehydes **1-3b** by *AlkJ*. Overoxidation to the respective carboxylic acids **1-3c** could occur.

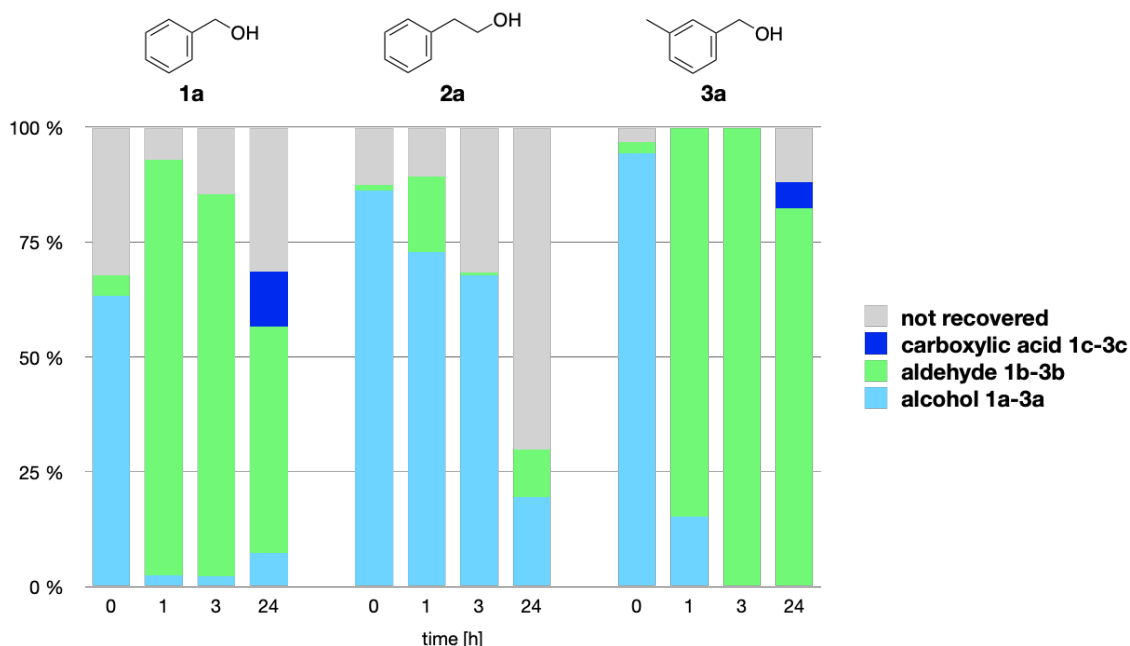


Figure 15: Oxidation of alcohols by *AlkJ*. Mean values of biological duplicates were analysed by calibrated GC/FID. The relative concentration of components over time is shown.

The alcohol **2a** showed a slower conversion to the corresponding aldehyde. A mass loss could be observed, which was explained by the alcohol's competing conversion to the acetic acid ester **2f** by chloramphenicol acetyltransferase (see Figure 16) [71]. The gene for chloramphenicol acetyltransferase was present in the pKA1 backbone and was used for selection by antibiotic resistance. Negligible amounts of the respective acetic acid esters of alcohols **1a** and **3a** were also detected.

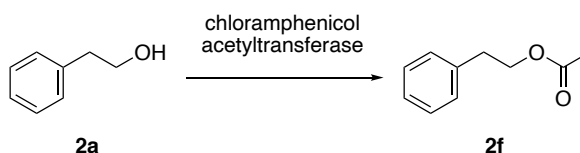


Figure 16: Formation of byproduct 2-phenylethyl acetate 2f. 2-Phenylethanol **2a** was converted to 2-phenylethyl acetate **2f** by chloramphenicol acetyltransferase.

With the purpose of comparing the activities of *AlkJ* with the truncated enzyme *AlkJ-short*, the substrate acceptance screening was repeated with *AlkJ-short* (as described in Chapter 11.4.3). Faster conversion of alcohol **2a** to aldehyde **2b** and overoxidation to **2c** could be observed employing variant *AlkJ-short* as biocatalyst. Moreover, a larger amount of **3b** was overoxidised to **3c** compared to the biotransformation employing enzyme *AlkJ* (see Figure 17).

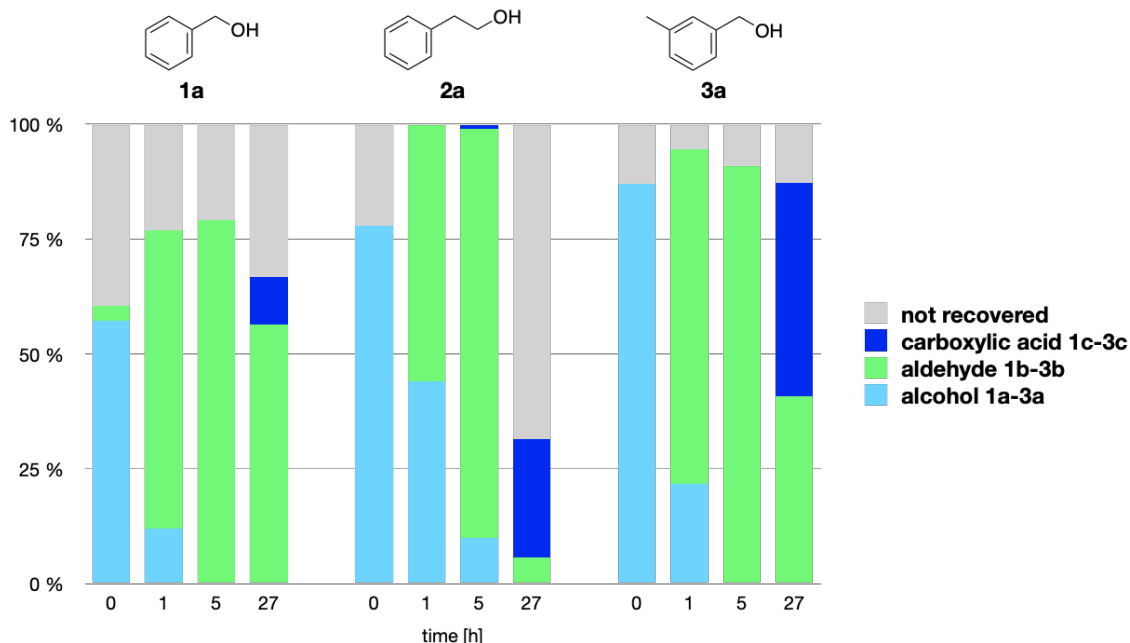


Figure 17: Oxidation of alcohols by *AlkJ-short*. Mean values of biological duplicates were analysed by calibrated GC/FID. The relative concentration of components over time is shown.

However, without introducing an enzyme to reverse the reducing activity of *E. coli* endogenous enzymes, the reactive aldehydes were metabolized very fast to their corresponding alcohols [32, 44]. This became apparent when the conversion of aldehydes by the *E. coli* enzymatic background was observed (as described in Chapter 11.4). Aldehydes **1b** and **3b** were converted to the corresponding alcohols **1a** and **3a** rapidly, whereas the metabolization of aldehyde **2b** appeared to happen slower, and a mass loss of more than 50 % could be observed (see Figure 18).

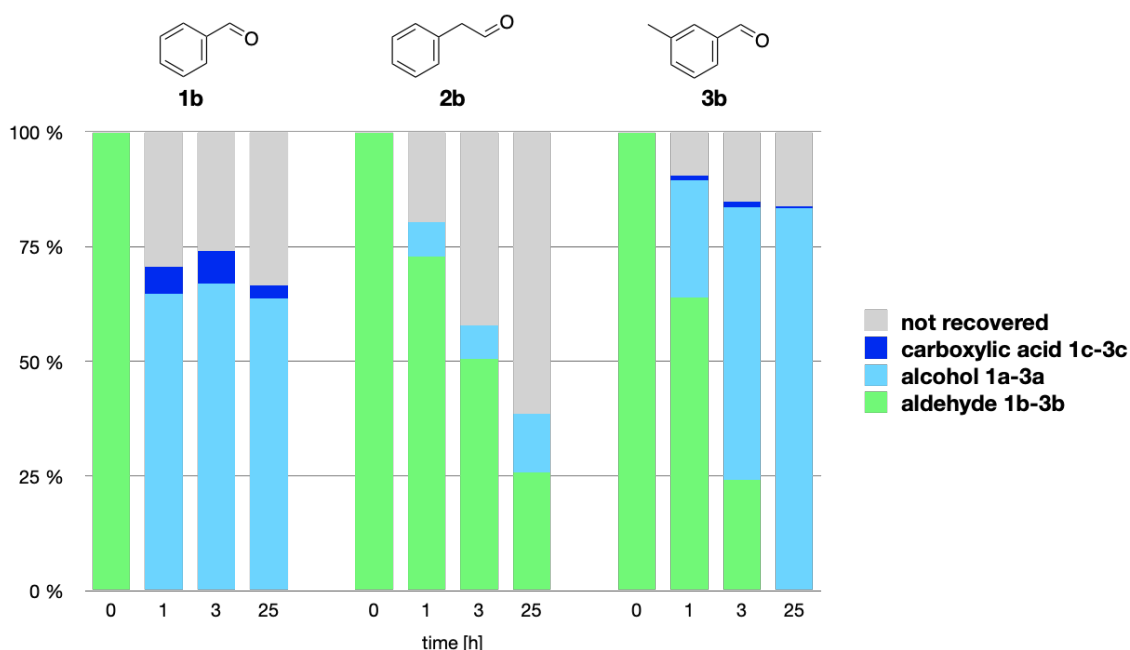


Figure 18: Metabolization of aldehydes by the *E. coli* enzymatic background. Mean values of biological duplicates were analysed by calibrated GC/FID. The relative concentration of components over time is shown.

7.2.1 Discussion

When comparing activities of corrected *AlkJ* and mutant *AlkJ-short*, the corrected variant showed poorer acceptance of substrate **2a**, while maintaining the same activity with substrates **1a** and **3a**. As a result of this rather slow conversion of **2a** by *AlkJ*, some mass loss could be observed due to conversion of **2a** to byproduct **2f** by chloramphenicol acetyl transferase expressed from the pKA1 plasmid (see Figure 16) [71]. Moreover, less overoxidation of the aldehydes to the corresponding carboxylic acids was observed with corrected *AlkJ* than with *AlkJ-short* (see Figures 15 and 17). Because compound **1a** was chosen as model substrate and the substrate scope was expanded subsequently, the activity of *AlkJ-short* was examined only after the construction of vectors for the co-expression of selected biocatalysts with *alkj*. Thus, all biocatalytic pathways were conducted employing the enzyme *AlkJ* with the corrected sequence.

7.3 Biocatalyst Selection for Reaction with the Aldehyde Species

In order to expand the applicability of the enzymatic redox equilibrium, which was developed by Thomas Bayer *et al.* through the combination of the enzymes *AlkJ* and *CAR_{Ni}*, several enzymes had to be taken into consideration [33, 43]. The reactive aldehyde species would serve as starting material for these enzymes opening the possibility to yield a range of different substance classes as the final product. In the following, the chosen enzymes and the verification of their biocatalytic activity will be described. The CFE was prepared as described in Chapter 10.9.3. Standard reaction conditions for biotransformations using the CFE are described in Chapter 10.12.1.

7.3.1 Pyruvate Decarboxylase *PDC_{Ap}* and Mutant *PDC_{Ap}_mutant*

The pyruvate decarboxylase from *Acetobacter Pasteurianus* has been previously described to exhibit carbolygating activity [55, 57]. Therefore, this enzyme was investigated as a potential catalyst for converting the reactive aldehyde **1b** to the value-added product phenylacetylcarbinol **1d** (see Figure 19). The *E. coli* strain harbouring the plasmid with the respective gene (pET22b(+)*_pdc_{Ap}*) was cultivated, and optimized enzyme production was performed according to Table 27 in Chapter 11.1. Either RCs or the cell free extract CFE were employed to test the biocatalytic conversion of **1b** to **1d** under different reaction conditions. However, no conversion to phenylacetylcarbinol was observed. This can be attributed to the rather low carbolygating activity of the enzyme. Successful carbolygation by *PDC_{Ap}* has been reported only with the purified enzyme [55, 57].

A new mutant of the enzyme *PDC_{Ap}* was obtained by Prof. Dörte Rother from the Forschungszentrum Jülich GmbH, Germany¹. The enzyme was produced in the *E. coli* strain (harbouring pET22b(+)*_pdc_{Ap}_mutant*), and the CFE was employed to test the biocatalytic conversion of **1b** with sodium pyruvate to **1d** (see Figure 19, as described in Chapter 11.4.5). Conversion to **1d** was observed already after 1 h reaction time (see Figure 20). Although the enantiomeric excess (ee) was not determined, it has been shown previously that wildtype *PDC_{Ap}* catalyses the formation of the (*R*)-enantiomer in 93 % ee [55]. The observed mass loss can be explained by cascade intermediates' volatility or by **1b** binding to/reacting with biomolecules such as proteins [70]. Moreover, the biotransformation was performed on a preparative scale, with the aim of isolating pure phenylacetylcarbinol as a reference material for the calibration by GC/FID. After purification of the product by column chromatography (silica gel, 9:1 petroleum ether/ethyl acetate), 60 % isolated yield was obtained as a yellow oil. Interestingly, a better conversion to the desired product **1d** and less conversion to byproduct **1a** was obtained in the preparative scale biotransformation than in the analytical scale biotransformation (see Figure 20).

¹ This mutant of the enzyme *PDC_{Ap}* has not been published yet. Therefore the respective mutation cannot be disclosed in this thesis.

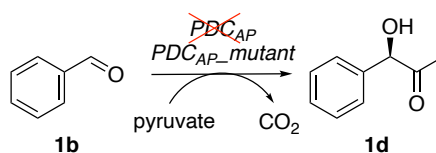


Figure 19: Model carboligation reaction catalysed by PDC_{AP} or PDC_{AP_mutant} . Benzaldehyde **1b** was not converted to phenylacetylcarbinol **1g** by PDC_{AP} . However, variant PDC_{AP_mutant} did yield conversion to **1g**.

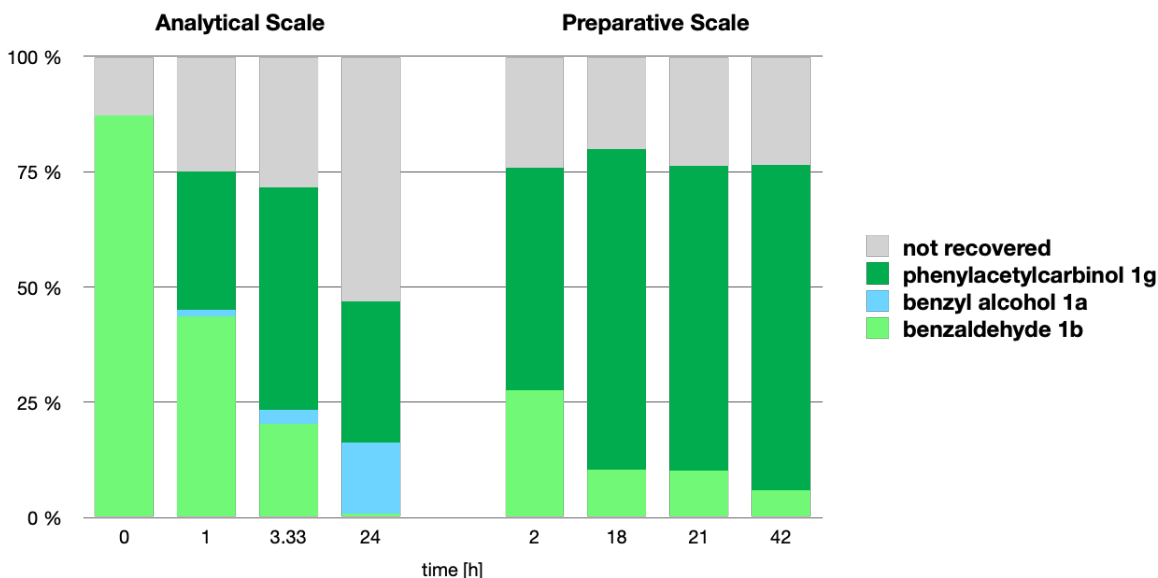


Figure 20: Conversion of benzaldehyde 1b with sodium pyruvate to phenylacetylcarbinol 1d by PDC_{AP_mutant} . Samples were analysed by calibrated GC/FID. The relative concentration of components over time is shown.

7.3.2 ω -Transaminases *VflH6*, *AspFum* and *AspTer*

As already mentioned in the introduction, ω -transaminases offer an interesting and environmentally friendly approach towards the synthesis of chiral amines [61]. Three ω -transaminases were chosen for the implementation into the biocatalytic cascade: ω -transaminase from *Vibrio fluvialis* *VflH6*, which has been studied extensively [28, 72-74], ω -transaminases from *Aspergillus fumigatus* *AspFum* [75] and *Aspergillus Terreus* *AspTer* [76]. The three enzymes were tested as potential catalysts for the conversion of ketone **4a** to amine **4b**. Therefore, the *E. coli* strains harbouring the plasmids with the respective genes (pET24a_vflh6, pET22b(+)_aspfum, pGASTON_aspter) were cultivated and optimized enzyme production was performed according to Table 27 in Chapter 11.1. The CFEs were employed to test the biocatalytic conversion of **4a** with L-alanine to **4b** (as described in Chapter 11.4.6). Additionally, lactate dehydrogenase *LDH*, NADH, glucose dehydrogenase *GDH* and D-Glucose were combined in order to consume emerging pyruvate and thereby push the reaction equilibrium to the product side (see Figure 21) [77]. Conversion was observed after 24 h reaction time for all three ω -transaminases. However, ω -transaminase *VflH6* showed the best conversion to product **4b** (see Figure 22).

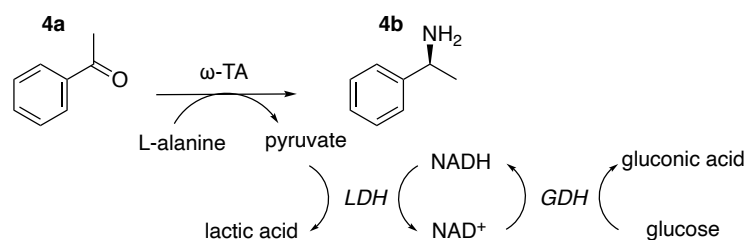


Figure 21: Model transamination reaction catalysed by ω -TAs. Acetophenone **4a** was converted to 1-phenylethylamine **4b** by ω -TAs *VfIH6*, *AspFum* or *AspTer*. Additionally, the combination of *LDH*, NADH, *GDH* and D-Glucose served to push the reaction equilibrium to the product side by the consumption of pyruvate.

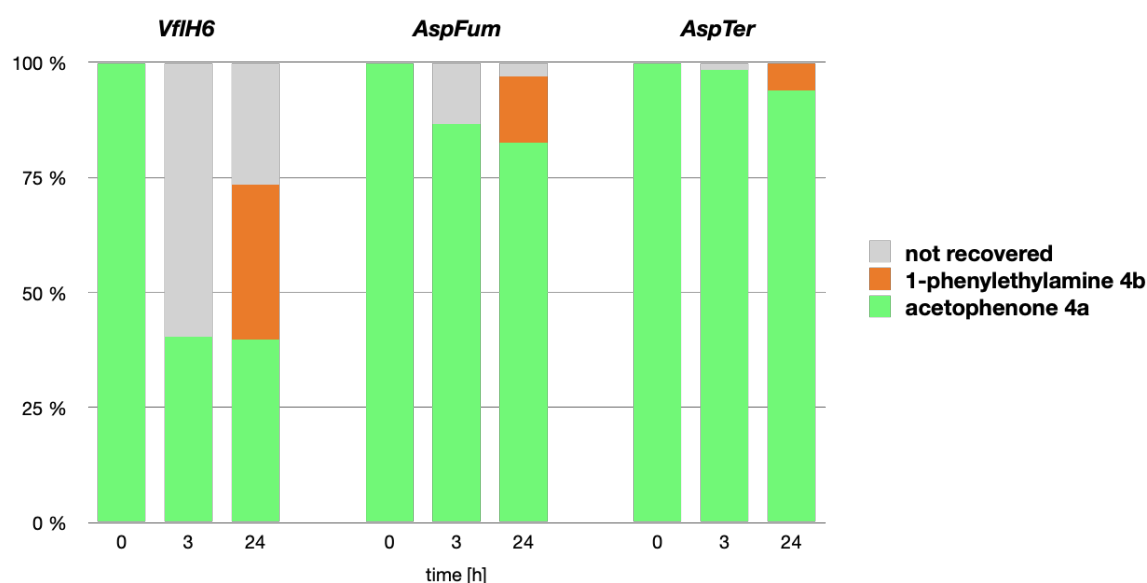
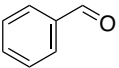
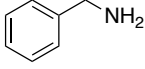
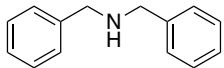
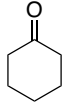
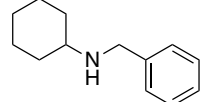


Figure 22: Conversion of acetophenone **4a with L-alanine to 1-phenylethylamine **4b** by *VfIH6*, *AspFum* and *AspTer*.** Samples were analysed by calibrated GC/FID. The relative concentration of components over time is shown.

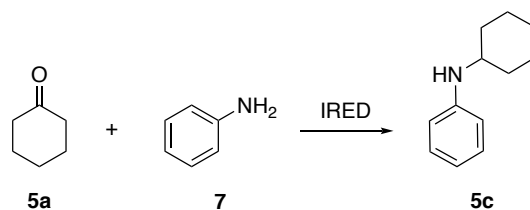
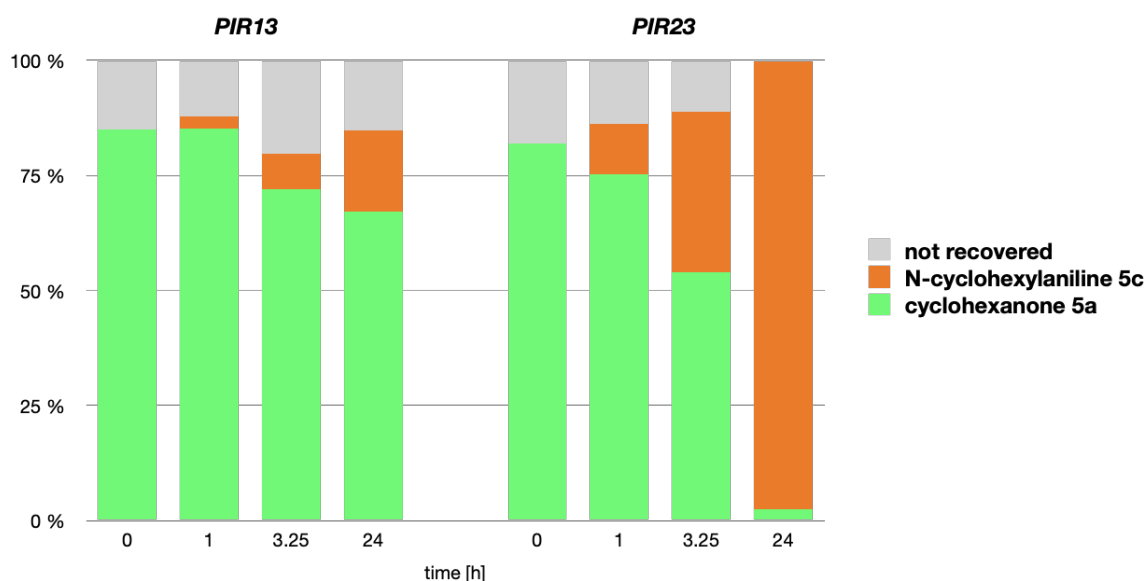
7.3.3 Reductive Aminase *AspRedAm* and Imine Reductases *PIR13* and *PIR23*

Reductive aminase from *Aspergillus oryzae* *AspRedAm* was shown to yield good conversions in reductive aminations with a small excess of amine [68, 78]. Therefore, this enzyme was investigated as a potential catalyst for converting the aldehyde **1b** to amine **1f** or ketone **5a** to secondary amine **5b** using **1d** as amine (see Table 1). The *E. coli* strain harbouring the plasmid with the gene (pET28a_*aspredam*) was cultivated, and optimized enzyme production was performed according to Table 27 in Chapter 11.1. The CFE was employed to test the biocatalytic conversion under different reaction conditions (as described in Chapter 11.4.7). However, no conversion was observed. This could be attributed to the rather poor heterologous expression of the enzyme in *E. coli* (possibly due to its fungal origin) [79]. Successful reductive amination by *AspRedAm* has been reported only with the purified enzyme [68, 78].

Table 1: Investigation of Enzymatic Activity of *AspRedAm* in Model Reductive Amination Reactions

Substrate + Amine		$\xrightarrow[\times]{AspRedAm}$	Product
Substrate	Amine	Product	Product formation after 24 h
1b 	1d 	1f 	n.a.
5a 		5b 	n.a.

Consequently, two imine reductases (IREDs) were chosen to be investigated towards their reductive amination activity: imine reductase from *Amycolatopsis regifaucium* *PIR13* and imine reductase from *Cystobacter ferrugineus* *PIR23* [79]. They were employed as catalysts in the conversion of ketone **5a** with amine **7** to secondary amine **5c** (see Figure 23). The *E. coli* strains harbouring the plasmids with the respective genes (pET28b(+)*_pir13* and pET28b(+)*_pir23*) were cultivated, and optimized enzyme production was performed according to Table 27 in Chapter 11.1. The CFEs were employed to test the biocatalytic conversion (as described in Chapter 11.4.8). Conversion to **5c** was observed after 24 h (see Figure 24). *PIR13* showed only partial conversion, whereas *PIR23* showed full conversion to the product.

**Figure 23: Model reductive amination reaction catalysed by IRED.** Acetophenone **5a** and aniline **7** were converted to the secondary amine *N*-cyclohexylaniline **5c** by IREDs *PIR13* and *PIR23*.**Figure 24: Reductive amination biotransformation of cyclohexanone **5a** with aniline **7** to *N*-cyclohexylaniline **5c** by *PIR13* and *PIR23*.** Samples were analysed by calibrated GC/FID. The relative concentration of components over time is shown.

Later in this research project, there were encountered some problems of the substrate acceptance of *PIR23* during the validation of the biocatalytic maxi-pathway (see Chapter 7.6.3). Therefore, the substrate scope was tested with two other amines **6** and **2d** (see Figures 25 and 26, as described in Chapter 11.4.8). Due to the high reactivity of aldehyde **1b** and fast metabolization to the corresponding alcohol **1a** by *E. coli* endogenous enzymes present in the CFE, relatively small conversions to the desired products were obtained. Formation of approximately 18 % product **1h** and only traces of product **1i** and were observed.

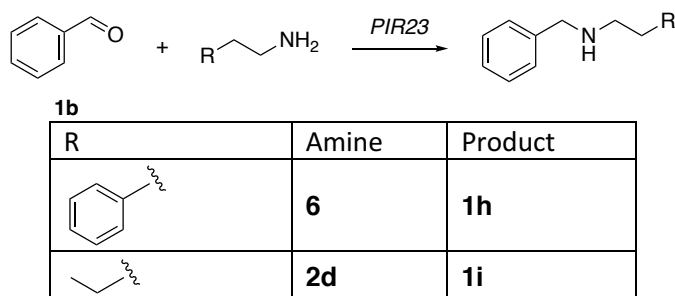


Figure 25: Model reductive amination reactions catalysed by *PIR23*. Benzaldehyde **1b** and amines **6** and **2d** were converted to the respective secondary amines **1h** and **1i** by *PIR23*.

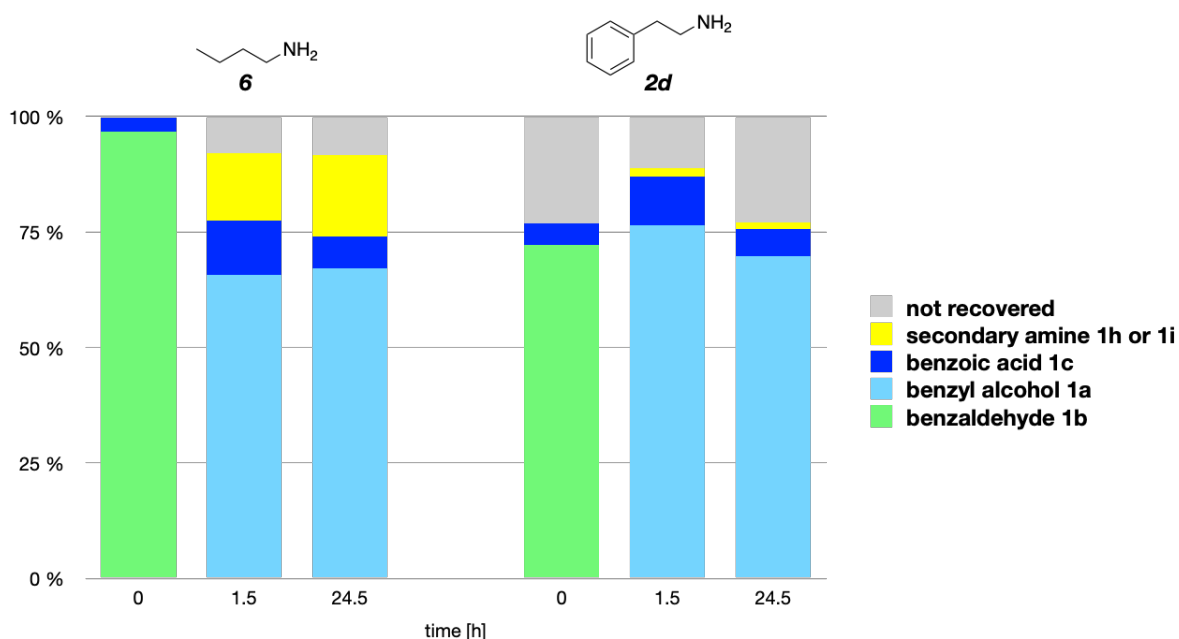


Figure 26: Reductive amination biotransformations of benzaldehyde **1b with different amines **6** and **2d** to secondary amines **1h** and **1i** by *PIR23*.** Samples were analysed by calibrated GC/FID. The relative concentration of components over time is shown. The reactive benzaldehyde **1b** was metabolized fast to benzyl alcohol **1a** by *E. coli* endogenous enzymes.

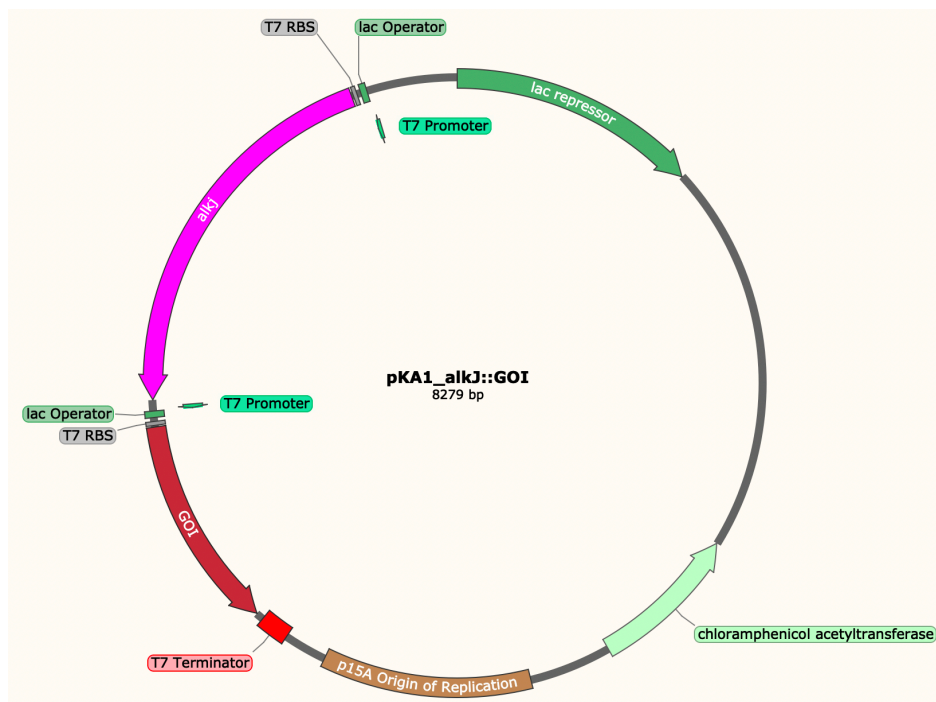
7.3.4 Discussion

During biocatalyst selection, main difficulties were encountered when testing the activity of enzymes *PDC_{Ap}* and *AspRedAm*. Substrates were not converted under various conditions, and the target products not produced. Previously, activity has been reported only with the purified enzymes, indicating the inherent low carbolygating activity of enzyme *PDC_{Ap}* [8, 9] and possibly no correct folding/inhibition of fungal enzyme activity (*AspRedAm*) during heterologous expression in *E. coli* [68, 78, 79]. Subsequently, mutant *PDC_{Ap}_mutant* showed high activity for carbolygation and bacterial imine reductase *PIR23* showed high activity for reductive amination using the unpurified cell free extract for biotransformations.

7.4 Construction of Vectors for the Co-expression of Selected Biocatalysts with *alkj*

Based on results obtained by Thomas Bayer [43], vectors for the co-expression of the selected genes of interest and *alkj* pKA1_alkj::GOI were constructed in pseudo-operon configuration (see Figure 27). The *alkj* gene from *P. putida* has been subcloned previously from the pGEc47 cosmid into the pKA1 vector for expression in *E. coli* [43]. The *LacI*/*P_{T7lac}* expression system is highly efficient on the level of transcription. Transcription is induced with IPTG, an α -lactose (α -Lac) analogue or via autoinduction media, containing a limited amount of glucose for cell proliferation and the inducing sugar α -lactose [80].

a



b



Figure 27: Design of the plasmid and close-up of the module for co-expression of *alkj* and *GOI*. a) The plasmid for co-expression of *alkj* and *GOI* was designed in pseudo-operon configuration, where two T7 promoters control the expression of each gene. b) Close-up of the regulatory elements in the model for co-expression of *alkj* and *GOI*.

The plasmids for co-expression were assembled by NEBuilder® HiFi DNA Assembly [19]. NEBuilder® HiFi DNA Assembly/Gibson assembly is a very convenient *in vitro* technique for the assembly of multiple DNA fragments (see Figure 28). It depends on homologous DNA overlaps, which must be carefully designed. In this cloning technique, three purified enzymes are combined: a high-fidelity DNA polymerase, a T5 exonuclease, and a *Taq* DNA ligase. However, secondary structures can interfere with the assembly, or repeated homologous sequences can lead to constructs either not containing the DNA fragment or unwanted configurations [21].

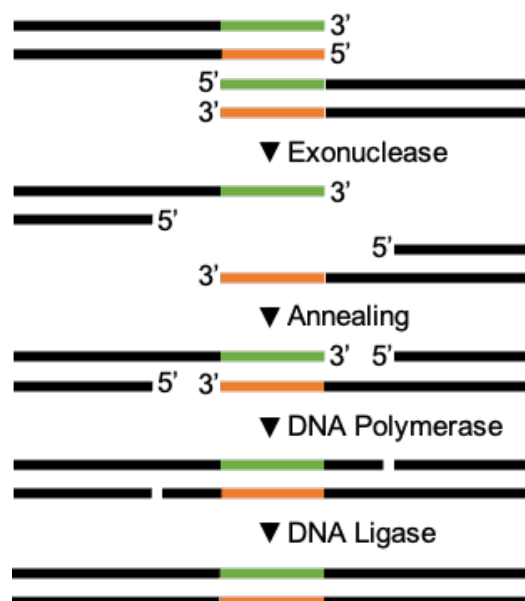


Figure 28: Gibson Assembly Overview. Schematic representation of the combination of two DNA fragments in a Gibson Assembly.

The detailed cloning procedure is described in Chapters 10.8 and 11.5. Successfully assembled constructs were verified by colony PCR and sequencing.

7.5 Co-Expression of GOI and *alkJ* from the Assembled Constructs and Validation of Biocatalytic Mini-Pathway

For the validation of the biocatalytic mini-pathways employing *AlkJ* and the respective enzyme, the successfully assembled constructs were transformed in *E. coli* BL21 (DE3) cells, and optimized enzyme production was performed following the protocol for cultivation in autoinduction media as described in Chapter 10.9.2. RCs were prepared as described in Chapter 10.9.4. Standard reaction conditions for biotransformations using RCs are described in Chapter 10.12.2.

7.5.1 *AlkJ* and *PDC_{Ap}*/Mutant *PDC_{Ap}_mutant*

First, the co-expression of *AlkJ* and pyruvate decarboxylase *PDC_{Ap}* was analysed. Unfortunately, only a minimal amount of the enzyme *PDC_{Ap}* was found in the soluble fraction according to SDS-PAGE (see Figure 29). However, in the insoluble fraction, it was impossible to distinguish between *AlkJ* and *PDC_{Ap}* bands because of their similar molecular weight. RCs were employed to test the biocatalytic conversion of alcohol **1a** to aldehyde **1b** and subsequent reaction with sodium pyruvate to product **1g** (see Figure 30). While there was conversion to **1b**, there was no conversion to **1g**, as already observed in Chapter 7.3.1.

Subsequently, the construct containing *alkj* and *pdc_{Ap}_mutant* was transformed in *E. coli* BL21 (DE3), and enzyme production was performed. Again, *PDC_{Ap}_mutant* was found in both soluble and insoluble fraction according to SDS-PAGE (see Figure 29), but it was not possible to distinguish between the bands of *AlkJ* and *PDC_{Ap}_mutant*.

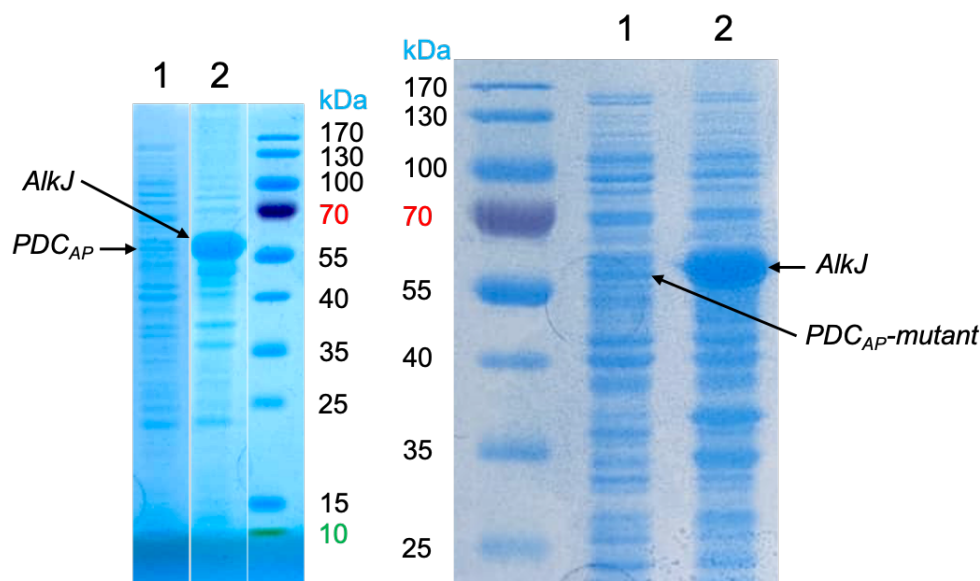


Figure 29: SDS-PAGE analysis of co-expression of *AlkJ* and *PDC_{AP}* or *PDC_{AP}-mutant*. In both cases, only a slight band for *PDC_{AP}-mutant* with the expected size of 60 kDa is visible in the soluble fraction (1). A strong band is visible in the insoluble fraction (2) with the expected size of 60 kDa, which would correspond to both, *AlkJ* and *PDC_{AP}-mutant*. Sample loading was normalized to 10 μg total protein per lane.

RCs were employed to test the biocatalytic conversion of alcohol **1a** to aldehyde **1b** and subsequent reaction with sodium pyruvate to product **1g** (see Figure 30, as described in Chapter 11.6.2). Conversion to **1b** and subsequent conversion to **1g** was observed (see Figure 31). However, using a higher biomass concentration ($\text{OD}_{590} = 20$ and $\text{OD}_{590} = 30$) resulted in better conversion, which could be explained by the enzyme's rather poor soluble expression.

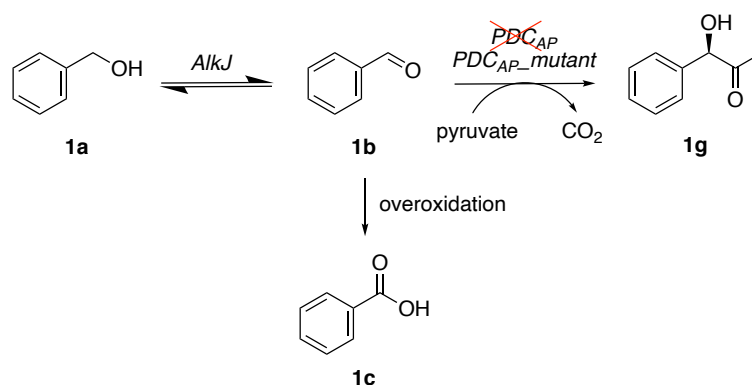


Figure 30: Mini-pathway consisting of oxidation reaction catalysed by *AlkJ* and carboligation reaction catalysed by *PDC_{AP}* or *PDC_{AP}-mutant*. Benzyl alcohol **1a** was converted to benzaldehyde **1b** and subsequent carboligation reaction by *PDC_{AP}-mutant* yielded phenylacetylcarbinol **1g** whereas *PDC_{AP}* did not show any conversion.

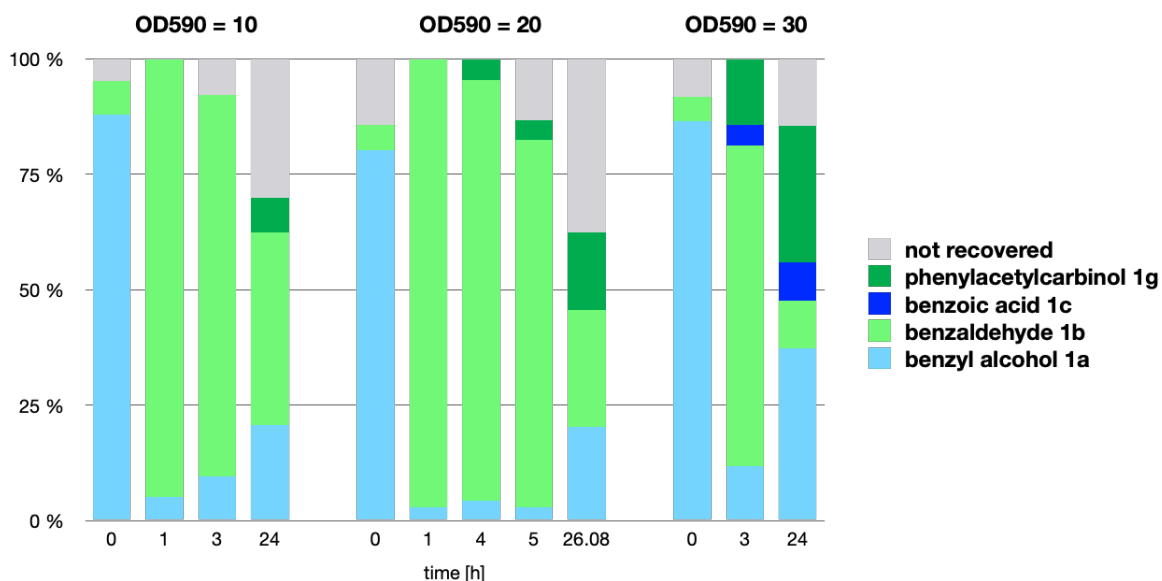


Figure 31: Conversion of benzyl alcohol 1a to benzaldehyde 1b by *AlkJ* and subsequent reaction with sodium pyruvate to phenylacetylcarbinol 1g by *PDC_{AP}* mutant. Samples were analysed by calibrated GC/FID. The relative concentration of components over time is shown.

7.5.2 *AlkJ* and *VflH6*/*AspFum*/*AspTer*

Moving on to the next biocatalytic mini-pathway, the ω -transaminases *VflH6*, *AspFum* and *AspTer* were found in the soluble fraction as well as the insoluble fraction according to SDS-PAGE (see Figure 32). The enzyme *AlkJ* was only found in the insoluble fraction, as expected.

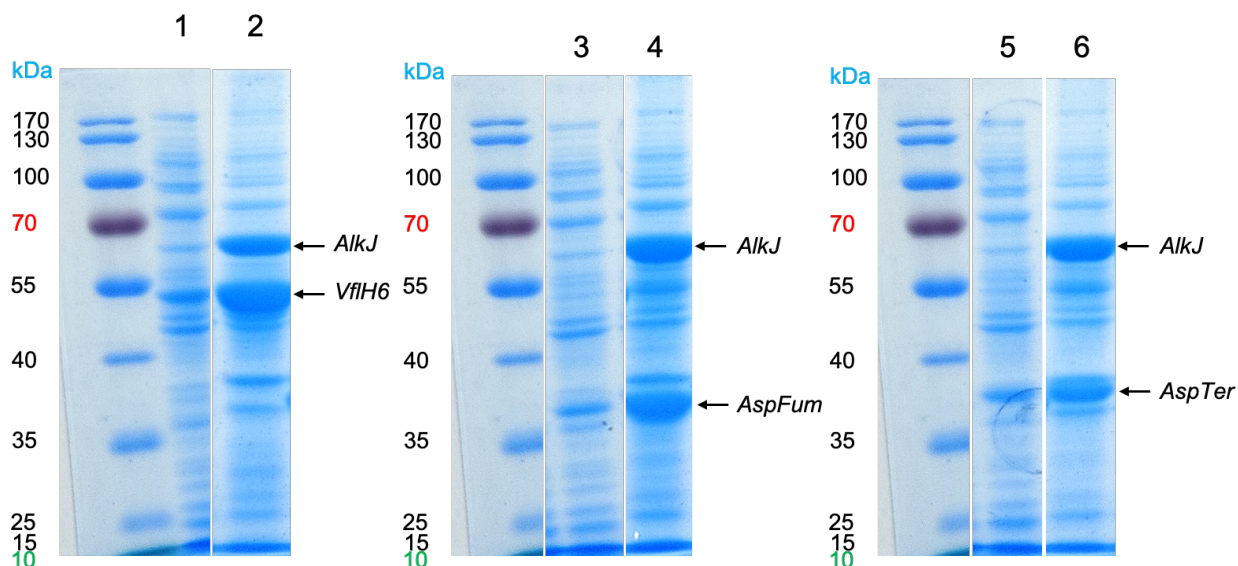


Figure 32: SDS-PAGE analysis of co-expression of *AlkJ* and *VflH6*/*AspFum*/*AspTer*. *VflH6* with the expected size of 52 kDa is visible in the soluble fraction (1) as well as the insoluble fraction (2). *AspFum* with the expected size of 37 kDa is visible in the soluble fraction (3) as well as the insoluble fraction (4). *AspTer* with the expected size of 38 kDa is visible in the soluble fraction (5) as well as the insoluble fraction (6). A strong band for *AlkJ* is visible in the insoluble fractions (2, 4 and 6) with the expected size of 60 kDa. Sample loading was normalized to 20 μ g total protein per lane.

RCs were employed to test the biocatalytic conversion of alcohol **1a** to aldehyde **1b** and subsequent reaction with 25 equivalents L-alanine to product **1d** (see Figure 33, as described in Chapter 11.6.3). Conversion to benzaldehyde and subsequent conversion to **1d** was observed (see Figure 34). As already observed during biocatalyst selection, the ω -transaminase *VfIH6* showed the highest activity and, thus, the best conversion to product **1d**. Interestingly, in the strains co-expressing *AlkJ* and *AspFum/AspTer*, the enzymatic background could not counter the aldehyde production by reducing the alcohol **1a** (even though conversion to the product **1d** was low and thereby aldehyde concentration high). Consequently, a bigger mass loss was observed, possibly due to cascade intermediates' volatility or due to **1b** binding to/reacting with biomolecules such as proteins [70].

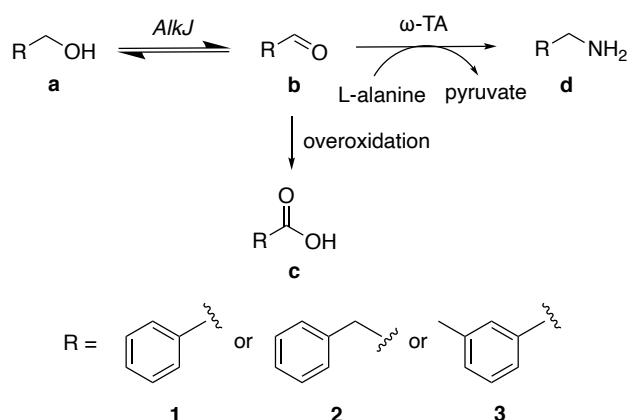


Figure 33: Mini-pathway consisting of oxidation reaction catalysed by *AlkJ* and transamination reaction catalysed by ω -TAs. Alcohol **1-3a was converted to aldehydes **1-3b**, and subsequent transamination reaction by ω -TAs yielded amines **1-3d**.**

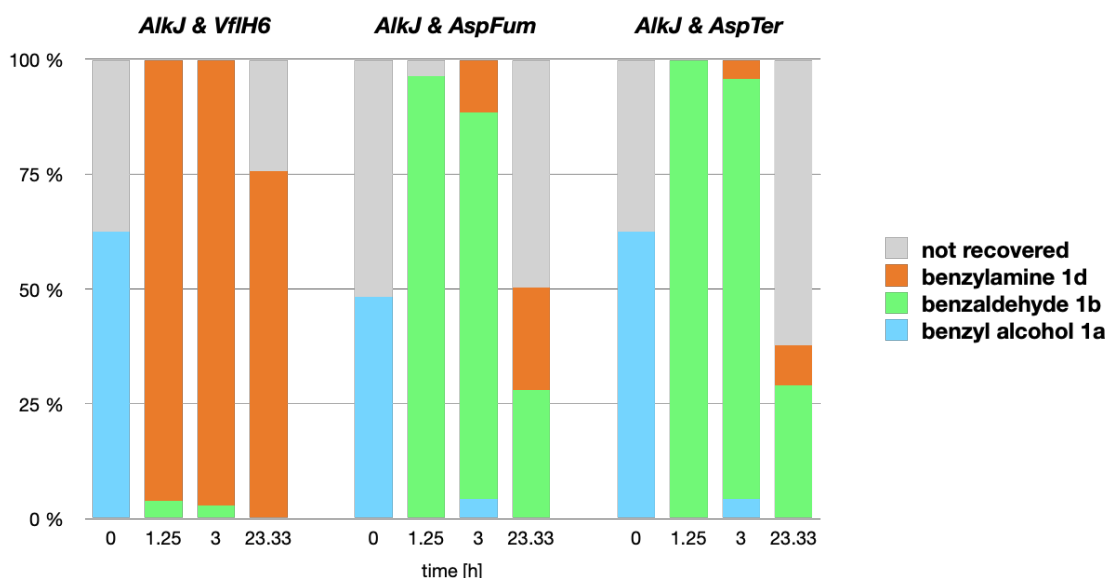


Figure 34: Conversion of benzyl alcohol **1a to benzaldehyde **1b** by *AlkJ* and subsequent reaction with 25 equivalents L-alanine to benzylamine **1d** by *VfIH6/AspFum/AspTer*. Samples were analysed by calibrated GC/FID. The relative concentration of components over time is shown.**

Moreover, the same biocatalytic pathway was repeated, employing only 10 equivalents L-alanine instead of 25 (see Figure 35). When comparing conversions over time, the final catalytic step's reversibility became apparent as the concentration of the final product **1d** was highest after 3 hours. After 24 hours, the concentration of **1d** decreased, and consequently, some of the reactive aldehyde intermediate **1b** has been reduced to starting material **1a** by the *E. coli* enzymatic background.

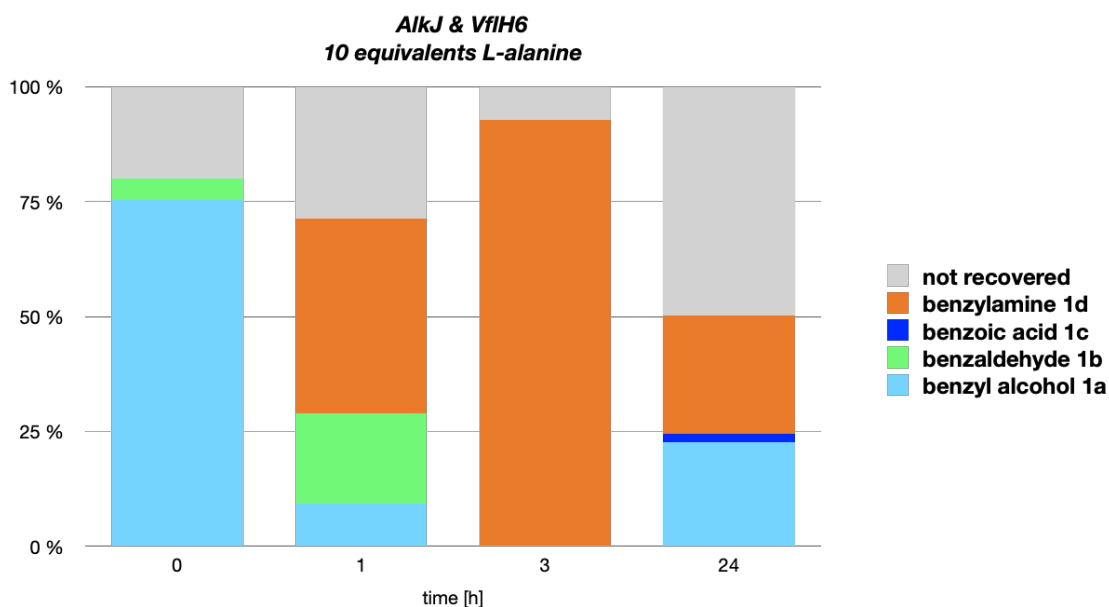


Figure 35: Conversion of benzyl alcohol 1a to benzaldehyde 1b by *AlkJ* and subsequent reaction with 10 equivalents L-alanine to benzylamine 1d by *VfIH6*. Mean values of biological duplicates were analysed by calibrated GC/FID. The relative concentration of components over time is shown.

The biocatalytic mini-pathway employing the enzymes *AlkJ* and *VfIH6* was tested with two other alcohols as starting material (**2a** and **3a**) to expand the substrate scope (as described in Chapter 11.6.3). Conversion to the aldehydes **2b** and **3b** and subsequent reaction with 10 equivalents L-alanine to the corresponding amines **2d** and **3d** was observed (see Figures 33 and 36). Due to the rather poor conversion when using **1a** as starting material, the substrate scope was not tested employing the other two ω -transaminases *AspFum* and *AspTer*.

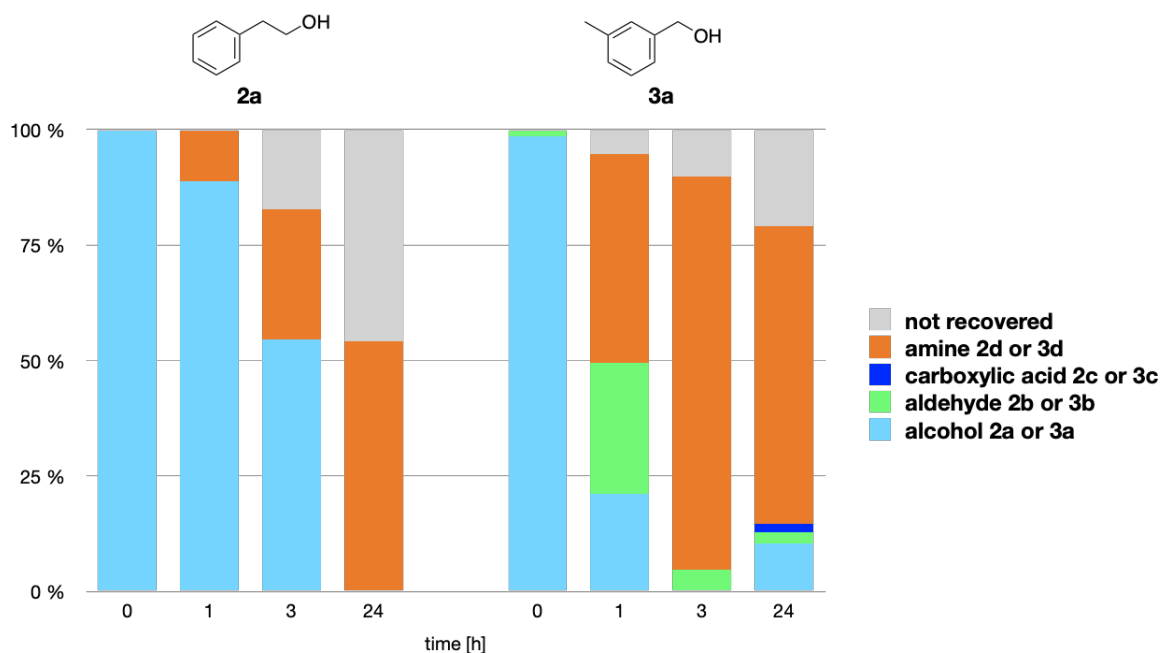


Figure 36: Conversion of alcohols 2a & 3a to corresponding aldehydes 2b & 3b by *AlkJ* and subsequent reaction with L-alanine to the amines 2d & 3d by *VfIH6*. Mean values of biological duplicates were analysed by calibrated GC/FID. The relative concentration of components over time is shown. The formation of **2f** could explain the mass loss during conversion of **2a** as a byproduct by chloramphenicol acetyl transferase [71].

7.5.3 *AlkJ* and *AspRedAm*/*PIR13*/*PIR23*

Next, the co-expression of *AlkJ* and reductive aminase *AspRedAm* was analysed. The enzyme *AspRedAm* was found in the soluble fraction as well as the insoluble fraction according to SDS-PAGE (see Figure 37), but overall, less expression was observed than usually. The enzyme *AlkJ* was only found in the insoluble fraction, as expected.

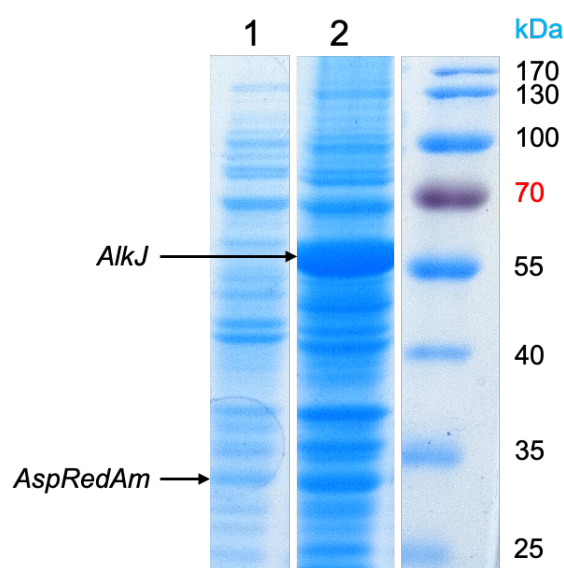


Figure 37: SDS-PAGE analysis of co-expression of *AlkJ* and *AspRedAm*. *AspRedAm* with the expected size of 31 kDa is visible in the soluble fraction (1) as well as the insoluble fraction (2). A strong band for *AlkJ* is visible in the insoluble fraction with the expected size of 60 kDa. Sample loading was normalized to 20 μ g total protein per lane.

RCs were employed to test the biocatalytic conversion of alcohol **1a** to aldehyde **1b** and subsequent reaction with **1d** to product **1f** (see Figure 38). Conversion to **1b** and subsequent imine formation was observed, but reductive amination to **1f** was not observed, as already mentioned in Chapter 7.3.3.

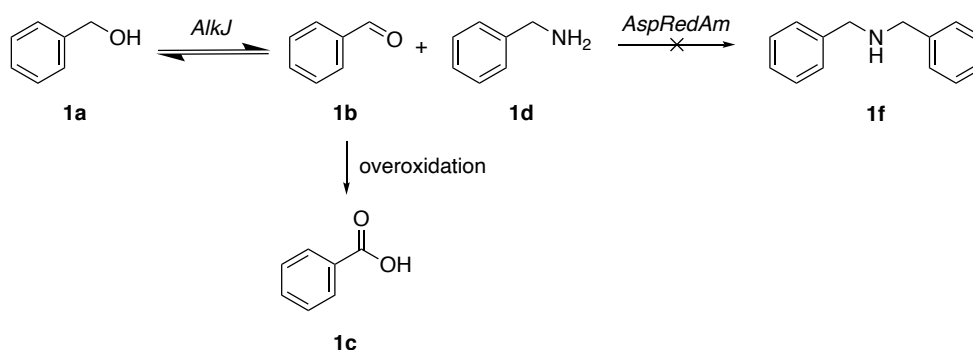


Figure 38: Mini-pathway consisting of oxidation reaction catalysed by *AlkJ* and reductive amination reaction catalysed by *AspRedAm*. Benzyl alcohol **1a** was converted to benzaldehyde **1b**, but subsequent reductive amination reaction to dibenzylamine **1f** by *AspRedAm* did not take place.

Subsequently, the construct containing *alkj* and imine reductases *pir13* and *pir23* were transformed in *E. coli* BL21 (DE3), and enzyme production was performed. According to SDS-PAGE, the enzymes *PIR13* and *PIR23* were found in the soluble fraction and the insoluble fraction (see Figure 39). The enzyme *AlkJ* was only found in the insoluble fraction, as expected.

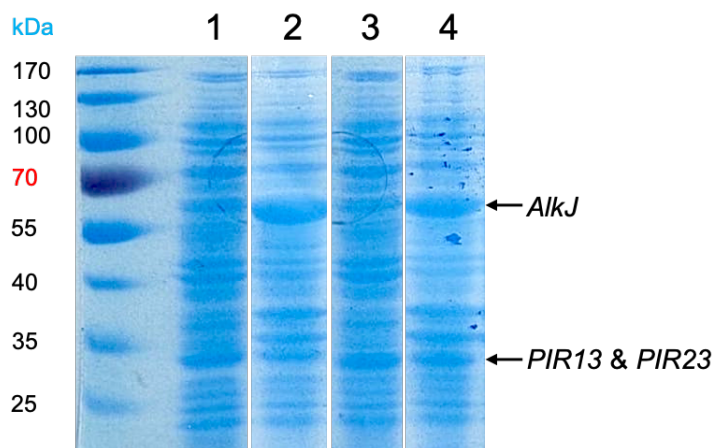


Figure 39: SDS-PAGE analysis of co-expression of *AlkJ* and *PIR13/PIR23*. *PIR13* with the expected size of 32 kDa is visible in the soluble fraction (1) as well as the insoluble fraction (2). *PIR23* with the expected size of 32 kDa is visible in the soluble fraction (3) as well as the insoluble fraction (4). A strong band for *AlkJ* is visible in the insoluble fractions (2 and 4) with the expected size of 60 kDa. Sample loading was normalized to 10 μ g total protein per lane.

RCs were employed to test the biocatalytic conversion of alcohol **1a** to aldehyde **1b** and subsequent reaction with **7** to product **1e** (see Figure 40, as described in Chapter 11.6.5). Conversion to **1b** and subsequent reductive amination to **1e** was observed employing *AlkJ* and *PIR23* (see Figure 41). However, using a higher biomass concentration ($OD_{590} = 30$) resulted in better conversion. A combination of *AlkJ* and *PIR13* showed conversion to benzaldehyde **1b** but did not show any reductive amination to the final product.

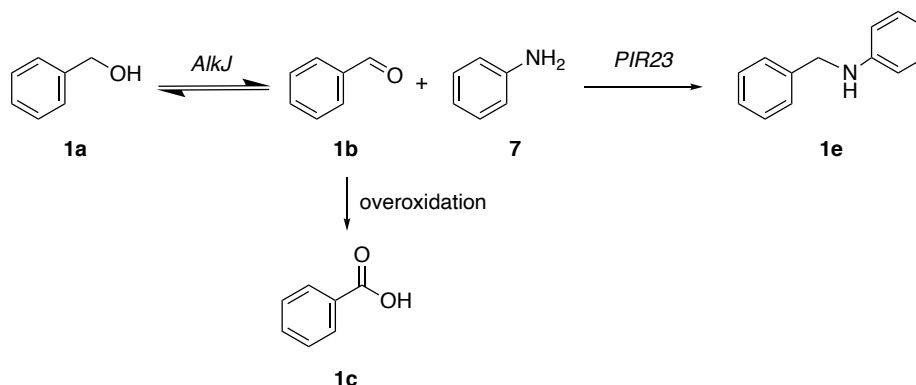


Figure 40: Mini-pathway consisting of oxidation reaction catalysed by *AlkJ* and reductive amination reaction catalysed by *PIR23*. Benzyl alcohol **1a** was converted to benzaldehyde **1b**, and subsequent reductive amination reaction catalysed by *PIR23* yielded N-benzylaniline **1e**.

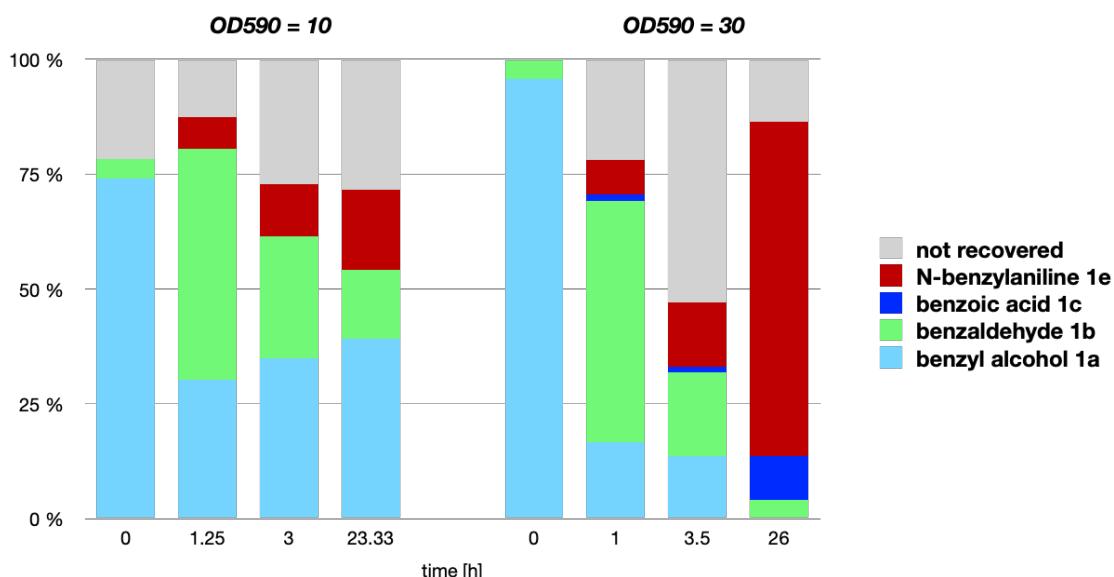


Figure 41: Conversion of benzyl alcohol to benzaldehyde by *AlkJ* and subsequent reaction with aniline to N-benzylaniline **1e** by *PIR23*. Samples were analysed by calibrated GC/FID. The relative concentration of components over time is shown.

7.5.4 Discussion

Successful co-production of pathway enzymes was confirmed in *E. coli* BL21 (DE3) cells transformed with the newly assembled plasmid harbouring *alkj* and the respective gene of interest. However, when co-expressed from the newly assembled plasmid, the amount of soluble protein was variable among the different enzymes. Only a small amount of soluble *PDC_{Ap}/PDC_{Ap}_mutant* was detected when co-expressed with *alkj*. As a result, the conversion efficiency of the reactive aldehyde **1b** to the desired product **1g** was rather low. Using a higher biomass concentration (OD₅₉₀ = 30) led to an improved final product yield. Formation of the byproduct carboxylic acid **1c** was observed.

Co-production of *AlkJ* with ω-transaminases *VfjH6* led to almost quantitative conversion to product **1d** after 3 hours, but reversibility of the transamination step depending on the excess of amine donor (10 or 25 equivalents) was observed. On this matter, using an excess of only 10 equivalents amine donor, some conversion back to alcohol **1a** by the enzymatic background and overoxidation to the respective carboxylic

acid **1c** did occur. Moreover, the mini-pathway was also tested successfully with two additional substrates **2a** and **3a**.

At last, a co-production of *AlkJ* with imine reductase *PIR23* led to almost quantitative conversion to desired product **1e** after 26 h when using a higher biomass concentration ($OD_{590} = 30$). This could not be explained by low soluble expression of the enzyme, but rather by low enzyme activity, as SDS-PAGE confirmed a substantial amount of soluble expression. Formation of the byproduct carboxylic acid **1c** was observed.

Mass loss was observed, mainly when performing biotransformations with *AlkJ* and the respective enzyme co-produced from the strain harbouring only one plasmid. A reason could be the volatility of cascade substrates/intermediates/products. When the observed mass loss correlates to higher aldehyde concentrations, a possible explanation can be binding to/reaction of the reactive aldehyde with biomolecules such as proteins [70]. The aldehyde can bind in particular to free amino groups of proteins (*e.g.* in cell membranes) [81, 82]. Moreover, a small amount of the unrecovered mass can be explained by undetectable carboxylic acid, if its concentration lied below the detection limit by GC/FID.

7.6 Co-Transformation of two Plasmids for Co-Production of all Cascade Enzymes and Validation of Biocatalytic Maxi-Pathway

Carboxylic acid reductase CAR_{Ni} and supplemental phosphopantetheinyl transferase (PPtase), necessary for its posttranslational modification [50, 83], were co-expressed from a Duet expression system (constructed by Dr. Margit Winkler from ACIB Graz, Austria). The Duet expression system is designed to harbour two target genes in pseudo-operon configuration and is useful for the co-expression of metabolically related enzymes [50]. To validate the biocatalytic maxi-pathways employing *AlkJ*, the respective enzyme and CAR_{Ni} , the successfully assembled constructs were co-transformed with pETDuet1_{pp_{tase}EC::car_{Ni}} in *E. coli* BL21 (DE3) cells. The pKA1 plasmid with medium-copy-number p15a origin of replication is compatible with the pETDuet1 plasmid with high-copy-number ColE1 (pBR322) origin of replication. Therefore, a successful co-production of all pathway enzymes was possible [21]. Plasmid uptake was verified by colony PCR as described in Chapter 10.6. If necessary, several clones were picked for protein expression. Optimized enzyme production was performed following the protocol for cultivation in autoinduction media as described in Chapter 10.9.2. RCs were prepared as described in Chapter 10.9.4. Standard reaction conditions for biotransformations using RCs are described in Chapter 10.12.2.

7.6.1 *AlkJ*, Mutant PDC_{Ap_mutant} and CAR_{Ni}

First, the biocatalytic maxi-pathway consisting of *AlkJ*, pyruvate decarboxylase mutant PDC_{Ap_mutant} and CAR_{Ni} was analysed. Ten co-transformed clones were picked for protein expression. Three out of ten clones showed successful production of the enzymes PDC_{Ap_mutant} , *AlkJ* and CAR_{Ni} , which was confirmed by SDS-PAGE (see Figure 42). However, it was not possible to distinguish between the bands of *AlkJ* and PDC_{Ap_mutant} , because of their similar molecular weight.

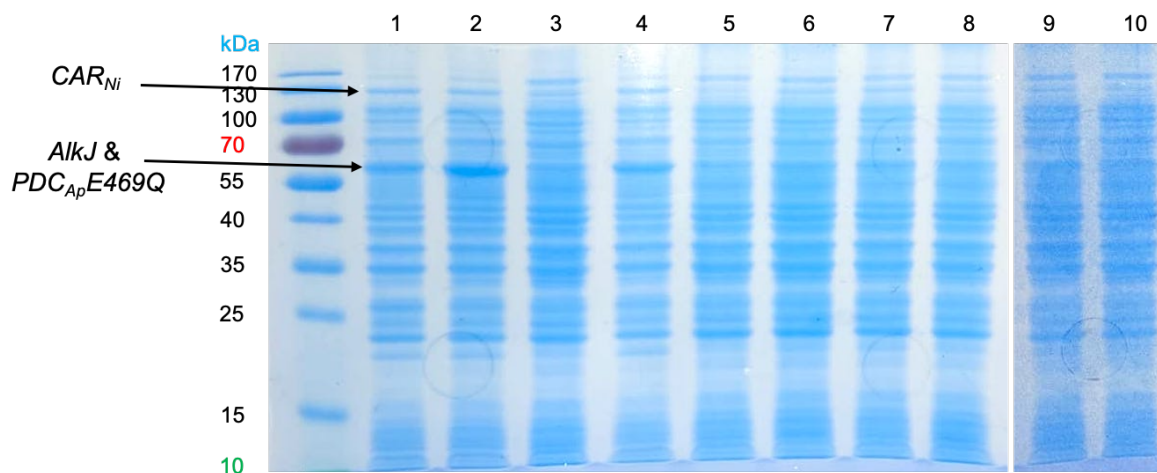


Figure 42: SDS-PAGE analysis of co-expression of $AlkJ$ and PDC_{Ap_mutant} and CAR_{Ni} . Bands for PDC_{Ap_mutant} and $AlkJ$ with the expected size of 60 kDa and for CAR_{Ni} with the expected size of 120 kDa are visible in RCs of clone 1, 2 and 4. Sample loading was normalized to 10 μ l per lane ($OD_{590} = 7$).

RCs were employed to test the biocatalytic conversion of either alcohol **1a**, acid **1c** or a 50:50 mixture of both to aldehyde **1b** and subsequent reaction with sodium pyruvate to product **1g** (see Figure 43, as described in Chapter 11.7.1). Conversion to **1b** and subsequent conversion to **1g** was observed (see Figure 44). However, conversion to the final product **1g** was rather low, probably because of the relatively poor soluble expression of the enzyme PDC_{Ap_mutant} .

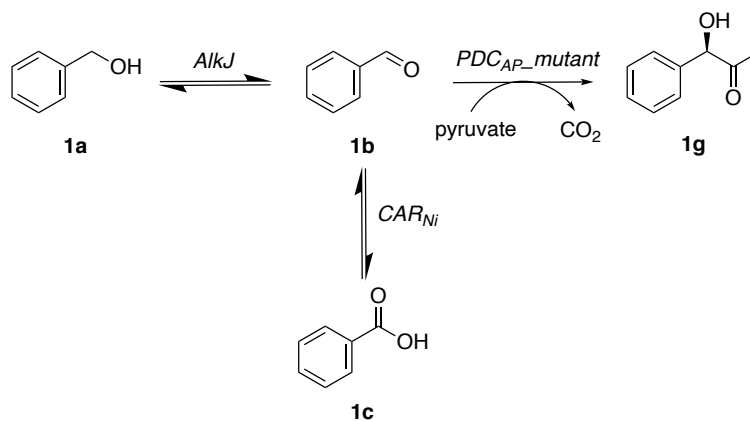


Figure 43: Maxi-pathway consisting of oxidation reaction catalysed by $AlkJ$, reduction reaction catalysed by CAR_{Ni} and carboligation reaction catalysed by PDC_{Ap_mutant} . Benzyl alcohol **1a** or benzoic acid **1c** was converted to benzaldehyde **1b** by $AlkJ$ and CAR_{Ni} respectively and subsequent carboligation reaction catalysed by PDC_{Ap_mutant} yielded phenylacetylcarbinol **1g**.

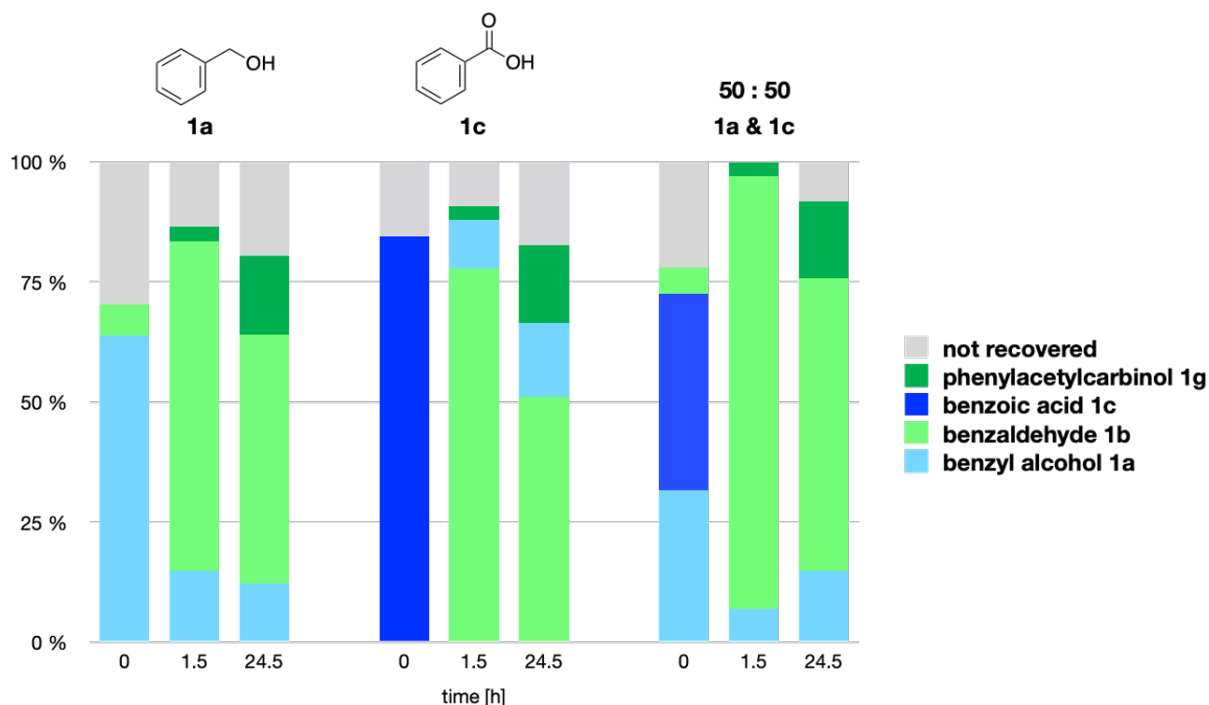


Figure 44: Conversion of benzyl alcohol or benzoic acid to benzaldehyde by *AlkJ* or *Car_{Ni}* respectively and subsequent reaction with sodium pyruvate to phenylacetylcarbinol by *PDC_{AP} mutant*. Mean values of biological duplicates were analysed by calibrated GC/FID. The relative concentration of components over time is shown.

7.6.2 *AlkJ*, *VfIH6/AspFum/AspTer* and *CAR_{Ni}*

Subsequently, the biocatalytic maxi-pathway consisting of *AlkJ*, the respective ω -transaminase and *CAR_{Ni}* was analysed. One clone of each co-transformation was picked for protein expression. All clones showed successful production of the enzymes *VfIH6/AspFum/AspTer*, *AlkJ* and *CAR_{Ni}*. According to SDS-PAGE, the enzymes *VfIH6*, *AspFum* and *AspTer* were found in both the soluble and insoluble fraction (see Figure 45). The enzyme *AlkJ* was only found in the insoluble fraction, as expected. The enzyme *CAR_{Ni}* was mainly found in the soluble fraction.

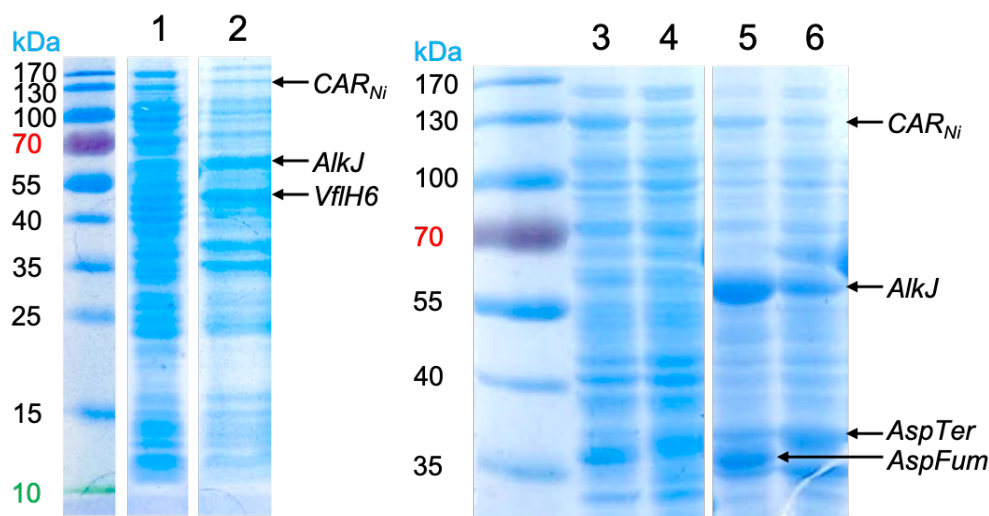


Figure 45: SDS-PAGE analysis of co-expression of *AlkJ* and *VflH6/AspFum/AspTer* and *CAR_{Ni}*. Bands for *VflH6* with the expected size of 52 kDa are visible in both the soluble (1) and insoluble (2) fraction. Bands for *AspFum* with the expected size of 37 kDa and *AspTer* with the expected size of 38 kDa are visible in both the soluble (3 and 4) and insoluble (5 and 6) fractions. Bands for *AlkJ* with the expected size of 60 kDa are visible mainly in the insoluble fractions (2, 5 and 6). Bands for *CAR_{Ni}* with the expected size of 120 kDa are visible mainly in the soluble fractions (1, 3 and 4). Sample loading was normalized to 10 μ g total protein per lane.

RCs were employed to test the biocatalytic conversion of either alcohol **1a**, acid **1c** or a 50:50 mixture of both to aldehyde **1b** and subsequent reaction with L-alanine to product **1d** (see Figure 46, as described in Chapter 11.7.2). Conversion to **1b** and subsequent conversion to **1d** was observed with *AlkJ*, *VflH6* and *CarNi* (see Figure 47). Biotransformations employing the other two transaminases *AspFum/AspTer* with *AlkJ* and *CAR_{Ni}* gave only traces of the product **1d** and therefore were not further investigated.

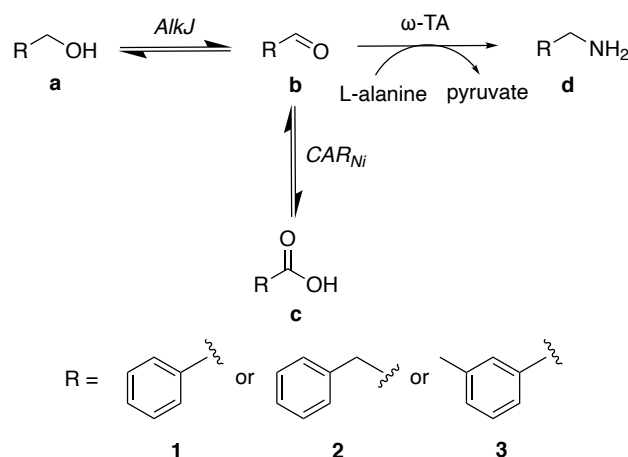


Figure 46: Maxi-pathway consisting of oxidation reaction catalysed by *AlkJ*, reduction reaction catalysed by *CAR_{Ni}* and transamination reaction catalysed by *VflH6*. Alcohols **1-3a** or carboxylic acids **1-3c** were converted to aldehydes **1-3b** by *AlkJ* and *CAR_{Ni}* respectively and subsequent transamination reaction catalysed by *VflH6* yielded amines **1-3d**.

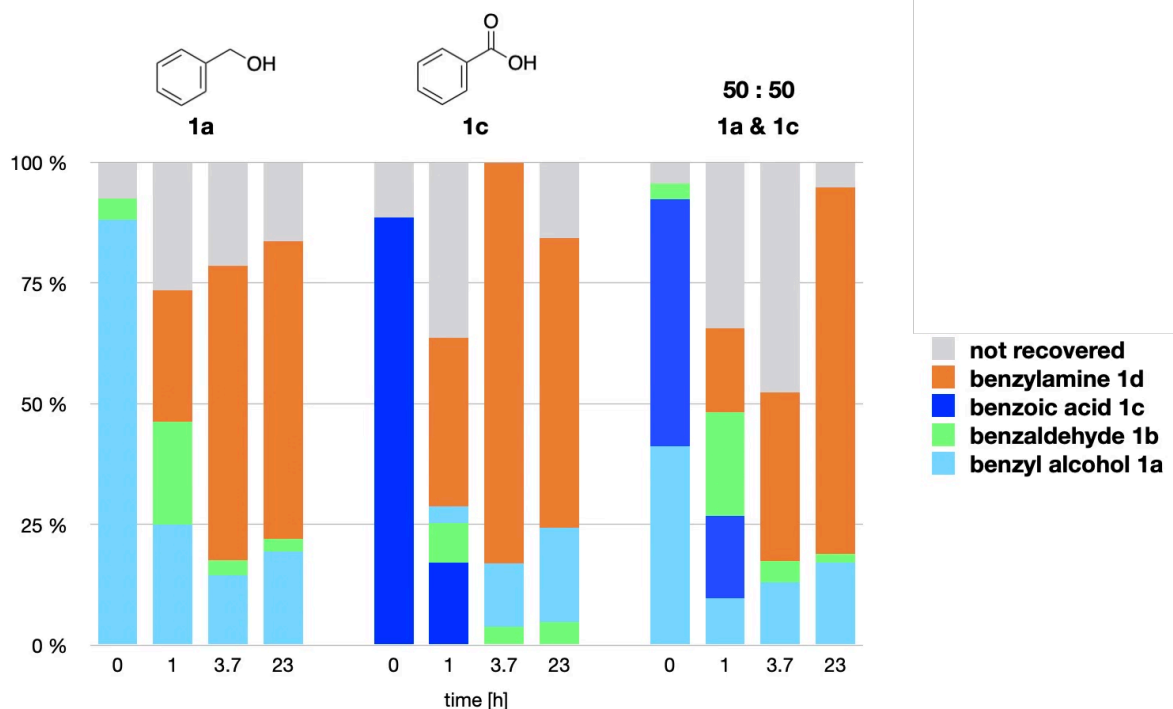


Figure 47: Conversion of benzyl alcohol **1a** or benzoic acid **1c** to benzaldehyde **1b** by *AlkJ* or *CAR_{Ni}* respectively and subsequent reaction with L-alanine to benzylamine **1d** by *VfIH6*. Mean values of biological duplicates were analysed by calibrated GC/FID. The relative concentration of components over time is shown.

To expand the substrate scope, the biocatalytic maxi-pathway employing the enzymes *AlkJ* and *VfIH6* and *CAR_{Ni}* was tested with two other alcohols **2a** and **3a**, the corresponding acids **2c** and **3c** and a 50:50 mixture of alcohol and acid as starting material (see Figure 46, as described in Chapter 11.7.2). Conversion to the aldehydes **2b** and **3b** and subsequent conversion to the corresponding amines **2d** and **3d** was observed (see Figure 48). Due to the poor conversion when using **1a** or **1c** as starting material, the substrate scope was not tested employing the other two ω -transaminases *AspFum* and *AspTer*.

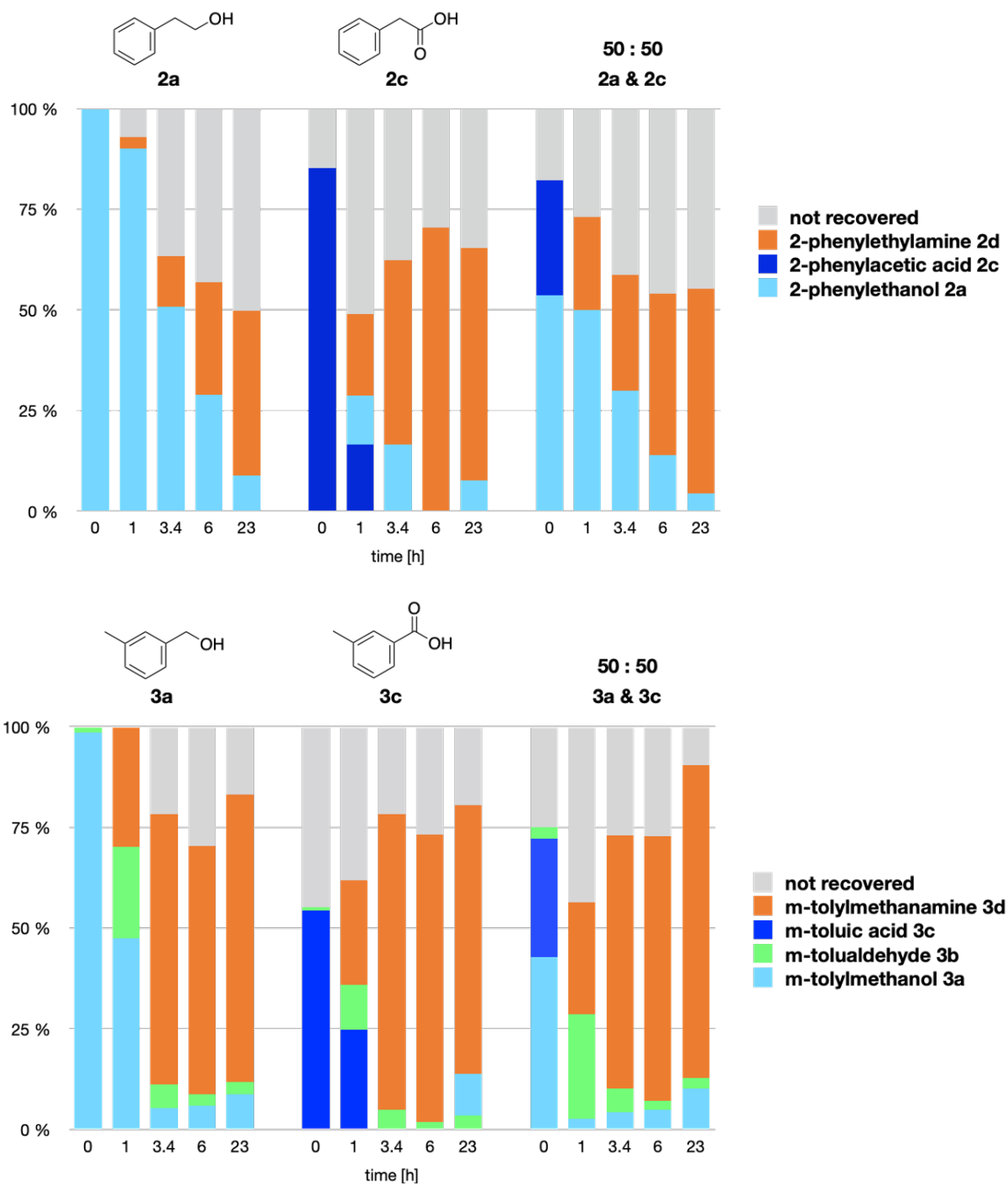


Figure 48: Conversion of alcohols **2a** & **3a** or acids **2c** & **3c** to corresponding aldehydes **2b** & **3b** by *AlkJ* or *CAR_{Ni}* respectively and subsequent reaction with L-alanine to the amines **2d** & **3d** by *VfiH6*. Mean values of biological duplicates were analysed by calibrated GC/FID (Method "7 min"). The relative concentration of components over time is shown. The formation of **2f** as a byproduct by chloramphenicol acetyl transferase explained the mass loss during conversion of **2a**, **2c** or the 50:50 mixture of **2a** and **2c** [71].

7.6.3 *AlkJ*, *PIR23* and *CAR_{Ni}*

Finally, the biocatalytic maxi-pathway consisting of *AlkJ*, imine reductase *PIR23* and *CAR_{Ni}* was analysed. Six co-transformed clones were picked for protein expression. Two out of six clones showed successful enzyme production. According to SDS-PAGE, the enzyme *PIR23* was found in both the soluble and insoluble fraction (see Figure 49). The enzyme *AlkJ* was only found in the insoluble fraction, as expected. The enzyme *CAR_{Ni}* was mainly found in the soluble fraction.

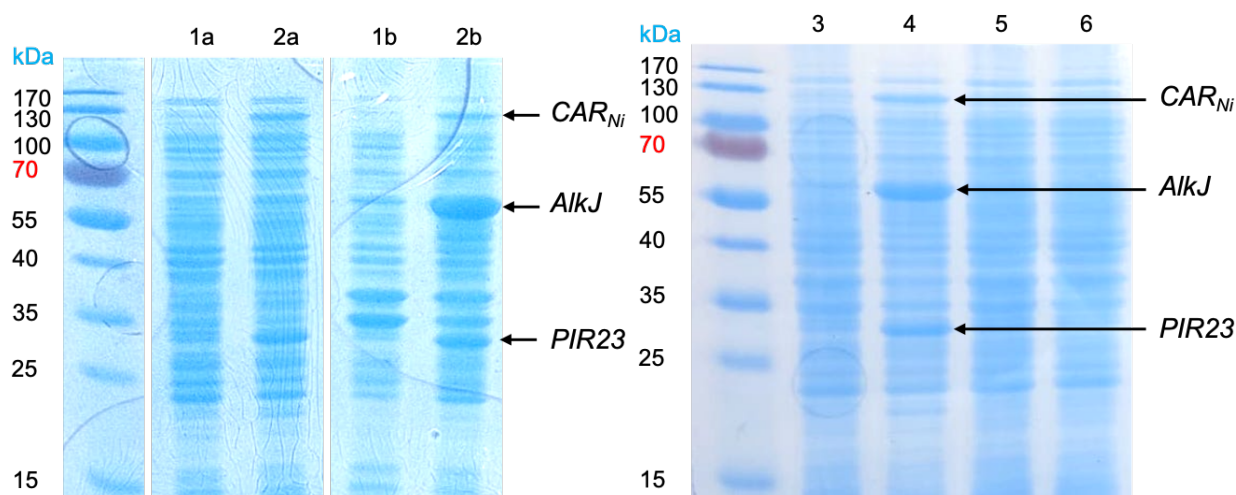


Figure 49: SDS-PAGE analysis of co-expression of *AlkJ* and *PIR23* and *CAR_{Ni}*. Bands for *PIR23* with the expected size of 32 kDa, for *AlkJ* with the expected size of 60 kDa and for *CAR_{Ni}* with the expected size of 120 kDa are visible in RCs of clone 2 and 4. *PIR23* is visible in both the soluble (**2a**) and insoluble (**2b**) fraction, *CAR_{Ni}* is visible mainly in the soluble fraction (**2a**), and *AlkJ* is visible mainly in the insoluble fraction (**2b**). All three enzymes are visible in RCs of clone (4). Sample loading was normalized to 10 μ g total protein per lane for the soluble and insoluble fractions (1 - 2) or 10 μ l (OD₅₉₀ = 7) for RCs (3-6).

RCs were employed to test the biocatalytic conversion of either alcohol **1a**, acid **1c** or a 50:50 mixture of both to aldehyde **1b** and subsequent reaction with amine **7** to product **1d** (see Figure 50, as described in Chapter 11.7.3). Conversion to **1b** and subsequent reductive amination to **1e** was observed employing (see Figure 51).

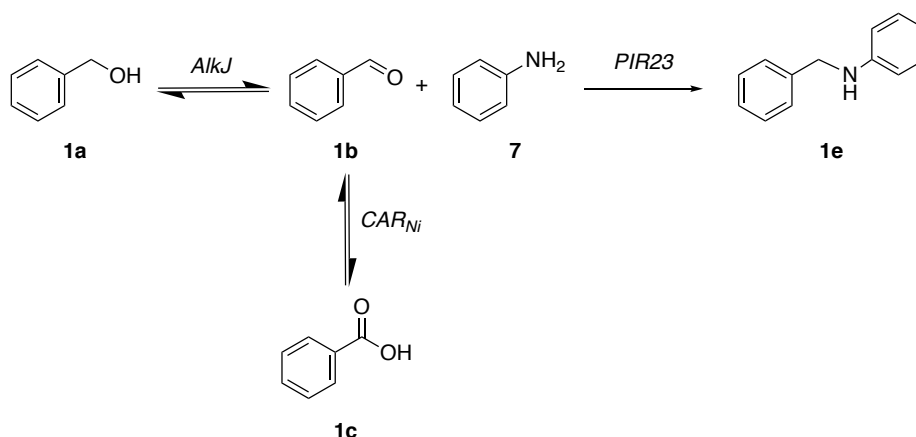


Figure 50: Maxi-pathway consisting of oxidation reaction catalysed by *AlkJ*, reduction reaction catalysed by *CAR_{Ni}* and reductive amination reaction catalysed by *PIR23*. Benzyl alcohol **1a** or benzoic acid **1c** was converted to benzaldehyde **1b** by *AlkJ* and *CAR_{Ni}* respectively and subsequent reductive amination reaction catalysed by *PIR23* yielded N-benzylaniline **1e**.

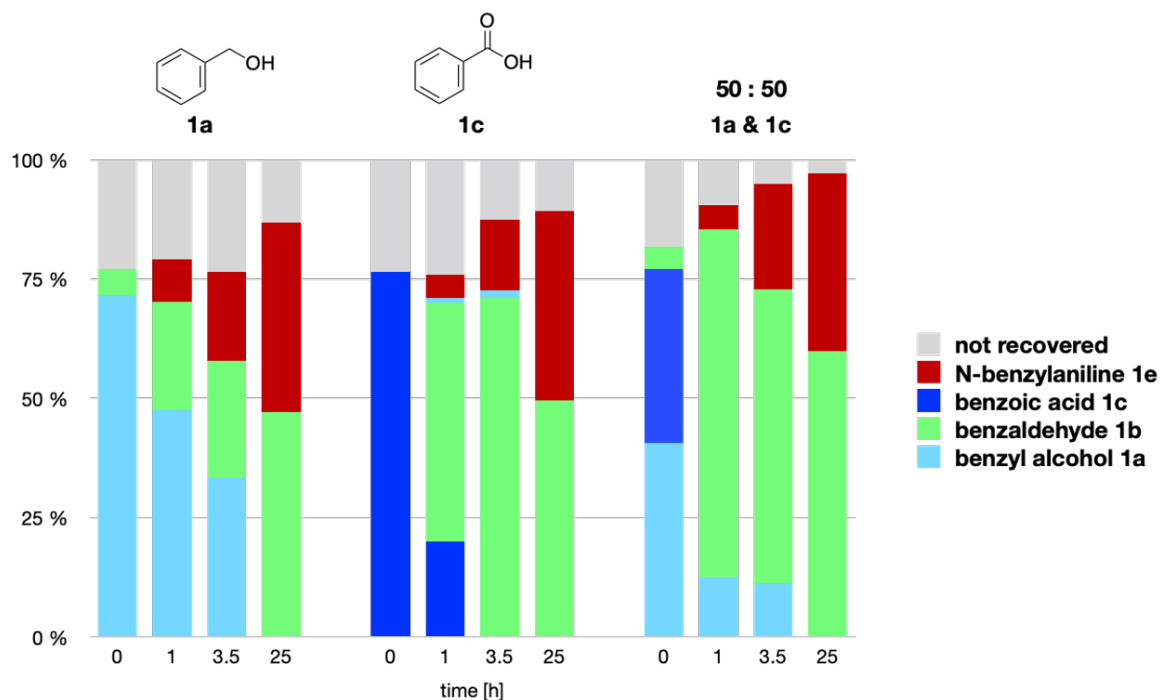


Figure 51: Conversion of benzyl alcohol **1a** or benzoic acid **1c** to benzaldehyde **1b** by *AlkJ* or *CAR_{Ni}* respectively and subsequent reaction with aniline to *N*-benzylaniline **1e** by *PIR23*. Mean values of biological duplicates were analysed by calibrated GC/FID. The relative concentration of components over time is shown.

To expand the substrate scope, the biocatalytic maxi-pathway was tested with two other alcohols, the corresponding acids and a 50:50 mixture of alcohol and acid as starting material (**2a/2c** and **3a/3c**). Conversion to the aldehydes **2b** and **3b**, however, the only formation of the imines, but no reduction to the corresponding secondary amines was observed. Moreover, three other amines (**2d**, **6** and **8**) for reductive amination were tested (see Table 2). Again, only the formation of the imines was observed, but not the reduction to the corresponding secondary amines. Employing amine **8**, traces of the desired product **1j** were formed. A reason to explain this could be that imine reductase *PIR23* only poorly accepts these rather bulky imines. Interestingly, with **2d** and **6** the imines were formed only temporarily and disappeared after approximately 3 hours. Previously, it was shown that *PIR23* accepts the imine formed by **1b** and **6**, yielding **1h** (see Chapter 7.3.3, Figure 26). Therefore, the failure to accept the imine when co-produced with all other cascade enzymes and the disappearance of the imine could not be explained.

7.6.4 Discussion

Co-production of all pathway enzymes was confirmed in *E. coli* BL21 (DE3) cells co-transformed with the newly assembled plasmid and a 2nd plasmid containing *CAR_{Ni}* and supplemental *PPTase_{EC}*. While all engineered strains successfully expressed *alkj* and the respective gene of interest in the 1-plasmid system, the gene expression from two plasmids after co-transformation imposed some difficulties. Although colony PCR confirmed the plasmid uptake in all clones, some clones showed low/now expression. In other words, transformed clones were not equivalent concerning their ability to produce active protein. This phenomenon was not observed after co-transformation of pKA1_alkj::vflh6 with pETDuet1_pptase_{EC}::car_{Ni}, but in the other two systems after co-transformation of pKA1_alkj::pdc_{Ap_mutant}/ pKA1_alkj::pir23 with pETDuet1_pptase_{EC}::car_{Ni} respectively. Ways to explain this heterogeneity in protein expression could be plasmid loss/low copy number of plasmids due to defects in machinery for the replication of plasmids (copy number control mechanism) or partitioning effects. As a result, the plasmid-free cells would outcompete the plasmid-containing cells, as the plasmid-free cells do not have to expend as much metabolic energy for plasmid maintenance [84]. However, other possible reasons could be insufficient transcription or translation in the respective clone due to defects in the transcription/translation machinery, which could be caused by the plasmid-related metabolic burden impeding host growth and metabolism [85].

The maxi-pathways were validated by using alcohol **1a**, acid **1c** or a 50:50 mixture as starting material. The formation of carboxylic acids could be completely prevented by the introduction of *CAR_{Ni}* in the 2-plasmid system. While the maxi-pathway employing ω -transaminases *VflH6* as the final enzyme showed good conversions to the final amine products (**1d-3d**) and acceptance towards a range of substrates (**1a-3a**), the maxi-pathways employing enzymes *PDC_{Ap_mutant}* and *PIR23* showed only moderate conversions to the respective final products (**1g** or **1e**, see Table 3). This can be explained by previously mentioned poor expression (*PDC_{Ap_mutant}*) or enzyme activity (*PIR23*). Attempts to expand the substrate scope of the maxi-pathway employing enzyme *PIR23* showed no or only poor results.

When comparing the strains harbouring two plasmids to the ones harbouring only one plasmid, activities of the enzymes *PDC_{Ap_mutant}* and *PIR23* and thereby product formation decreased probably due to reduced/unbalanced enzyme production (see Table 3). This could potentially be improved by further engineering of the strains through balancing of gene expression by *e.g.* either different genetic configurations, the use of different promoter/RBS systems or a different expression vector [11, 21, 86]. Finally, the cytotoxicity of aldehydes remains a major obstacle for biotransformations in resting cells. All in all, the enzymatic background was able to reduce the reactive aldehyde species better in the 1-plasmid system than in the 2-plasmid system. This indicates that the 2-plasmid system probably is less viable than the less burdened strain overproducing only two enzymes from one plasmid.

Table 3: Yields of Final Cascade Products Obtained in Biocatalytic Mini- and Maxi-Pathways

	System ^a	Co-expressed Enzymes	Final product	Yield [%] ^d	Byproduct alcohol & acid [%] ^d	Unreacted aldehyde [%] ^d
Pyruvate Decarboxylase <i>PDC_{AP}_mutant</i> ^b	mini-pathway	<i>AlkJ</i> & <i>PDC_{AP}_mutant</i>	1g	30	46	10
	maxi-pathway	<i>CAR_{Ni}</i> & <i>AlkJ</i> & <i>PDC_{AP}_mutant</i>	1g	16	12	52
ω-Transaminase <i>VfIH6</i> ^c	mini-pathway	<i>AlkJ</i> & <i>VfIH6</i>	1d	26	24	/
	mini-pathway	<i>AlkJ</i> & <i>VfIH6</i>	2d	54	/	/
	mini-pathway	<i>AlkJ</i> & <i>VfIH6</i>	3d	64	12	2
	maxi-pathway	<i>CAR_{Ni}</i> & <i>AlkJ</i> & <i>VfIH6</i>	1d	76	17	2
	maxi-pathway	<i>CAR_{Ni}</i> & <i>AlkJ</i> & <i>VfIH6</i>	2d	58	8	/
	maxi-pathway	<i>CAR_{Ni}</i> & <i>AlkJ</i> & <i>VfIH6</i>	3d	78	10	3
Imine Reductase <i>PIR23</i> ^b	mini-pathway	<i>AlkJ</i> & <i>PIR23</i>	1e	73	10	4
	maxi-pathway	<i>CAR_{Ni}</i> & <i>AlkJ</i> & <i>PIR23</i>	1e	40	/	47

^a *E. coli* BL21 (DE3) resting cells were used in all experiments

^b A biomass concentration of OD₅₉₀ = 30 was used

^c A biomass concentration of OD₅₉₀ = 10 was used, 10 equivalents of L-alanine were employed as amine donor

^d observed after 24 h, according to calibrated GC/FID

8 Conclusion

To conclude, the applicability of the previously developed biocatalytic redox-equilibrium given by alcohol dehydrogenase *AlkJ* and carboxylic acid reductase *CAR_{Ni}* [33, 43] was expanded successfully by the incorporation of three new enzymes: pyruvate decarboxylase *PDC_{Ap_mutant}*, ω -transaminases *VfIH6* and imine reductase *PIR23* (see Figure 52). This enabled the synthesis of α -hydroxy ketones, primary and secondary amines in *E. coli* resting cells. For the success of the biocatalytic cascade reactions, many factors had to be taken into consideration and addressed. First, the genetic sequences of pathway enzymes had to be validated and if necessary, corrected. Then, appropriate biocatalysts had to be selected and their biocatalytic activity verified. For the combination of all pathway enzymes in one cell, the genes of interest were combined via molecular cloning and co-transformation of two plasmids. Even though simultaneous co-production of all pathway enzymes in the 2-plasmid system presented some difficulties, a successful co-production of all pathway enzymes was achieved. However, the amount of protein production was variable among the different enzymes. The three new biocatalytic cascades were verified by the successful formation of the final cascade products. The intact biocatalytic redox equilibrium was confirmed by employing either the alcohol or the carboxylic acid starting material for the cascade reaction. In the cascade employing ω -transaminases *VfIH6* as final biocatalyst, best yields of the final cascade product and acceptance of three different substrates could be demonstrated, whereas the cascades with *PDC_{Ap_mutant}* or *PIR23* as final biocatalyst showed moderate yields of the final products. This can be explained by rather low/unbalanced enzyme production in the case of *PDC_{Ap_mutant}* or rather low enzyme activity in the case of *PIR23*. However, this problem could potentially be tackled by various possible changes/adjustments in the expression system [11, 21, 86].

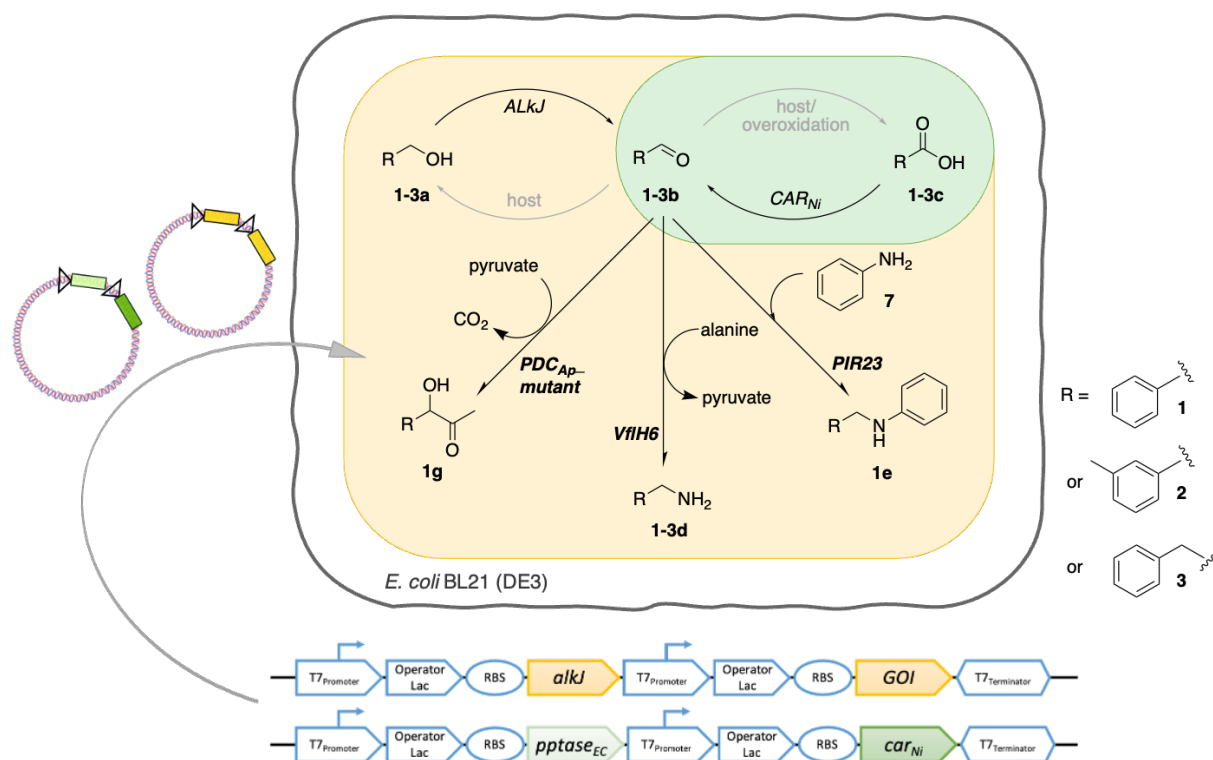


Figure 52: Synthetic pathways developed in this thesis. The biocatalytic aldehyde reservoir by *AlkJ* and *CAR_{Ni}* was expanded and three new enzymatic cascades were developed by incorporation of three new enzymes: pyruvate decarboxylase (*PDC_{Ap_mutant}*), ω -transaminase (*VfIH6*) or imine reductase (*PIR23*). A two-plasmid approach was used for the co-expression of all pathway enzymes in the enzymatic cascades respectively. Genetic configurations (organisation in pseudo-operons) of the two plasmids are depicted.

9 Material and Methods - General Preparations

All glassware, media and other solutions which were used during the cultivation of *E. coli* were sterilized prior to use by autoclaving (220 °C until elevated pressure, then 120 °C, 20 min; WMF Pressure Cooker Cromargan Stainless Steel) or by filtration (sterile syringe filter, 0.2 µm cellulose acetate, Roth Rotilabo).

9.1 General Stock Solutions

Table 4: Antibiotic Stock Solutions^a

Antibiotic	Stock conc. [mg/ml]	Working conc. [µg/ml]
Ampicillin (Amp) in dH ₂ O	100	100 or 50
Chloramphenicol (Cam) in abs. EtOH	34	34
Kanamycin (Kan) in dH ₂ O	50	50

^a Solutions were sterilized by filtration and stored at – 20 °C.

Table 5: Compound Stock Solutions used in Biotransformations

Compound	Stock conc.
Alanine in Tris-HCl buffer or RCM	1 M
Sodium pyruvate in Tris-HCl buffer or RCM	100 mM
Benzaldehyde in organic solvent ^a	100 mM (ACN)/1 M (DMSO)
Benzoic acid in organic solvent	100 mM (ACN)/1 M (DMSO)
Benzyl alcohol in organic solvent	100 mM (ACN)/1 M (DMSO)
Benzylamine in organic solvent	100 mM (ACN)/1 M (DMSO)
Dibenzylamine in organic solvent	100 mM (ACN)
Cyclohexanone in organic solvent	100 mM (ACN)/200 mM or 1 M (DMSO)
N-Cyclohexylaniline	1 M (DMSO)
Acetophenone in organic solvent	100 mM (ACN)/1 M (DMSO)
1-Phenylethylamine in ACN/DMSO	100 mM (ACN)/1 M (DMSO)
2-Phenylethylamine in DMSO	1 M (DMSO)
2-Phenylethanal	1 M (DMSO)
2-Phenylacetaldehyde	1 M (DMSO)
2-Phenylacetic acid	1 M (DMSO)
m-tolylmethanol	1 M (DMSO)
m-tolualdehyde	1 M (DMSO)
m-toluic acid	1 M (DMSO)
m-tolylmethanamine	1 M (DMSO)
Phenylacetylcarbinol	1 M (DMSO)
Aniline	1 M (DMSO)
N-Benzylaniline	1 M (DMSO)
n-butylamine	1 M (DMSO)
N-Butylbenzylamine	1 M (DMSO)
N-Benzyl-2-phenylethylamine	1 M (DMSO)
4-Phenylcyclohexylamine	1 M (DMSO)
o-toluidine	1 M (DMSO)
Methyl benzoate	1 mM (EtOAc)

^a Solutions were kept at -20 °C

^b Solutions were kept at 4 °C

Table 6: Other Stock Solutions used in Biotransformations

Compound	Stock conc.
NADH disodium salt hydrate in respective buffer ^a	10 mM
NADP disodium salt	10 or 100 mM
Pyridoxal phosphate in respective buffer or RCM ^a	10 mM
Thiamine diphosphate in respective buffer or RCM ^a	10 mM
D-Glucose in respective buffer ^b	1 M
Magnesium sulfate respective buffer or RCM ^b	10 mM

^a Solutions were always prepared on the day of use and kept on ice.

^b Solutions were kept at -20 °C

Table 7: Other Stock Solutions

Compound	Stock conc.
IPTG in dH ₂ O	0.1 M
PMSF in abs. <i>i</i> PrOH	0.1 M

9.2 Standard Media and Buffer

Media were stored in the dark at rt or at 4 °C if stored for a longer period.

Table 8: Composition of Bacterial Media

LB-Miller medium (400 ml) ^a	TB medium (400 ml) ^b	10 x TB salts (1 l) ^c	2 x YT medium (400 ml) ^a	SOC medium (400 ml) ^d
4.0 g bacto-peptone	4.8 g bacto-tryptone	23.1 g KH ₂ PO ₄	6.4 g bacto-tryptone	8 g bacto-tryptone
2.0 g yeast extract	9.6 g yeast extract	168.5 g K ₂ HPO ₄ *3H ₂ O	4.0 g yeast extract	2 g yeast extract
4.0 g NaCl	40 ml 10 x TB salts		2.0 g NaCl	0.076 g KCl
				3.6 ml 40 % (w/v) glucose ^e
				4 ml 1 M MgCl ₂ ^e

^a Filled up to 400 ml dH₂O and autoclaved

^b Before the addition of 10 x TB salts, it was filled up to 360 ml dH₂O and autoclaved.

^c Filled up to 1 l dH₂O and autoclaved

^d Before the addition of glucose and MgCl₂, it was adjusted to pH 7, filled up to 392.4 ml and autoclaved.

^e Sterilized by filtration separately and added under sterile conditions

Table 9: Composition of LB-Agar Plates

LB-Agar (400 ml) ^a
4.0 g bacto-peptone
2.0 g yeast extract
4.0 g NaCl
6.0 g Agar No.1

^a Filled up to 400 ml dH₂O and autoclaved; after cooling down to approximately 50 °C, the respective antibiotic was added, and the plates were poured (in standard petri dishes, 94x16 mm).

Table 10: Composition of Bacterial Autinduction Medium (AIM)

LB-0.8G (400 ml) ^a	LB-5052 (400 ml) ^a	20 x NPS (400 ml) ^b	50 x 5052 (250 ml) ^c
4.0 g bacto-peptone	4.0 g bacto-peptone	26.4 g (NH ₄) ₂ SO ₄	62.5 g glycerol
2.0 g yeast extract	2.0 g yeast extract	54.4 g KH ₂ PO ₄	6.25 g glucose
4.0 g NaCl	4.0 g NaCl	56.8 g Na ₂ HPO ₄	25.0 g a-lactose
0.4 ml 1M MgSO ₄ ^d	0.4 ml 1M MgSO ₄ ^d		
8 ml 40 % (w/v) glucose ^e	8 ml 50 x 5052		
20 ml 20 x NPS	20 ml 20 x NPS		

^a After the addition of bacto-peptone, yeast extract and NaCl, it was filled up to 371.6 ml dH₂O and autoclaved.

^b Filled up to 400 ml dH₂O and autoclaved

^c Filled up to 250 ml dH₂O and sterilized by filtration

^d Autoclaved separately and added under sterile conditions

^e Sterilized by filtration separately and added under sterile conditions

Table 11: Composition of Resting Cell Medium (RCM)

RCM (400 ml)	10 x M9 salts (N-free, 100 ml) ^a
423 ml dH ₂ O ^a	0.5 g NaCl
50 ml 10 x M9 salts (N-free)	3.0 g KH ₂ PO ₄
1.5 ml 1M MgSO ₄	5.98 g Na ₂ HPO ₄
0.5 ml 1 M CaCl ₂ ^b	
25 ml 20 % (w/v) glucose ^c	

^a Filled up to 100 ml dH₂O and autoclaved

^b Autoclaved separately and added under sterile conditions

^c Sterilized by filtration separately and added under sterile conditions

Table 12: Composition of Diverse Buffers:

50 mM Tris-HCl (1 l, pH 7.5 or pH 9) ^a	100 mM Tris-HCl (200 ml, pH 8) ^a	100 mM Sodium phosphate buffer (50 ml, pH 7.5) ^d	50 mM Potassium phosphate buffer (50 ml, pH 7) ^e	50 x TAE buffer
6.057 g Trizma [®] base	2.4228 g Trizma [®] base	685.493 mg Na ₂ HPO ₄ · 2 H ₂ O in 38.5 ml dH ₂ O ^b	113.6 mg KH ₂ PO ₄	2 M Tris
		158.7 mg NaH ₂ PO ₄ · H ₂ O in 11.5 ml dH ₂ O ^c	290 mg K ₂ HPO ₄	5.71 % (v/v) acetic acid
				50 mM EDTA ^f

^a pH was adjusted with 2 M HCl

^b Dissolved in 50 ml dH₂O

^c Dissolved in 20 ml dH₂O

^d Na₂HPO₄ · 2 H₂O was mixed with NaH₂PO₄ · H₂O. The pH was adjusted to 7.5 with 2 M HCl or 3 M NaOH.

^e It was filled up to 30 ml, then pH adjusted to 7 and then filled up to 50 ml

^f From 0.5 M stock solution adjusted to pH 8

Table 13: Composition of Buffers for Preparation of RbCl Competent Cells

RF1 buffer (100 ml, pH 5.8) ^a	RF2 buffer (100 ml, pH 6.8) ^a
1.21 g RbCl	0.12 g RbCl
0.99 g MnCl ₂ · 2 H ₂ O	0.21 g MOPS
0.294 g KOAc	0.11 g CaCl ₂ · 2 H ₂ O
0.148 g CaCl ₂ · 2 H ₂ O	15 g glycerol
15 g glycerol	

^a pH was adjusted by addition of 0.2 M acetic acid or 1 M NaOH and it was sterilized by filtration.

Table 14: Composition of Reagents for SDS-PAGE

30 % (w/v) Acrylamide (100 ml)	10 % (w/v) APS (10 ml)
29.2 g acrylamide	1 g APS
0.80 g N',N'-bis-methylene acrylamide	

^a After dissolving in 100 ml dH₂O, the solution was filtered into a container with dark glass and kept in the dark at 4 °C.

^c Dissolved in dH₂O, dispensed in 1 ml aliquots and stored at -20 °C

Table 15: Composition of Buffers for SDS-PAGE

10 x SDS running buffer (1l)	Resolving Gel Buffer (250 ml, pH 8.8) ^a	Stacking Gel Buffer (50 ml, pH 6.8) ^a	Sample Buffer ^b
30.3 g Trizma [®] base	46.2 g Tris (1.5 M)	15.15 g Tris (0.5 M)	7.3 ml dH ₂ O
144 g glycine	10 ml 10 % (w/v) SDS stock	10 ml 10 % (w/v) SDS stock	2.5 ml stacking gel buffer
10 g SDS			5 ml glycerol
			4 ml 10 % (w/v) SDS
			0.2 ml 1 % (w/v) bromphenol blue
			1 ml β-mercapto ethanol

^a After the addition of SDS, it was filled up to approximately 200 ml and the pH adjusted with 2 M or concentrated HCl. Then, it was filled up to 250 ml and solutions were sterilized.

^b Stored at 4 °C

10 Material and Methods - General Procedures

10.1 Cultivation of Bacteria

10.1.1 Overnight Culture

There was picked a colony from a LB-agar plate (using a pipette tip) and grown in 10 ml LB-Miller medium in a 50 ml falcon tube (supplemented with respective antibiotic). The lid was not closed completely and fixed to the tube with adhesive tape. It was incubated at 37 °C for 12-24 h (180 rpm; InforsHT Multitron Standard).

10.1.2 Preparation of Cryostocks

For each *E. coli* strain cryostocks were prepared and stored at -80 °C. Therefore, 0.5 ml 60 % (v/v) glycerol + 0.5 ml overnight culture were combined and stored in a cryogenic vial.

10.1.3 Cultivation on LB-agar Plates (Recovery of Bacteria from Cryostock)

While keeping cryostocks on ice, there was used a pipette tip to take up some cell material and streak it on a LB-agar plate (with the respective antibiotic). The plates were incubated upside down at 37 °C (INCULINE VWR) for 12-24 h. Plates were stored in the dark at 4 °C and propagated approximately every six weeks onto new LB-agar plates.

10.2 Preparation Chemically Competent *E. coli* Cells

All steps were carried out on ice and under sterile conditions if applicable. A single colony of the respective *E. coli* strain was incubated in 4 ml LB-Miller medium at 37 °C with shaking (200 rpm, InforsHT Multitron Standard) for approximately 12 h. A LB-Miller main culture (100 ml) was inoculated with 1 % (v/v) of the overnight culture (1 ml) and grown to an OD₅₉₀ of approximately 0.35.

Preparation of CaCl ₂ competent cells	Preparation of RbCl competent cells for storage
The culture was divided into 3 ml aliquots in Eppendorf tubes and centrifuged (2 292 x g, 4 °C, 10 min, Sigma Laboratory Centrifuge 3K15). The supernatant was discarded and cells were resuspended in 0.5 ml ice-cold 0.1 M CaCl ₂ . Cells were incubated for 15 min, centrifuged and resuspended in 0.1 ml ice-cold 0.1 M CaCl ₂ .	Cells were harvested by centrifugation (4000 x g, 4 °C, 10 min, Sigma Laboratory Centrifuge 6K15 or 3K30) and resuspended in 20 ml RF1 buffer (1/5 volume of the main culture). Cells were incubated for 15 min, centrifuged, and resuspended in 4 ml RF2 buffer (1/5 volume of the RF1 suspension). Cells were divided into 100 µl aliquots (1.5 ml Eppendorf tubes), snap frozen in liquid nitrogen and stored at -80 °C.

10.3 Transformation of Chemically Competent Cells

1 μ l of plasmid DNA (with a concentration of 50–100 ng/ μ l) or 5 μ l of KLD mix were added to 100 μ l of RbCl or CaCl₂ competent cells. Cells were incubated on ice for 1 h. The heat shock was performed at 42 °C for 30 seconds or 1 minute (Biometra TS1 Thermoshaker Analytik Jena) and cells were put on ice for 2 min. 0.5 ml prewarmed SOC medium were added for recovery and cells were incubated at 37 °C with shaking (650 rpm, Biometra TS1 Thermoshaker Analytik Jena) for 1 h. Subsequently, 50 μ l were plated on one half of a pre-warmed LB agar plate supplemented with the appropriate antibiotic and the rest was centrifuged (7000 rpm, 1 min). The supernatant was discarded, cells were resuspended and plated on the other half of the plate. Plates were incubated upside down at 37 °C for 12–24 h (INCU-line VWR). For co-transformations of two plasmids, the concentrations of the respective antibiotics in the LB agar plate were reduced to half.

10.4 Plasmid DNA Isolation and Quantification

The GeneJET Plasmid Miniprep Kit by Thermo Scientific was used following enclosed instructions. 7.6 ml of a respective overnight culture were pelleted in four centrifugation steps (16162 x g, 1 min, Sigma Tabletop Centrifuge 1-14) in 2 ml Eppendorf tubes. The pellets were resuspended in 250 μ l of Resuspension Solution (stored at 4 °C) by vortexing and pipetting. 250 μ l of Lysis Solution were added, it was mixed by inverting 4-6 times and incubated for 5 minutes. 350 μ l of Neutralization Solution were added, it was mixed by inverting 4-6 times and subsequently centrifuged (16162 x g, 10 min). Afterwards, the supernatant was transferred to a GeneJET spin column by decanting or pipetting with caution. The column was centrifuged (16162 x g, 1 min) and the flow-through discarded. Two consecutive washing steps with 500 μ l of wash solution, (16162 x g, 1 min) were performed. The flow-through was discarded and the empty column was centrifuged (16162 x g, 2 min). The column was transferred into a clean 2 ml Eppendorf tube and placed into a heat block (approximately 50 °C, Grant Instruments BTA Dry Block Heating System) for evaporation of residual EtOH. Pre-warmed 35 μ l nuclease-free water was added to the center of the purification column, it was incubated for at least 5 minutes and it was centrifuged (16162 x g, 2 min). The purified plasmid-DNA was quantified by NanoDrop (NanoDrop™ OneC Microvolume UV-Vis Spectrophotometer, Thermo Scientific) in the measurement mode “dsDNA” using 1.5 μ l of the sample. Afterwards, the purification columns were discarded and the samples were stored at -20 °C.

10.4.1 Verification of DNA by Sequencing (Plasmid Template)

Samples were prepared for sequencing (480 – 1200 ng DNA in 12 μ l, + 3 μ l sequencing primer = 15 μ l in total). Primers were added immediately from 10 μ M stock solutions or chosen from a standard primer list.

10.5 Dilution of Primers

Primers (obtained from Sigma-Aldrich) were centrifuged at max. speed 1 minute and diluted in nuclease-free water for 100 μ M. After vortexing, they were diluted in nuclease-free water for 10 μ M and stored at -20 °C.

10.6 Colony PCR

For colony PCR, Opti Taq DNA Polymerase was used (5 U/ μ l, OptiTaq DNA Polymerase EURx). The following PCR reaction mix was prepared on ice:

Table 16: Colony PCR Reaction Mix

Component	Amount [μ l]
Primer <i>fwd</i> (10 μ M)	0.125
Primer <i>rev</i> (10 μ M)	0.125
10 x Buffer C (EURx)	0.5
MgCl ₂ (25 mM)	0.2
DMSO	0.1
dNTP mix (2 mM)	0.5
Nuclease-free water	3.4
Opti Taq DNA Polymerase 5 U/ μ l	0.05

After adding the polymerase, 5 μ l of the master mix were aliquoted into pre-cooled PCR tubes. Usually, five colonies were picked with a 10 μ l pipette tip from an agar plate. Each clone was streaked onto a separate agar plate for later use. Then, the pipette tip was put into the PCR tube containing the master mix, incubated for at least 10 seconds and pipetted up and down. As positive controls, there were done PCR reactions of one colony of a previously verified plasmid and of a purified plasmid (diluted to approximately 1 ng/ μ l). The PCR samples were spun down and the PCR program performed under the following temperature conditions (Biometra TAdvanced Twin Analytik Jena):

Table 17: Temperature Program

PCR Step	Temperature [$^{\circ}$ C]	Time	Number of Cycles
Initial Denaturation	95	5 minutes	1
Denaturation	95	30 seconds	
Annealing	50-72 ^a	30 seconds	30
Extension	72	1min/kb	
Final Extension	72	7 minutes	1
Hold	4	indefinite	

^a 5 $^{\circ}$ C below melting temperature of the primer with the lowest melting temperature

The PCR reactions were analysed on a 1 % (w/v) agarose gel as described in Chapter 10.7.

10.7 Gel Electrophoresis

If not noted otherwise, 1 % (m/V) agarose gel was prepared. 1.80 g (or 0.80 g) agarose were resolved in 180 ml (or 80 ml) TAE buffer for approximately 5 min in the microwave. 18 μ l (or 8 μ l) SYBR Safe gel stain (SYBR[®] Safe DNA gel stain; S33102, Thermo Scientific) were added and the gel was poured. The electrophoresis chamber was filled with TAE buffer, the gel was positioned and loaded. Therefore, the DNA containing mixture was previously combined 5:1 with purple 6 x Purple DNA gel loading dye (B7024S, NEB). Samples from colony PCR were loaded directly, without the addition of purple DNA gel loading dye. 6 μ l DNA marker (GeneRuler[™] 1 kb DNA Ladder; SM01313, Thermo Scientific) were loaded. The electrophoresis was run at 120 V for 30-45 min. For preparative purposes, the gel electrophoresis was run at 90 V for 70-90 min. A picture was made visualizing DNA fragments in UV light (UVP UVsolo touch, Analytik Jena).

10.8 NEBuilder® HiFi DNA Assembly

10.8.1 Primer Design

The online NEBuilder assembly tool from New England Biolabs Inc. (<https://nebuilder.neb.com/#!/>) was used to assemble the desired plasmid harbouring the target gene *in silico*. Primer pairs for amplification of the backbone as well as the target insert were chosen using previous work as an example [43]. Moreover, primers were chosen to have approximately 20 bp annealing to the DNA sequencing to be amplified and to have more than 30 bp overlapping overhangs for DNA assembly. Primers had terminal GC pairs and the GC content was kept below 60 %. All used primers are summarized in Table 42, Chapter 12.2.

10.8.2 PCR Amplification of Target DNA Fragments

Target inserts and backbone were both generated by PCR using Q5 High-Fidelity DNA Polymerase (M0491, NEB). Recommendations from NEB (<https://international.neb.com/protocols/2013/12/13/pcr-using-q5-high-fidelity-dna-polymerase-m0491>) were followed. The following reaction mix was prepared on ice:

Table 18: PCR Reaction Mix (50 µl volume)

Component	Amount [µl]	Final Concentration
Primer <i>fwd</i> (10 µM)	2.5 µl	0.5 µM
10 µM Primer <i>rev</i> (10 µM)	2.5 µl	0.5 µM
Template DNA (~1 ng/µl)	1 µl	~1 ng/50 µl
dNTP mix (2 mM)	5 µl	200 µM
Nuclease-free water	28.5 µl/18.5 µl	-
5 x Q5 Reaction Buffer	10 µl	1 x
Q5 High-Fidelity DNA Polymerase (2 U/µl)	0.5 µl	0.02 U/µl
Optional: 5X Q5 High GC Enhancer ^a	10 µl	1 x

^a Q5 High GC Enhancer was used for the amplification of backbone as it can improve reaction performance of difficult targets, like GC-rich templates or those with secondary structures.

After adding Q5 High-Fidelity DNA Polymerase to the reaction mix, 44 µl were aliquoted into pre-cooled PCR tubes. The PCR samples were spun down and the PCR program was performed under the following temperature conditions (Biometra TAdvanced Twin Analytik Jena):

Table 19: Temperature Program

PCR Step	Temperature [°C]	Time	Number of Cycles
Initial Denaturation	98 °C	30 seconds	1
Denaturation	98 °C	10 seconds	
Annealing	T _{a1} 50-72 °C ^a	30 seconds	10
Extension	72 °C	30-45 seconds/kb ^b	
Denaturation	98 °C	10 seconds	
Annealing	T _{a2} 50-72 °C ^a	30 seconds	20
Extension	72 °C	30-45 seconds/kb ^b	
Final Extension	72 °C	2 minutes	1
Hold	4 °C		1

^a Annealing temperature was calculated according to NEB Tm calculator (<https://tmcalsculator.neb.com/#!/main>)

^b 30 seconds were used for the amplification of target inserts and 45 seconds were used for the amplification of backbone

The PCR reactions were analysed on a 1% (w/v) agarose gel as described in Chapter 10.7.

10.8.3 Gel Purification of PCR Amplified DNA Fragments

The target DNA band was visualized by exposure to UV light (UV Transilluminator 2000 Bio-Rad) and excised. For purification the GeneJET gel extraction kit from Thermo Scientific) was used following enclosed instructions. An equal volume of binding buffer was added to the gel slices and the resulting gel mixtures were incubated at 50 °C for 10 minutes until the gel was dissolved. The solubilized gel solution was transferred to the GeneJET purification column, centrifuged (16162 x g, 1 min, Sigma Tabletop Centrifuge 1-14) and the flow-through discarded. An additional binding step (application of 100 µl additional binding buffer to the column and centrifugation) was done if the purified DNA subsequently was used for sequencing. Two consecutive washing steps with 700 µl and 500 µl of wash solution, (16162 x g, 1 min) were performed. The flow-through was discarded and the empty column was centrifuged (16162 x g, 2 min). The column was transferred into a clean 1.5 ml Eppendorf tube and placed into a heat block (approximately 50 °C, Grant Instruments BTA Dry Block Heating System) for evaporation of residual EtOH. Pre-warmed 35 µl nuclease-free water was added to the center of the purification column, it was incubated for at 10 min and it was centrifuged (16162 x g, 2 min). The purified plasmid-DNA was quantified by NanoDrop® (NanoDrop™ OneC Microvolume UV-Vis Spectrophotometer, Thermo Scientific) in the measurement mode “dsDNA” using 1.5 µl of the sample. Afterwards, the purification columns were discarded and the samples were stored at -20 °C.

10.8.4 Assembly

For the assembly of backbone with the target insert, recommendations from NEBuilder HiFi DNA assembly reaction protocol (<https://international.neb.com/protocols/2014/11/26/nebuilder-hifi-dna-assembly-reaction-protocol>) were followed. The amount of backbone was set to 100 ng and the molar ratio 1:10 backbone to insert resulted in the best assembly efficiency. DNA containing solutions were diluted for better pipetting if necessary and the following mix was prepared:

Table 20: Assembly Reaction Mix

Component	Amount
Backbone DNA	100 ng = 0.02 pmol
Target insert DNA	0.2 pmol
Nuclease-free water	fill up to 10 µl
NEBuilder HiFi DNA assembly master mix	10 µl

The assembly reaction mix was prepared in pre-cooled PCR tubes. If necessary, there was also prepared a positive control:

Table 21: Positive Control Reaction Mix

Component	Amount
NEBuilder positive control	10 µl
NEBuilder HiFi DNA assembly master mix	10 µl

For best assembly efficiency, samples were incubated at 50 °C in the thermocycler (Biometra TAdvanced Twin Analytik Jena) for 3 hours.

10.8.5 Chemical Transformation

10 µl of the assembly reaction mix were used directly for the transformation in chemically competent *E. coli* Top 10 cells as described in Chapter 10.3.

10.8.6 Verification by Colony PCR

5 transformants from each plate were picked and amplification of the insert DNA was analysed by colony PCR and subsequent gel electrophoresis as described in Chapters 10.6 and 10.7.

10.8.7 Plasmid DNA isolation and Verification by Sequencing

The plasmid DNA of positive clones was isolated from the corresponding colonies and verified by sequencing as described in Chapter 10.4.

10.9 Enzyme Expression in *E. coli*

10.9.1 Cultivation in LB-Miller and TB Media for Conventional Induction

A preculture of the respective *E. coli* strain was grown in 4 ml LB-Miller medium supplemented with appropriate antibiotic (37 °C, 200 rpm, InforsHT Multitron Standard) for 12-24 h. If not noted otherwise, the TB medium main culture (usually 50 ml in a 250 ml baffled shake flask) supplemented with appropriate antibiotic was inoculated with 1 % (v/v) of the preculture and grown (37 °C, 200 rpm) until a suitable OD₅₉₀ for induction (WPA colourwave, CO7500 Colorimeter). Protein production was performed for approximately 20 h.

10.9.2 Cultivation in Autoinduction Media

A preculture of the respective *E. coli* strain was grown in 12 ml LB-0.8G supplemented with appropriate antibiotic in a 50 ml falcon tube for approximately 16 h (37 °C, 275 rpm, InforsHT Multitron Standard). The LB-5052 medium main culture (usually 50 ml in a 250 ml baffled shake flask) supplemented with appropriate antibiotic was inoculated with 0.2 % (v/v) of the preculture and grown for 4 h (37 °C, 150 rpm). Protein production was performed for approximately 20 h (20 °C, 150 rpm).

10.9.3 Preparation of *E. coli* Cell-free Extracts (CFEs)

Cells were harvested from the main culture by centrifugation (6 000 x g, 4 °C, 15 min, Sigma Laboratory Centrifuge 6K15 or 3K30). Subsequently, the cell pellet was washed by resuspending in 1/10 volume of the main culture in 50 mM Tris-HCl buffer (pH 7.5) and centrifuging. Then, the pellet was either stored at -20 °C for later use or resuspended in 1/40 volume of the main culture in 50 mM Tris-HCl buffer (pH 7.5) if not noted otherwise. 0.1 mM PMSF was added to a final concentration of 0.1 µM before to cell lysis, which was conducted on ice by sonication (5 s/min pulse for 9 min, 40 % amplitude, TS106 probe, Bandelin Sonoplus HD4100). If necessary, the respective cofactors were also added prior to lysis. Cellular debris was pelleted by centrifugation (14 000 x g, 4 °C, 25 min). The insoluble fraction was resuspended in a sufficient volume of 50 mM Tris-HCl buffer (pH 7.5). Consequently, the total amount of protein was determined by Bradford assay for both the insoluble and the soluble fraction (CFE) before analysis by SDS-PAGE. CFEs were stored on ice for immediate use or kept at -20 °C for long time storage if possible.

10.9.4 Preparation of *E. coli* Resting Cells (RCs)

Cells were harvested from the main culture by centrifugation (6 000 x g, 4 °C, 15 min, Sigma Laboratory Centrifuge 6K15 or 3K30). The pellet was washed by resuspending in 1/10 volume of the main culture in

RCM and centrifuging. Then, the pellet was either stored at -20 °C for later use or resuspended in a sufficient volume of RCM until an OD₅₉₀ = 20.0 was reached. RCs were stored at 4 °C if necessary (changing the RCM once a day). Protein production was analysed by SDS-PAGE.

10.10 Bradford Assay for Determination of Protein Concentration

For the determination of the total protein concentration, the insoluble and soluble fractions were diluted with dH₂O (1:30 or 1:50). Therefore, 200 µl of 1:5-diluted Bradford reagent (Bio-Rad Protein Assay Dye Reagent Concentrate) were mixed with 5 µl of the diluted protein solutions in 96-well plates for 5 seconds (1350 rpm, Heidolph Titramax 1000) and incubated at rt for 15 min (protein solutions were pipetted first, and then the Bradford reagent was added quickly). All samples (including a dH₂O blank) were measured in triplicates. The absorbance was measured at 595 nm with a plate reader (Anthos Zenyth 3100) and the amount of protein was calculated by bovine serum albumin (BSA) calibration. The calibration was done for fresh Bradford reagents. In this regard, a dilution series of BSA (0-1 mg/ml) was prepared in 50 mM Tris-HCl buffer (pH 7.5) and measured in triplicates. An example BSA calibration is shown in Figure 53.

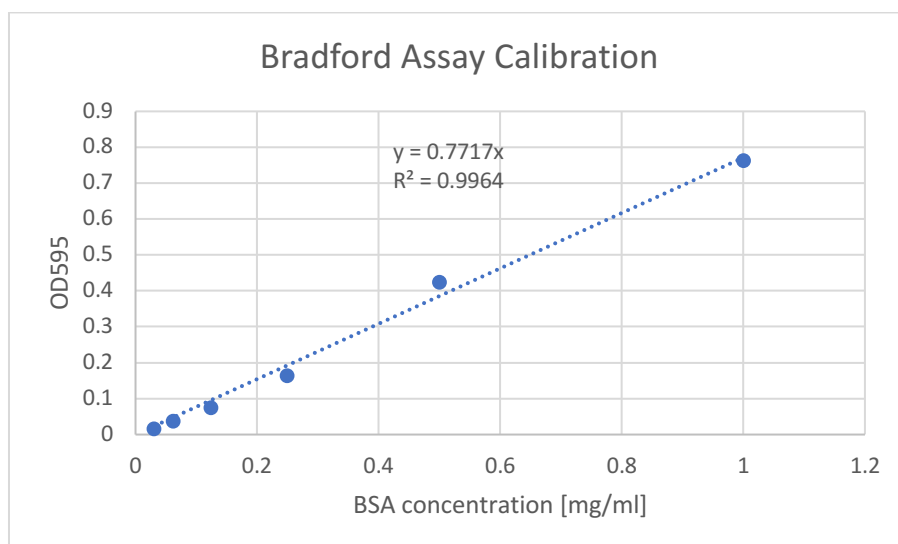


Figure 53: Bradford assay calibration. The calibration was performed with BSA (0-1 mg/ml) in 50 mM Tris-HCl buffer (pH 7.5).

10.11 Sodium Dodecylsulfate Polyacrylamide Gel Electrophoresis (SDS-PAGE)

12 % (w/v) polyacrylamide gels (0.75 mm or 1.5 mm thickness) were used for SDS-PAGE (the composition of resolving and stacking gel is summarized in Table 22).

Table 22: Preparation of Resolving and Stacking Gel

Resolving gel (12%) ^a	Stacking gel ^a
3.2 ml dH ₂ O	2.2 ml dH ₂ O
2.5 ml resolving gel buffer	1.3 ml stacking gel buffer
4.2 ml 30% (w/v) acrylamide ^b	0.50 ml 30% (w/v) acrylamide ^b
50 µl 10% (w/v) APS	30 µl bromphenolblue
8 µl TEMED	25 µl 10 % (w/v) APS
	8.0 µl TEMED

^a Amounts account for the preparation of two gels

^b Acrylamide was added with a sterile pipette

After addition of 10% (w/v) APS and TEMED the resolving gel was poured immediately (it was covered with *i*PrOH which was removed again before pouring of stacking gel). After 20 min the stacking gel was prepared and immediately added on top. The protein samples were denatured with SDS-PAGE sample buffer usually 1:1 (5 or 10 μ l sample + 5 or 10 μ l SDS-PAGE sample buffer) at 95 °C for 4 min before loading onto the gel. Whole cell samples (5 or 10 μ l RCs) were incubated with SDS-PAGE sample buffer (20 or 40 μ l) and denatured at 95 °C for 10 min. 5 or 10 μ l (depending on the thickness of the gel) of the respective denatured protein solution were loaded onto the gel. For comparison between different gels, sample loading was normalized to 10 μ g (0.75 mm thick gel) or 20 μ g (1.5 mm thick gel) protein per lane or samples from expressing cultures were normalized to OD₅₉₀ = 7.0. 5 μ l of prestained protein marker (PageRuler™ Prestained Protein Ladder 26616, Thermo Scientific) were loaded onto each gel. Gel electrophoresis was performed in 1 x SDS-PAGE running buffer at 80-120 V. Afterwards, gels were stained according to a microwave staining procedure. Therefore, the stacking gel was carefully removed. The resolving gels were covered with dH₂O and incubated at 750 W in the microwave for 1 min. The gels were slightly shaken at rt for 2 min (PSU-10i Orbital Shaking Platform, Grant-bio) and then covered in fresh dH₂O, incubated at 500 W for 1 min, and once more shaken at rt for 2 min. After discarding the dH₂O, the gels were covered in dyeing solution (Invitrogen™ SimplyBlue™ SafeStain, LC6065) and incubated at 350 W for 45 s. The gels were slightly shaken at rt for 5 min, the dyeing solution was removed and the gels were washed in dH₂O with shaking for at least 10 min. At last, the gels were preserved in dH₂O overnight or over the weekend. A picture was made for documentation. The gel was preserved in 20% (w/v) NaCl and a picture was made for documentation.

10.12 Biotransformations

Biotransformations were carried out in glass vials. Biotransformation products were analysed by calibrated GC/FID.

10.12.1 Standard Reaction Conditions for Biotransformations employing CFEs

Biotransformations employing CFEs usually were carried out in 1.0 ml containing 5 mg/ml CFE in Tris-HCl buffer (50 mM, pH 7.5) if not noted otherwise. The substrate was added last (from 100 mM stock solutions in ACN or 1 M stock solutions in DMSO) to a concentration of 4 mM or 8 mM (composition of biotransformation mix see Table 23). Therefore, the reaction mixture contained 0.8 - 5 % (v/v) organic solvent. Biotransformations were performed at 25 °C or 30 °C with shaking (250 rpm).

Table 23: Biotransformation Mix

Biotransformation mix (1.0 ml)	Amount	Final concentration
CFE (OD ₅₉₀ = 20)	variable	5 mg/ml
Substrate (100 mM) or Substrate (1 M)	40 μ l or 8 μ l	4 mM or 8 mM
Tris-HCl buffer (50 mM, pH 7.5)	variable	-
Optional		
Reactant	variable	variable
Cofactor(s)	variable	variable
Enzymes for cofactor recycling	variable	variable

10.12.2 Standard Reaction Conditions for Biotransformations using RCs

Biotransformations employing RCs usually were carried out at $OD_{590} = 10.0$ in 2.0 ml if not noted otherwise. The substrate was added last (from 100 mM stock solutions in ACN or 1 M stock solutions in DMSO) to a concentration of 5 or 8 mM (composition of biotransformation mix see Table 24). Therefore, the reaction mixture contained 0.8 - 5 % (v/v) organic solvent. Reactions were performed at 25 °C or 30 °C with shaking (250 rpm).

Table 24: Biotransformation Mix

Biotransformation mix (2.0 ml)	Amount	Final concentration
RCs ($OD_{590} = 20$)	1 ml	$OD_{590}=10$
Substrate (100 mM) or Substrate (1 M)	100 μ l or 16 μ l	5 mM or 8 mM
RCM	variable	-
Optional		
Reactant	variable	variable
Cofactor(s)	variable	variable

10.12.3 Analysis of Product Formation with Calibrated Gas Chromatography (GC)

For analysis by GC, 100 μ l or 200 μ l samples were taken at different time points and prepared for analysis. The first sample was taken directly after adding the substrate and mixing by inverting a few times. It was transferred into an Eppendorf tube, which already contained 1 mM methylbenzoate in EtOAc as internal standard (IS) and 10 μ l 2 M HCl (extraction protocol 1) or 10 μ l 3 M NaOH (extraction protocol 2). The sample was extracted by vortexing at maximal speed for 35 seconds (IKA® Vortex 4 basic) and centrifuging at maximal speed for 1 min. The organic layer (upper layer) was separated by pipetting into a new Eppendorf tube. Then, the sample was extracted a second time with 200 μ l 1 mM methylbenzoate (and 20 μ l 2 M HCl in case of extraction protocol 2). The organic layers were combined and dried over Na_2SO_4 . Samples were measured in a 1.5 ml GC vial using a 0.1 ml micro-insert after crimping with an aluminium cap with rubber septum. The injected sample volume was 1 μ l. Samples were usually taken immediately, 1 h, 2 h or 3 h, and 24 h after mixing.

10.12.4 Sample Preparation for Calibration by GC/FID

Calibration curves were generated for the respective compounds. Therefore, dilutions (0.125 - 4 mM) of the respective 1 M stock solutions were prepared in the respective reaction buffer or RCM and extraction in EtOAc (containing 1 mM methyl benzoate ad IS) was performed under same conditions as during reaction monitoring. GC methods and retention times of all compounds are summarized in table 25.

Table 25: Achiral GC/FID Methods

Name	Method	Compound	Retention time [min]	Extraction Protocol
6 min (Thermo Scientific Focus GC)	Initial temperature of 80 °C, hold 0.5 min, ramp 1 at 40 °C min ⁻¹ to 220 °C, ramp 2 at 80 °C min ⁻¹ to 300 °C, hold 1 min	1a	3.35	1
		1b	3.09	
		1c	3.82	
		1a	3.16	
		1b	2.84	
		1c	3.68	
		1d	3.09	
		1e	5.71	
		1f	-	
		1g	4.05	
		1h	4.36	
		1i	5.98	
		7 min (Thermo Scientific Trace Dual, Restek Rtx-5, 10250)	Initial temperature of 80 °C, hold 1 min, ramp at 40 °C min ⁻¹ to 280 °C, hold 1 min	
2a	3.55			
2b	3.24			
2c	4.03			
2d	3.49			
2e	-			
2f	4.10			
3a	3.61			
3b	3.36			
3c	4.08			
3d	3.55			
3e	-			
3f	-			
4a	3.35			
4b	3.25			
5a	2.48			
5b	-			
5c	5.24			
6	-			
7	3.36			
8	3.36			

11 Experimental

11.1 Enzyme Library

Characteristics and expression conditions for single enzymes in a respective *E. coli* strain are summarized in the following tables. Cultivation and expression were performed as described in Chapter 10.9 if not noted otherwise.

Table 26: Enzyme Characteristics

<i>Enzyme</i>	Enzyme Class	Primary host	Reference	Gene Size	Amino Acids	Experimental molecular Mass
<i>CAR_{Ni}</i>	Carboxylic Acid Reductase (CAR)	<i>Nocardia iowensis</i>	GenBank: AAR91681.1	3522 bp	1174	120 kDa
<i>PPtase_{Ec}</i>	Phosphopantetheinyl Transferase (PPtase)	<i>Escherichia coli</i>	GenBank: CAQ31055.1	627 bp	209	24 kDa
<i>AlkJ</i>	Alcohol Dehydrogenase (ADH)	<i>Pseudomonas putida</i>	GenBank: CAB54054.1	1674 bp	558	60 kDa
<i>PDC_{Ap}</i>	Pyruvate Decarboxylase	<i>Acetobacter pasteurianus</i>	Variant ApPDC_Pohl from Rother <i>et al.</i> [57]	1698 bp	566	60 kDa
<i>PDC_{Ap}_mutant</i>	Pyruvate Decarboxylase	<i>Acetobacter pasteurianus</i>	Not yet published variant from Dörte Rother <i>et al.</i>	1698 bp	566	60 kDa
<i>VfIH6</i>	ω -Transaminase	<i>Vibrio fluvialis</i>	GenBank: AEA39183.1	1359 bp	453	52 kDa
<i>AspFum</i>	ω -Transaminase	<i>Aspergillus fumigatus</i>	Genbank: EAL86783.1	969 bp	323	37 kDa
<i>AspTer</i>	ω -Transaminase	<i>Aspergillus terreus</i>	Genbank: EAU29472.1	975 bp	325	38 kDa
<i>AspRedAm</i>	Reductive Aminase	<i>Aspergillus oryzae</i>	Genbank: BAE66526.1	885 bp	295	31 kDa
<i>PIR13</i>	Imine Reductase	<i>Amycolatopsis regifaucium</i>	GenBank: KZB85949.1	873 bp	291	32 kDa
<i>PIR23</i>	Imine Reductase	<i>Cystobacter ferrugineus</i>	GenBank: OJH34016.1	873 bp	291	32 kDa

Table 27: Growth and Expression Conditions of all Enzymes

Enzyme	<i>E. coli</i> Strain	Vector/Selectable Marker	Expression Conditions					
			Inducer	Inducer Conc.	OD ₅₉₀ for Induction	Temp. [°C]	Rotational Speed [rpm]	Time [h]
<i>CAR_{Ni}</i> & <i>PPtase_{Ec}</i> ^a	BL21-Gold(DE3)	pETDuet-1/amp ^R	α-Lac	0.2 (w/v)	AIM	20	150	approximately 20
<i>AlkJ</i>	BL21(DE3)	pKA1/cam ^R	IPTG	0.5 mM	0.5	25	120	approximately 20
<i>PDC_{Ap}</i> ^b	BL21(DE3)	pET22b(+)/amp ^R	α-Lac	0.2 (w/v)	AIM	20	150	approximately 20
<i>PDC_{Ap} mutant</i> ^b	BL21(DE3)	pET22b(+)/amp ^R	α-Lac	0.2 (w/v)	AIM	20	150	approximately 20
<i>VfIH6</i> ^c	BL21(DE3)	pET24a/kan ^R	α-Lac	0.2 (w/v)	AIM	20	150	approximately 20
<i>AspFum</i> ^c	BL21(DE3)	pET22b(+)/amp ^R	α-Lac	0.2 (w/v)	AIM	20	150	approximately 20
<i>AspTer</i> ^c	BL21(DE3)	pGASTON/amp ^R	L-Rhm	0.2 (w/v)	0.7	20	200	approximately 20
<i>AspRedAm</i> ^d	BL21(DE3)	pET28a/kan ^R	α-Lac	0.2 (w/v)	AIM	20	150	approximately 20
<i>PIR13</i> ^d	BL21(DE3)	pET28b/kan ^R	α-Lac	0.2 (w/v)	AIM	20	150	approximately 20
<i>PIR23</i> ^d	BL21(DE3)	pET28b/kan ^R	α-Lac	0.2 (w/v)	AIM	20	150	approximately 20

^a Enzymes were always co-expressed.

^b Provided by Prof. Dörte Rother from the Forschungszentrum Jülich GmbH, Germany.

^c Provided by Prof. Uwe T. Bornscheuer from the University of Greifswald, Germany.

^d Provided by Prof. Nicholas Turner from the University of Manchester, United Kingdom.

11.2 Preliminary Verification of Correct Enzyme Sequences

In order to assure correct gene sequence of the enzymes of interest, all constructs were isolated and the correct enzyme sequence verified by sequencing using primers outlined in Table 28. Therefore, strains containing the constructs of interest were either recovered from *E. coli* BL21 (DE3) or *E. coli* BL21-Gold (DE3) cryostocks (as described in Chapter 10.1.3) or if obtained as isolated plasmid, it was transformed in the respective *E. coli* strain, then cultivated for plasmid preparation and prepared for sequencing (as described in Chapters 10.1.1 and 10.4).

Table 28: Sequencing Primers used for Verification of Enzyme Sequences

Construct	Primer
	tom1
pETDuet1_ <i>pptase_{EC}::car_{NI}</i>	tom2
	tom3
	tom4
	t7probis
pKA1_ <i>alkj</i>	t7terbis
pPOP	t7terbis
pET22b(+)_ <i>pdc_{Ap}</i>	t7probis
	t7terbis
pET22b(+)_ <i>pdc_{Ap}_mutant</i>	t7probis
	t7terbis
pET24a_ <i>vflh6</i>	t7probis
	t7terbis
pET22b(+)_ <i>aspfum</i>	t7probis
pGASTON_ <i>aspter</i>	pBADrev
pET28a_ <i>aspredam</i> ^a	t7probis
	t7terbis
pET28b_ <i>pir13</i>	t7probis
	t7terbis
pET28b_ <i>pir23</i>	t7probis
	t7terbis/t7term

A point mutation (deletion of one basepair) in the *alkj* gene sequence was detected in the constructs pKA1_*alkj* and pPOP (=pKA1_*alkj::fsa1-A129S*). This mutation had to be corrected prior to further construction of vectors for co-expression of enzymes as it causes a frameshift in the enzyme resulting in a protein sequence six amino acids (MIAVCM) shorter than the reported one [43] (see Chapter 7.1).

11.3 Correction of Mutation in *AlkJ* by Q5[®] Site-directed Mutagenesis

The correction of the mutation found in pKA1_*alkj* and pPOP was performed by Q5[®] site-directed mutagenesis (Q5[®] Site-Directed Mutagenesis Kit, New England Biolabs Inc.). Mutagenesis primers were designed by the online tool NEBaseChanger[®] (<https://nebasechanger.neb.com>). The following primers were used for Q5[®] site-directed mutagenesis:

plysu001: 5'-catgatagctgtctgcatg-3'

plysu002: 5'-Gccaactctagctctgcac-3'

Table 29: Mutagenesis Plan

Mutagenesis Reaction	Template	Amount (1-25 ng)	Fwd Primer	Rev Primer	Annealing T _m	length
pKA1_alkj_mutag2	pKA1_alkJ(TBA)	18.6 ng	plysu001	plysu002	61 °C	7200 bp
pPOP_mutag	pPOP	18.3 ng	plysu001	plysu002	61 °C	7950 bp

Step1: Exponential Amplification

The correction of the mutation was introduced in the first step of Q5® site-directed mutagenesis by exponentially amplifying the whole plasmid performing PCR using the respective mutagenesis primers.

Table 30: PCR Reaction Mix

Component	Volume (25 µl reaction)	Final Conc.
Q5 Hot Start High-Fidelity 2 x Master Mix	12.5 µl	1 x
10 µM fwd Primer	1.25 µl	0.5 µM
10 µM rev Primer	1.25 µl	0.5 µM
Template DNA (1-25 ng/µl)	1 µl	0.04-1 ng/µl
Nuclease-free water	9 µl	-

Table 31: Temperature Program

PCR Step	Temp.	Time (pKA1_alkj_mutag2)	Time (pPOP_mutag)	Number Of Cycles
Initial Denaturation	98 °C	30 seconds	30 seconds	1
Denaturation	98 °C	10 seconds	10 seconds	
Annealing	61 °C	30 seconds	30 seconds	25
Extension	72 °C	3 min 36 seconds	3 min 59 seconds	
Final Extension	72 °C	2 min	2 min	1
Hold	4 °C		∞	1

There was performed a gel electrophoresis of the mutagenesis reactions pKA1_alkj_mutag2 and pPOP_mutag in order to confirm the efficiency of the PCR (see Figure 1 in Chapter 7.1).

Step2: KLD Reaction

In the 2nd step, the KLD reaction, intramolecular ligation and template removal was performed in one step. It was incubated for 5 minutes at room temperature.

Table 32: Reaction Mix for the KLD Reaction

Component	Volume (10 µl reaction)	Final Conc.
PCR Product	1 µl	-
2x KLD Reaction Buffer	5 µl	1 x
10X KLD Enzyme Mix	1 µl	1 x
Nuclease-free water	3 µl	-

Step 3: Transformation in E. coli BL21 (DE3)

Immediately after performing the reaction, 5 µl of KLD reaction mix were transformed in RbCl competent cells (as described in Chapter 10.3). In both cases (pKA1_alkj_mutag2 and pPOP_mutag) approximately 60 colonies were obtained. Two colonies were picked for the preparation of overnight cultures (as described in Chapter 10.1.1). After plasmid preparation (as described in Chapter 10.4) the successful correction of the mutation was confirmed by sequencing using following primers:

t7probis: 5'-tcccgcgaaattaatac-3'

t7terbis: 5'-aacccctcaagaccg-3'

Regarding pPOP_mutag only clone 2 showed correct alignment. Clone 1 did not show correct alignment. Overnight cultures of pKA1_alkj_mutag2 and pPOP_mutag_c2 were prepared for subsequent plasmid isolation, yielding a concentration of 163.7 ng/ μ l and 220.0 ng/ μ l respectively.

11.4 Characterizations of Single Enzymes

All single enzymes were already in suitable vectors for expression. *E. coli* strains harboring the respective vectors were cultivated according to standard cultivation conditions (by conventional induction as described in Chapter 10.9.1 or by autoinduction as described in Chapter 10.9.2) and protein content analysed by Bradford Assay and SDS-PAGE (as described in Chapters 10.10 and 10.11). Expression conditions are summarized in Table 27, Chapter 11.1. The CFE and RCs were prepared as described in Chapters 10.9.3 and 10.9.4. Standard reaction conditions for biotransformations using the CFE or RCs are described in Chapters 10.12.1 and 10.12.2. The reaction progress was monitored via calibrated GC as described in Chapter 10.12.3.

For comparison to background protein expression, the *E. coli* host strains (*E. coli* BL21 (DE3) and *E. coli* BL21-Gold (DE3)) were cultivated and the protein background analysed by SDS-PAGE (see Figure 54).

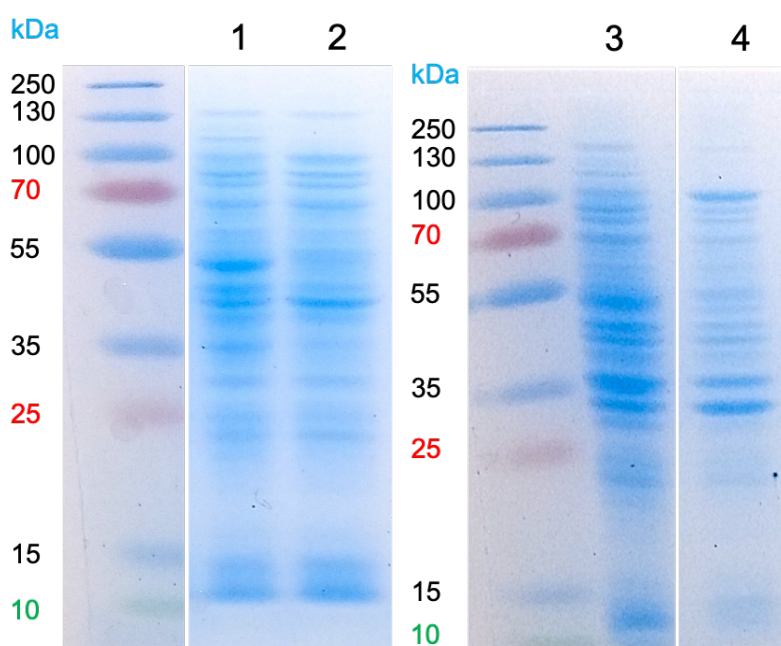


Figure 54: SDS-PAGE analysis of background protein expression in *E. coli* host strains. Background protein expression in *E. coli* BL21-Gold (DE3) in soluble (1) and insoluble (3) fractions and *E. coli* BL21 (DE3) in soluble (2) and insoluble (4) fractions. Sample loading was normalized to 10 μ g total protein per lane.

Conversion of Aldehydes by the Metabolic Background of *E. coli*

The reduction/oxidation of aldehydes by the host background was analysed. Mainly reducing activity of the enzymatic host background was verified by the conversion of 8 mM benzaldehyde, 2-phenylacetaldehyde and *m*-tolualdehyde respectively in RCs at 30 °C, 250 rpm. The reaction volume was 1 ml. After 25 h, 64 %, 13 % and 83 % conversion to the alcohols (1a, 2a and 3a respectively) and 3 % and 1 % conversion to the carboxylic acids (1a and 3a respectively) by the enzymatic background was observed (see Figure 18 in Chapter 7.2).

11.4.1 Characterization of Carboxylic Acid Reductase CAR_{Ni} for Reduction of Carboxylic Acids to Aldehydes

Enzyme Expression by Autoinduction

A preculture was started with the *E. coli* BL21-Gold (DE3) cells harbouring plasmid pETDuet1_*pptase_{Ec}::car_{Ni}*. Optimized enzyme production was performed following the protocol for cultivation in autoinduction media. The CFE and RCs were prepared. The enzyme CAR_{Ni} was mainly found in the soluble fraction according to SDS-PAGE (see Figure 55). The enzyme *Pptase_{Ec}* was not detectable by SDS-PAGE under experimental conditions as already reported in previous research [43].

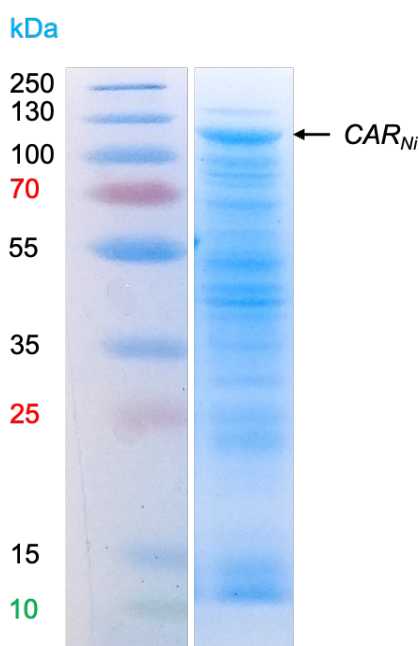


Figure 55: SDS-PAGE analysis of expression of CAR_{Ni} . CAR_{Ni} is visible in the soluble fraction with the expected size of 120 kDa. Sample loading was normalized to 10 μ g total protein per lane. Co-expressed *Pptase_{Ec}* was below detection limit under experimental conditions.

Verification of Biocatalytic Activity

Reducing activity of the enzyme was verified by the conversion of 5 mM benzoic acid **1c** to benzaldehyde **1b** and subsequently to benzyl alcohol **1a** in RCs at 25 °C, 250 rpm. Full conversion to **1a** was observed after 2 hours reaction time (see Figure 13 in Chapter 7.2).

11.4.2 Characterization of Alcohol Dehydrogenase *AlkJ* for Oxidation of Primary Alcohols to Aldehydes

Enzyme Expression by IPTG induction

A preculture was started with the *E. coli* BL21(DE3) cells harbouring plasmid pKA1_alkj_mutag2 which contained the correct *alkj* gene. Optimized enzyme production was performed following the protocol for conventional induction. The CFE and RCs were prepared. As *AlkJ* is a membrane-associated enzyme, it was mainly found in the insoluble fraction according to SDS-PAGE (see Figure 56).

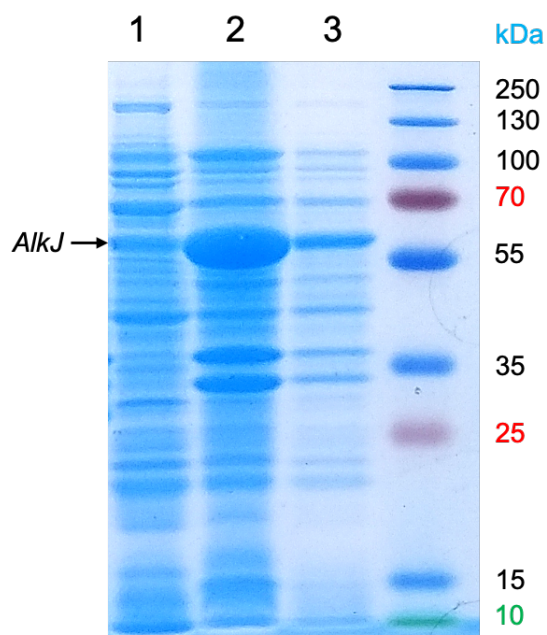


Figure 56: SDS-PAGE analysis of expression of *AlkJ*. *AlkJ* is partially visible in soluble (1), but mostly expressed in insoluble (2) fraction with the expected size of 60 kDa. Sample loading was normalized to 20 µg total protein per lane. Additionally, expressed *AlkJ* is shown in RCs (3).

Substrate Acceptance Screening

Oxidising activity of the enzyme was verified by the conversion of 8 mM alcohols in RCs at 25 °C, 250 rpm. The reaction volume was 1 ml. After 24 h, 49 %, 10 % and 82 % conversion to the aldehydes (**1b**, **2b** and **3b** respectively) and 12 % and 5 % conversion to the carboxylic acids (**1c** and **3c** respectively) was observed (see Figure 15 in Chapter 7.2).

11.4.3 Characterization of Alcohol Dehydrogenase *AlkJ-short* for Oxidation of Primary Alcohols to Aldehydes

Enzyme Expression by Autoinduction

A preculture was started with the *E. coli* BL21 (DE3) cells harbouring plasmid pKA1_alkj-short. Optimized enzyme production was performed following the protocol for cultivation in autoinduction. The CFE and RCs were prepared. The enzyme *AlkJ-short* was mainly found in the insoluble fraction according to SDS-PAGE (see Figure 57).

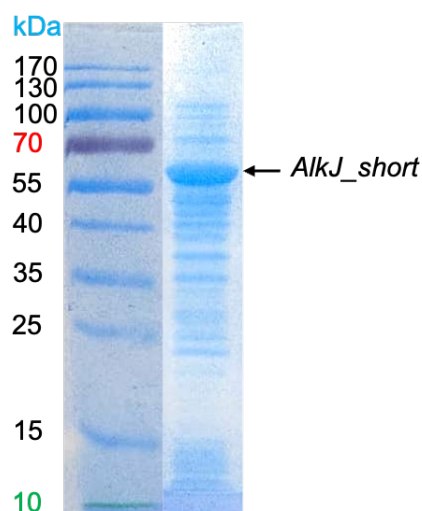


Figure 57: SDS-PAGE analysis of expression of *AlkJ-short*. Expressed *AlkJ-short* is shown in RCs.

Substrate Acceptance Screening

Oxidising activity of the enzyme was verified by the conversion of 8 mM alcohols **1a-3a** to aldehydes **1b-3b** in RCs at 25 °C, 180 rpm. The reaction volume was 1 ml. After 27 h, 56 %, 6 % and 41 % conversion to the aldehydes (**1b**, **2b** and **3b** respectively) and 10 %, 26 % and 46 % conversion to the carboxylic acids (**1c**, **2c** and **3c** respectively) was observed (see Figure 17 in Chapter 7.2).

11.4.4 Characterization of Pyruvate Decarboxylase PDC_{Ap} for C–C Bond Formation

Enzyme Expression by Autoinduction

A preculture was started with the *E. coli* BL21 (DE3) cells harbouring plasmid pET22b(+) $_{pdc_{Ap}}$. The preculture was grown in 20 ml LB-0.8G. Optimized enzyme production was performed following the protocol for cultivation in autoinduction media. The CFE was prepared. The cofactors $MgSO_4$ and ThDP were added to a final conc. of 2.5 mM and 0.1 mM respectively to the cell suspension prior to lysis by sonication in 50 mM potassium phosphate buffer (pH 7). The enzyme PDC_{Ap} was mainly found in the soluble fraction according to SDS-PAGE (see Figure 58).

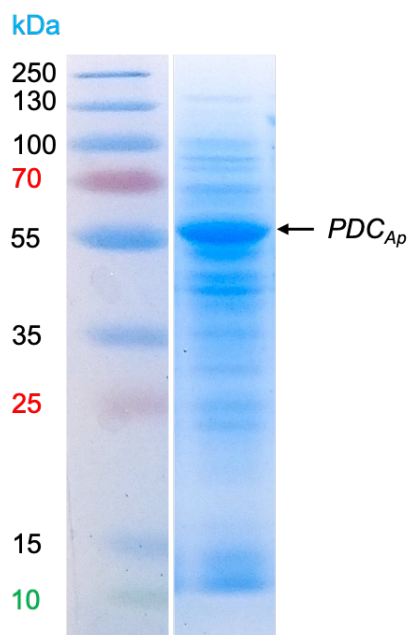


Figure 58: SDS-PAGE analysis of expression of PDC_{Ap} . PDC_{Ap} is visible in the soluble fraction with the expected size of 60 kDa. Sample loading was normalized to 10 μ g total protein per lane.

11.4.5 Characterization of Pyruvate Decarboxylase PDC_{Ap_mutant} for C–C Bond Formation

Enzyme Expression by Autoinduction

A preculture was started with the *E. coli* BL21 (DE3) cells harbouring plasmid pET22b(+) $_{pdc_{Ap_mutant}}$. The preculture was grown in 12 ml LB-0.8G. Optimized enzyme production was performed following the protocol for cultivation in autoinduction media. The CFE was prepared. The cofactors $MgSO_4$ and ThDP were added to a final conc. of 2.5 mM and 0.1 mM respectively to the cell suspension prior to lysis by sonication in 50 mM potassium phosphate buffer (pH 7). The enzyme PDC_{Ap_mutant} was mainly found in the soluble fraction according to SDS-PAGE (see Figure 59).

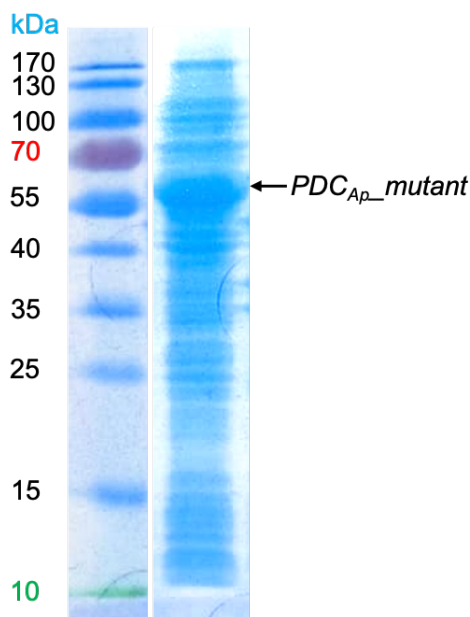


Figure 59: SDS-PAGE analysis of expression of *PDC_{Ap}_mutant*. *PDC_{Ap}_mutant* is visible in the soluble fraction with the expected size of 60 kDa. Sample loading was normalized to 10 µg total protein per lane.

Verification of Biocatalytic Activity

The carboligating activity of the enzyme was tested by the conversion of 8 mM benzaldehyde **1b** with 10 mM sodium pyruvate to phenylacetylcarbinol **1g** under the addition of 2.5 mM MgSO₄ and 0.1 mM ThDP in 50 mM potassium phosphate buffer (pH 7) using the CFE at 30 °C, 250 rpm. The reaction volume was 2 ml. After 3 h, 48 % conversion to **1g** was observed (see Figure 20 in Chapter 7.3.1).

Preparative Scale Biotransformation for the Isolation and Characterization of Phenylacetylcarbinol

With the aim to obtain pure Phenylacetylcarbinol **1g** as a reference material for GC calibration, the biotransformation was performed on a preparative scale. Therefore, benzaldehyde (0.72 mmol, 76.42 mg, 1 equivalent) were stirred with (0.90 mmol, 99 mg, 1.25 equivalents) sodium pyruvate under the addition of 2.5 mM MgSO₄ and 0.1 mM ThDP in 50 mM potassium phosphate buffer (pH 7) using the CFE at 30 °C, 250 rpm. The total reaction volume was 30.6 ml. After 22 h, there were added another 0.25 equivalents (0.18 mmol, 19.8 mg) sodium pyruvate and additional 500 µl CFE (47.6 mg/ml protein). After 42 h, 70 % conversion to **1g** was observed (see Figure 20 in Chapter 7.3.1). The biotransformation mixture was extracted three times with 25 ml EtOAc, dried with Na₂SO₄ and the solvent was removed by evaporation. The residue was dissolved in 5 ml Et₂O to remove traces of DMSO, washed with brine, dried with Na₂SO₄ and the solvent removed. Purification of the crude product (85.4 mg, yellow oil) by column chromatography (silica gel, 9:1 petroleum ether/ethyl acetate) yielded the product (0.43 mmol, 64.5 mg, 60 % yield) as a yellow oil. Spectroscopic data are according to literature [55].

¹H NMR (200 MHz, CDCl₃) δ 2.01 (3H, s, CH₃), 4.24 (1H, br, OH), 5.02 (1H, s, CHOH), 7.19-7.37 (5H, m, Ar-H); GCMS (EI, Thermo Scientific ISQ Series): [M/Z] calculated for C₉H₁₀O₂: 150.068, found: 150.064 (2.5 %) [M⁺], 107.048 (100 %), 79.063 (93 %)

11.4.6 Characterization of Different ω-Transaminases for C-N Formation (by Transamination)

Enzyme Expression by Autoinduction and L-Rhamnose Induction

Precultures were started with the *E. coli* BL21 (DE3) cells harbouring plasmids containing the genes of ω-transaminases (pET24a_ *vflh6*, pET22b(+)_ *aspfum* and pGASTON_ *aspter*). Optimized enzyme production was performed following the protocol for cultivation in autoinduction media (enzymes *VflH6* and *AspFum*)

and following the protocol for conventional induction (enzyme *AspTer*). The CFE was prepared. The cofactor PLP was added to a final concentration of 1 mM to the cell suspension prior to lysis by sonication. The enzymes *VfIH6*, *AspFum* and *AspTer* were found in both, the soluble and insoluble fraction according to SDS-PAGE (see Figure 60).

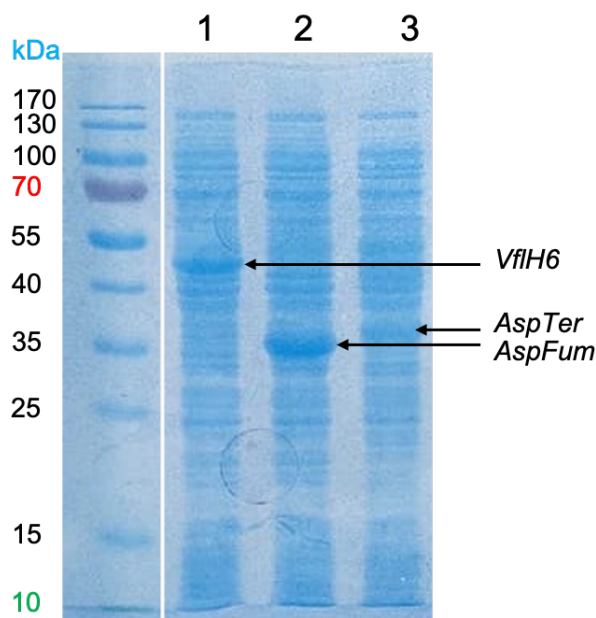


Figure 60: SDS-PAGE analysis of expression of *VfIH6*, *AspFum* and *AspTer*. Enzymes are visible in the soluble fractions: *VfIH6* with the expected size of 52 kDa (1), *AspFum* with the expected size of 37 kDa (2) and *AspTer* with the expected size of 38 kDa (3). Sample loading was normalized to 20 µg total protein per lane.

Verification of Biocatalytic Activity

The activity of the enzymes was tested by the conversion of 8 mM acetophenone **4a** with 160 mM L-alanine to 1-phenylethylamine **4b** under the addition of 0.1 mM PLP in potassium sodium buffer using the CFE with a protein concentration of 10 mg/ml at 30 °C, 250 rpm. Additionally, 90 U/ml *LDH* solution (520U/mg; 14 mg/ml solution), 2 mM NADH, 165 mM D-Glucose and 15 U/ml *GDH* (340 U/mg) were combined in order to consume emerging pyruvate and thereby push the reaction equilibrium to the product side [77]. After 24 h, 33 % (*VfIH6*), 15 % (*AspFum*) and 6 % (*AspTer*) conversion to **4b** was observed (see Figure 22 in Chapter 7.3.2).

11.4.7 Characterization of Reductive Aminase *AspRedAm* for C-N Formation (by Reductive Amination)

Enzyme Expression by Autoinduction

A preculture was started with the *E. coli* BL21 (DE3) cells harbouring the plasmid pET28a_*aspredam*. Optimized enzyme production was performed following the protocol for cultivation in autoinduction media. The CFE was prepared. The enzyme *AspRedAm* was found in the soluble and insoluble fraction according to SDS-PAGE (see Figure 61), but overall less expression was observed than usually.

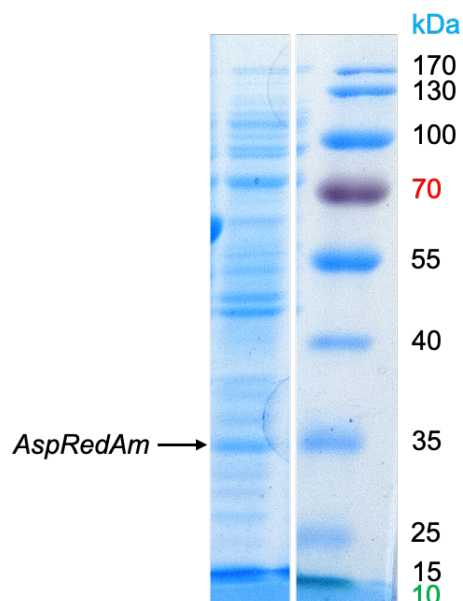


Figure 61: SDS-PAGE analysis of expression of *AspRedAm*. *AspRedAm* is visible in the soluble fraction with the expected size of 31 kDa. Sample loading was normalized to 20 μ g total protein per lane.

11.4.8 Characterization of Imine Reductases *PIR13* & *PIR23* for C-N Formation (by Reductive Amination)

Enzyme Expression by Autoinduction

Precultures were started with the *E. coli* BL21 (DE3) cells harbouring the plasmid pET28b_*pir13* and pET28b_*pir23* respectively. Optimized enzyme production was performed following the protocol for cultivation in autoinduction media. The CFE was prepared. The enzymes *PIR13* and *PIR23* were mainly found in the soluble fraction according to SDS-PAGE (see Figure 62).

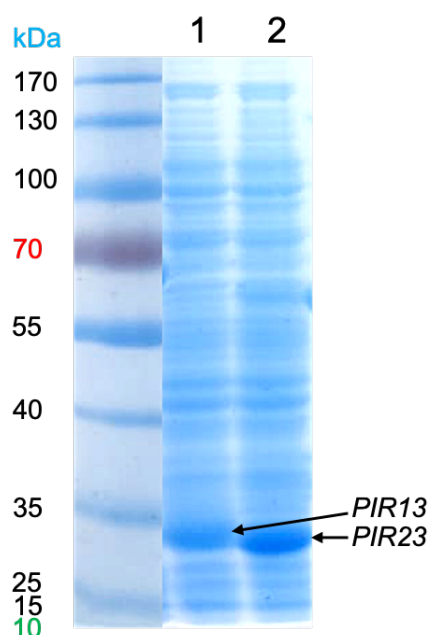


Figure 62: SDS-PAGE analysis of expression of *PIR13* and *PIR23*. *PIR13* (1) and *PIR23* (2) are visible in the soluble fraction with the expected size of 32 kDa. Sample loading was normalized to 10 μ g total protein per lane.

Verification of biocatalytic Activity

The reductive amination activity of the enzymes was tested by the conversion of 8 mM cyclohexanone **5a** with 16 mM aniline **7** to *N*-cyclohexylaniline **5c** under the addition of 0.5 mM NADP⁺, 40 mM D-Glucose and 30 U/ml *GDH* (340 U/mg) in 100 mM Tris-HCl (pH 8) using the CFE at 30 °C, 250 rpm. The reaction volume was 2 ml. After 24 h, 18 % (*PIR13*) and full conversion (*PIR23*) to **5c** was observed (see Figure 24 in Chapter 7.3.3).

Substrate Acceptance Screening

The substrate acceptance employing different amines was tested with the CFE of *PIR23*. Therefore, the conversion of 8 mM benzaldehyde **1b** with 16 mM 2-phenylethylamine **2d** or *n*-butylamine **6** under the addition of 0.5 mM NADP⁺, 40 mM D-Glucose and 30 U/ml *GDH* (340 U/mg) in 100 mM Tris-HCl (pH 8) was followed at 30 °C, 250 rpm. After 24 h, 18 % conversion to *N*-benzylbutan-1-amine **1h** and 1 % conversion to *N*-benzyl-2-phenylethan-1-amine **1i** was observed (see Figure 26 in Chapter 7.3.3).

11.5 Construction of Vectors for the Co-expression of Pathway Enzymes

For Co-production of *alkj* with target genes of interest, the vectors pKA1_alkj::GOI were constructed in pseudo-operon configuration. In the following, the cloning procedure is described.

11.5.1 Generation of Backbone1 for Assembly of

pKA1_alkj::pdc_{Ap}/pdc_{Ap}_mutant/vflh6/aspfum/aspredam/pir13/pir23

The backbone (7226 bp) was amplified by PCR, using previously corrected pKA1_alkj_mutag2 (see Chapter 11.3) as a template. Originally, the following primer pair was used:

plysu003: 5'-cgcgggatcggttagcagccGGATCCTTAC-3'

plysu004: 5'-cccgaaggaagctgagttgGCTGCTGC-3'

However, after several rounds of unsuccessful assemblies, the primers were adjusted to have 30 bp overlapping overhangs for DNA assembly instead of 20 bp.

Finally, the following primers were used for amplification of the backbone:

plysu014: 5'-gtattaatttcgcgggatcggttagcagccGGATCCTTAC-3'

plysu015: 5'-gctaacaagcccgaag-3'

Annealing was done at 64 °C (10 cycles) and 65 °C (20 cycles). Annealing temperatures were calculated according to NEB Tm calculator. Extension was done at 72 °C for 5 minutes and 25 seconds. Q5 High GC Enhancer was used for the amplification of the backbone. Conditions for the amplification via PCR are summarized in Chapter 10.8.2. Successful amplification of the backbone was verified with preparative gel electrophoresis as described in Chapter 10.7 (see Figure 63). Because the efficiency of the amplification was rather low, the PCR reaction was repeated four times and combined before subsequent gel purification as described in Chapter 10.8.3 yielding a concentration of 45.1 ng/μl.

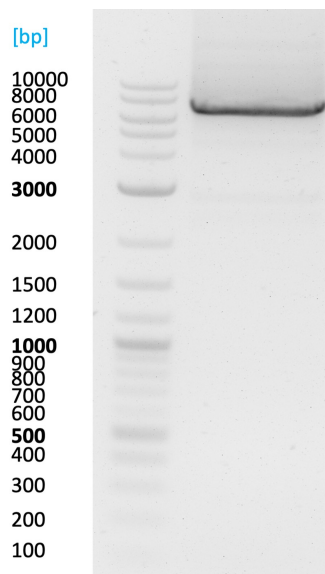


Figure 63: Gel electrophoresis of PCR reaction for the generation of backbone1. There is a band visible at approximately 7000 bp, as expected (7226 bp).

11.5.2 Successful Assembly of pKA1_alkj::pdc_{AP} by NEBuilder® HiFi DNA Assembly

The insert (1832 bp) for assembly of pKA1_alkj::pdc_{AP} was amplified by PCR, using pET22b(+)_pdc_{AP} (provided by Prof. Dörte Rother from the Forschungszentrum Jülich GmbH, Germany) as a template. The following primer pair was used:

plysu006: 5'-ggctgctaaccgatcccgcgaaattaatac-3'

plysu005: 5'-caactcagcttcctttcgggctttgtag-3'

Annealing was done at 71 °C (10 cycles) and 72 °C (20 cycles). Annealing temperatures were calculated according to NEB Tm calculator. Extension was done for 55 seconds. Conditions for the amplification via PCR are summarized in Chapter 10.8.2. Successful amplification of the target insert was verified with preparative gel electrophoresis as described in Chapter 10.7 (see Figure 64) and after excision of the corresponding band, purified as described in Chapter 10.8.3 for further use in the assembly.

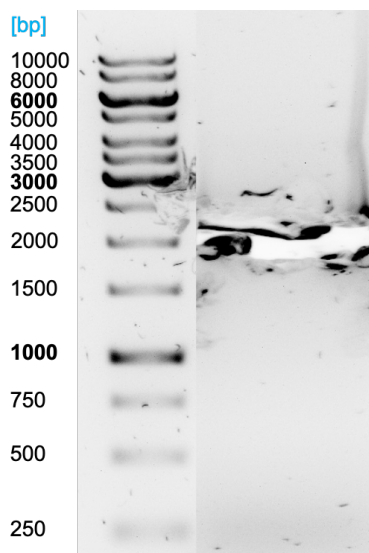


Figure 64: Gel electrophoresis of PCR reaction for the generation of the target insert pdc_{AP}. There is a band visible at approximately 1900 bp, as expected (1832 bp).

The assembly of backbone1 with target insert *pd_{CAP}* was conducted as described in Chapter 10.8.4. The following reaction mix was prepared and incubated at 50 °C in the thermocycler (Biometra TAdvanced Twin Analytik Jena) for 3 hours:

Table 33: Assembly Reaction Mix

Assembly 4 pKA1_alkj::pd _{CAP}	Size	Amount [ng]	Concentration [ng/μl]	Volume [μl]
Backbone1	7226	100	45.1	2.22
<i>pd_{CAP}</i>	1834	253.81	79.8	3.18
Nuclease-free water	-	-	-	4.6
NEBuilder HiFi DNA assembly master mix	-	-	-	10

After transformation in chemically competent *E. coli* Top cells (see Chapter 10.3), three transformants were obtained. Colony PCR (see Chapter 10.6) using following primers and subsequent gel electrophoresis (see Chapter 10.7) verified correct assembly in clone 2 and 3 (see Figure 65):

plysu012: 5'-gggtgcagagctagagttg-3'

plysu011: 5'-gggttatgctagttattgctcag-3'

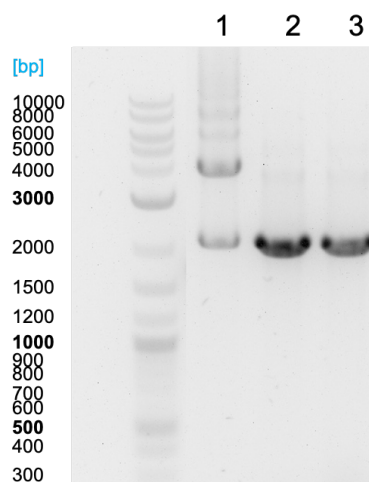


Figure 65: Gel electrophoresis of Colony PCR reaction to verify target insert *pd_{CAP}*. There is a band visible at approximately 1900 bp, as expected (1937 bp) in clone 2 and 3. Clone 1 shows a second band at approximately 4000 bp and was therefore ruled out.

An overnight culture of clone 2 was prepared for subsequent plasmid isolation (see Chapter 10.4) yielding a concentration of 198 ng/μl. The correct assembly of the target insert *pd_{CAP}* as well as the presence of *alkj* were confirmed by sequencing using following primers:

plysu012: 5'-gggtgcagagctagagttg-3'

t7terbis: 5'-aaccctcaagaccg-3'

plysu018: 5'-gaagcagcccagtagtaggttgag-3'

plysu019: 5'-gatccttacatgcagacagctatc-3'

11.5.3 Successful Assembly of pKA1_alkj::pdc_{AP}_mutant by NEBuilder® HiFi DNA

Assembly

Assembly of pKA1_alkj::pdc_{AP}_mutant was performed under equal conditions as pKA1_alkj::pdc_{AP} (outlined in the previous Chapter 10.5.2). The insert (1832 bp) for assembly of pKA1_alkj::pdc_{AP}_mutant was amplified by PCR (see Figure 66), using pET22b(+)_pdc_{AP}_mutant as a template (provided by Prof. Dörte Rother from the Forschungszentrum Jülich GmbH, Germany). Annealing was done at 61 °C (10 cycles) and 71 °C (20 cycles).

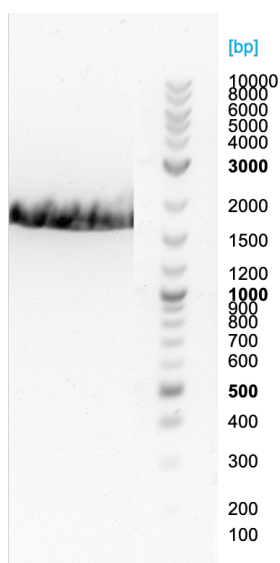


Figure 66: Gel electrophoresis of PCR reaction for the generation of the target insert *pdc_{AP}_mutant*. There is a band visible at approximately 1900 bp, as expected (1832 bp).

The following reaction mix was prepared:

Table 34: Assembly Reaction Mix

Assembly 6 pKA1_alkj::pdc _{AP} _mutant	Size	Amount [ng]	Concentration [ng/μl]	Volume [μl]
Backbone1	7226	100	45.1	2.22
<i>pdc_{AP}_mutant</i>	1834	253.81	122.4	2.07
Nuclease-free water	-	-	-	5.71
NEBuilder HiFi DNA assembly master mix	-	-	-	10

After transformation in chemically competent *E. coli* Top10 cells, seven transformants were obtained and confirmed by colony PCR (see Figure 67):

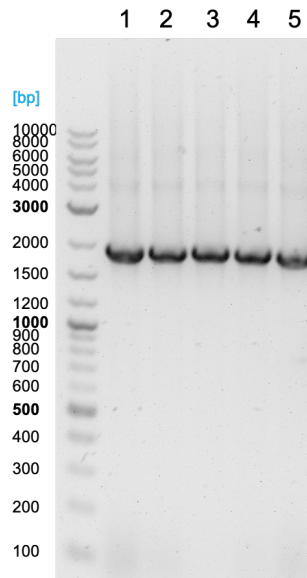


Figure 67: Gel electrophoresis of Colony PCR reaction to verify target insert *pd_{CAP}_mutant*. There is a band visible at approximately 1900 bp, as expected (1937 bp) in clones 1-5.

An overnight culture of clone 2 was prepared for subsequent plasmid isolation, yielding a concentration of 199 ng/ μ l.

11.5.4 Successful Assembly of pKA1_alkj::vflh6 by NEBuilder® HiFi DNA Assembly

Assembly of pKA1_alkj::vflh6 was performed under equal conditions as pKA1_alkj::pd_{CAP} (outlined in the previous Chapter 11.5.2). The insert (1580 bp) for assembly of pKA1_alkj::vflh6 was amplified by PCR (see Figure 68), using pET24a_vflh6 (provided by Prof. Uwe T. Bornscheuer from the University of Greifswald, Germany) as a template. Annealing was done at 71 °C (10 cycles) and 72 °C (20 cycles).

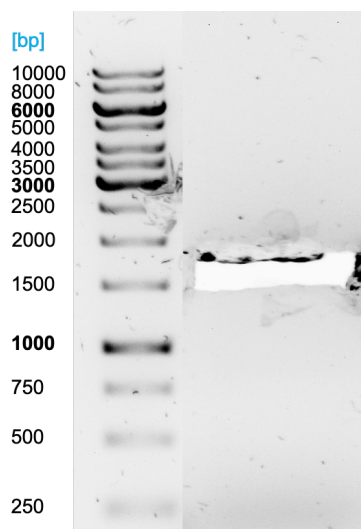


Figure 68: Gel electrophoresis of PCR reaction for the generation of the target insert *vflh6*. There is a band visible at approximately 1500 bp, as expected (1580 bp).

The following reaction mix was prepared and incubated at 50 °C for 2 hours instead of 3 hours:

Table 35: Assembly Reaction Mix

Assembly 1_5 pKA1_alkj::vflh6	Size	Amount [ng]	Concentration [ng/μl]	Volume [μl]
Backbone1	7226	100	45.1	2.22
<i>vflh6</i>	1580	218.65	82.8	2.64
Nuclease-free water	-	-	-	5.14
NEBuilder HiFi DNA assembly master mix	-	-	-	10

After transformation in chemically competent *E. coli* Top10 cells, six transformants were obtained and confirmed by colony PCR (see Figure 69):

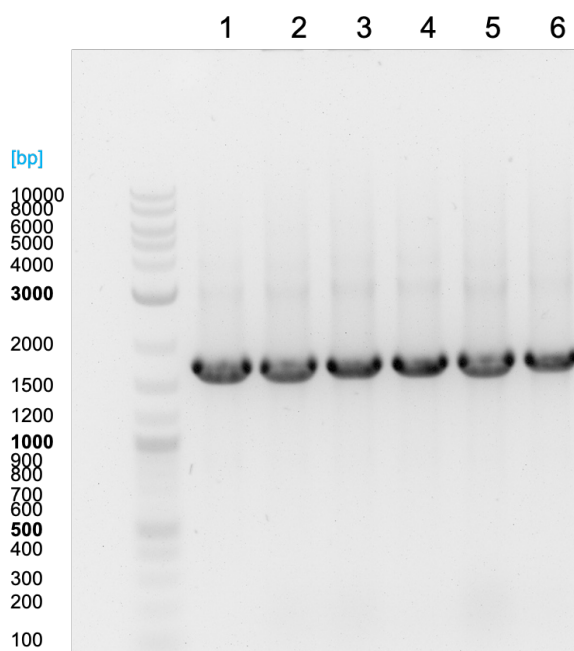


Figure 69: Gel electrophoresis of Colony PCR reaction to verify target insert *vflh6*. There is a band visible at approximately 1600 bp, as expected (1665 bp) in clones 1-6.

An overnight culture of clone 1 was prepared for subsequent plasmid isolation, yielding a concentration of 154.6 ng/μl.

11.5.5 Successful Assembly of pKA1_alkj::*aspfum* by NEBuilder® HiFi DNA Assembly

Assembly of pKA1_alkj::*aspfum* was performed under equal conditions as pKA1_alkj::*pdC_{Ap}* (outlined in the previous Chapter 11.5.2). The insert (1192 bp) for assembly of pKA1_alkj::*aspfum* was amplified by PCR (see Figure 70), using pET22b(+)_{*aspfum*} (provided by Prof. Uwe T. Bornscheuer from the University of Greifswald, Germany) as a template. Annealing was done at 71 °C (10 cycles) and 72 °C (20 cycles).

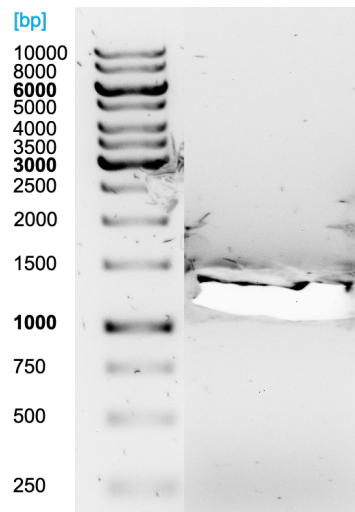


Figure 70: Gel electrophoresis of PCR reaction for the generation of the target insert *aspfum*. There is a band visible at approximately 1200 bp, as expected (1192 bp).

The following reaction mix was prepared:

Table 36: Assembly Reaction Mix

Assembly 2_4 <i>pKA1_alkj::aspfum</i>	Size	Amount [ng]	Concentration [ng/ μ l]	Volume [μ l]
Backbone1	7226	100	45.1	2.22
<i>aspfum</i>	1192	164.96	104.7	1.58
Nuclease-free water	-	-	-	6.2
NEBuilder HiFi DNA assembly master mix	-	-	-	10

After transformation in chemically competent *E. coli* Top10 cells, three transformants were obtained and confirmed by colony PCR (see Figure 71):

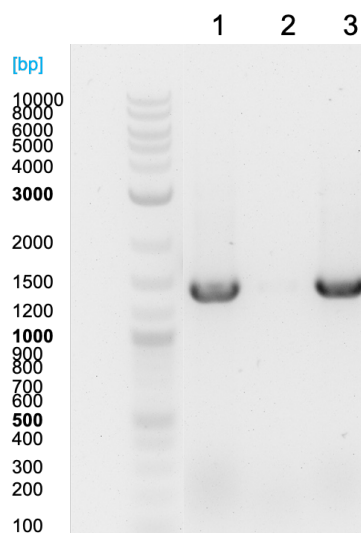


Figure 71: Gel electrophoresis of Colony PCR reaction to verify target insert *aspfum*. There is a band visible at approximately 1300 bp, as expected (1277 bp) in clones 1 and 3. Clone 2 does not show any band and was therefore ruled out.

An overnight culture of clone 1 was prepared for subsequent plasmid isolation, yielding a concentration of 165.1 ng/μl.

11.5.6 Successful Assembly of pKA1_alkj::aspredam by NEBuilder® HiFi DNA Assembly

Assembly of pKA1_alkj::aspredam was performed under equal conditions as pKA1_alkj::pdc_{Ap} (outlined in the previous Chapter 11.5.2). The insert (1128 bp) for assembly of pKA1_alkj::aspredam was amplified by PCR (see Figure 72), using pET28a_aspredam (provided by Prof. Nicholas Turner from the University of Manchester, United Kingdom) as a template. Annealing was done at 71 °C (10 cycles) and 72 °C (20 cycles).

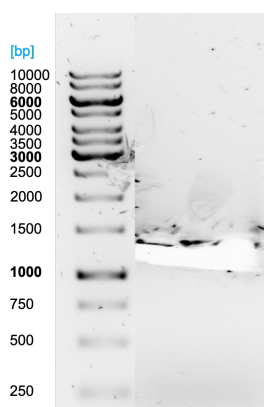


Figure 72: Gel electrophoresis of PCR reaction for the generation of the target insert *aspredam*. There is a band visible at approximately 1100 bp, as expected (1128 bp).

The following reaction mix was prepared:

Table 37: Assembly Reaction Mix

Assembly 5 pKA1_alkj::aspredam	Size	Amount [ng]	Concentration [ng/μl]	Volume [μl]
Backbone1	7226	100	45.1	2.22
<i>aspredam</i>	1128	156.10	120.5	1.30
Nuclease-free water	-	-	-	6.48
NEBuilder HiFi DNA assembly master mix	-	-	-	10

For transformation in chemically competent *E. coli* Top cells, only 2 μl were used. Two transformants were obtained and confirmed by colony PCR (see Figure 73):

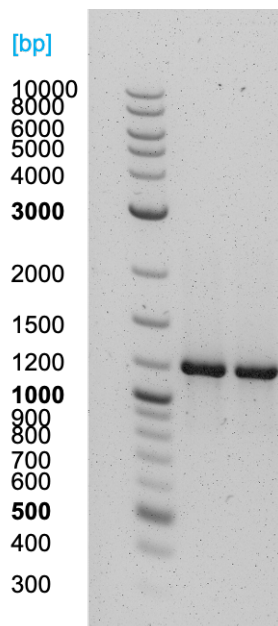


Figure 73: Gel electrophoresis of Colony PCR reaction to verify target insert *aspredam*. There is a band visible at approximately 1200 bp, as expected (1210 bp) in clones 1 and 2.

An overnight culture of clone 1 was prepared for subsequent plasmid isolation, yielding a concentration of 179.5 ng/ μ l. Primer plysu011 was used instead of t7terbis for verification of the correct assembly of the target insert *aspredam* by sequencing:

plysu011: 5'-gggttatgctagttattgctcag-3'

11.5.7 Successful Assembly of pKA1_alkj::pir13 by NEBuilder® HiFi DNA Assembly

Assembly of pKA1_alkj::pir13 was performed under equal conditions as pKA1_alkj::pdc_{Ap} (outlined in the previous Chapter 11.5.2). The insert (1113 bp) for assembly of pKA1_alkj::pir13 was amplified by PCR (see Figure 74), using pET28b(+)_pir13 (provided by Prof. Nicholas Turner from the University of Manchester, United Kingdom) as a template. Annealing was done at 61 °C (10 cycles) and 71 °C (20 cycles).

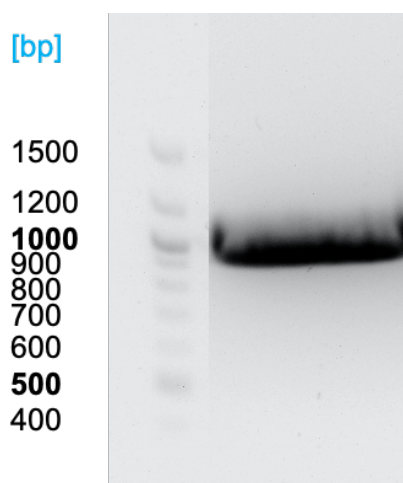


Figure 74: Gel electrophoresis of PCR reaction for the generation of the target insert *pir13*. There is a band visible at approximately 1000 bp, as expected (1113 bp).

The following reaction mix was prepared:

Table 38: Assembly Reaction Mix

Assembly 7 pKA1_alkj::pir13	Size	Amount [ng]	Concentration [ng/μl]	Volume [μl]
Backbone1	7226	100	45.1	2.22
<i>pir13</i>	1113	154.03	115.8	1.33
Nuclease-free water	-	-	-	6.45
NEBuilder HiFi DNA assembly master mix	-	-	-	10

Eleven transformants were obtained and five were confirmed by colony PCR (see Figure 75):

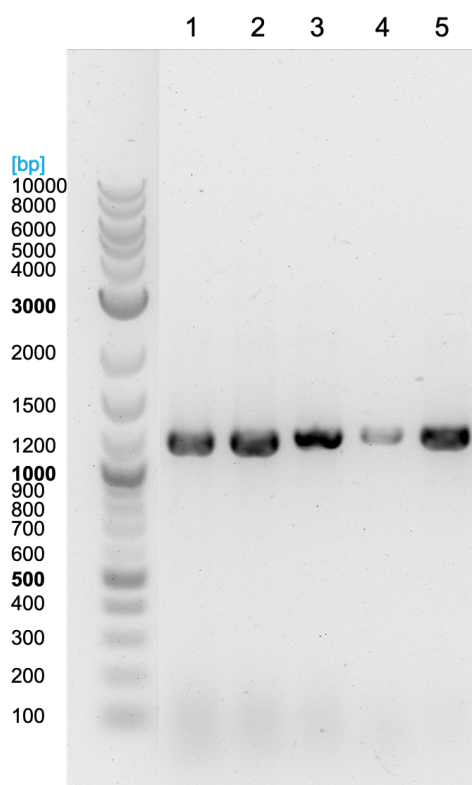


Figure 75: Gel electrophoresis of Colony PCR reaction to verify target insert *pir13*. There is a band visible at approximately 1200 bp, as expected (1198 bp) in clones 1 - 5.

An overnight culture of clone 1 was prepared for subsequent plasmid isolation, yielding a concentration of 125.4 ng/μl.

11.5.8 Successful Assembly of pKA1_alkj::pir23 by NEBuilder® HiFi DNA Assembly

Assembly of pKA1_alkj::pir23 was performed under equal conditions as pKA1_alkj::pdcAp (outlined in the previous Chapter 11.5.2). The insert (1113 bp) for assembly of pKA1_alkj::pir23 was amplified by PCR (see Figure 76), using pET28b(+)_pir23 (provided by Prof. Nicholas Turner from the University of Manchester, United Kingdom) as a template. Annealing was done at 61 °C (10 cycles) and 71 °C (20 cycles).

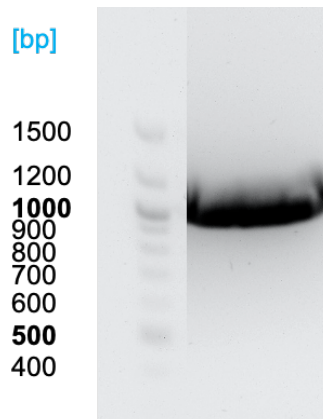


Figure 76: Gel electrophoresis of PCR reaction for the generation of the target insert *pir23*. There is a band visible at approximately 1000 bp, as expected (1113 bp).

The following reaction mix was prepared:

Table 39: Assembly Reaction Mix

Assembly 8 <i>pKA1_alkj::pir23</i>	Size	Amount [ng]	Concentration [ng/ μ l]	Volume [μ l]
Backbone1	7226	100	45.1	2.22
<i>pir23</i>	1113	154.03	140.5	1.10
Nuclease-free water	-	-	-	6.68
NEBuilder HiFi DNA assembly master mix	-	-	-	10

18 transformants were obtained and five were confirmed by colony PCR (see Figure 77):

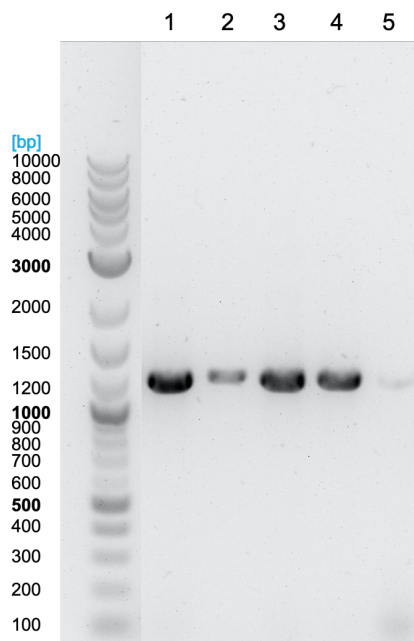


Figure 77: Gel electrophoresis of Colony PCR reaction to verify target insert *pir23*. There is a band visible at approximately 1200 bp, as expected (1198 bp) in clones 1 - 4. Clone 4 showed a very weak band and was therefore ruled out.

An overnight culture of clone 1 was prepared for subsequent plasmid isolation, yielding a concentration of 134.6 ng/μl.

11.5.9 Generation of Backbone2 for Assembly of pKA1_alkj::aspter

The backbone2 (7307 bp) was amplified by PCR, using previously corrected pPOP_mutag_c2 (see Chapter 11.3) as a template. The following primer pair was used:

plysu007: 5'-tgcttgccatggtatatctccttcttaagTTAAACAAAATTATTTCTAGAG-3'

plysu008: 5'-ttgactgcagagctgagttggctgctgc-3'

Annealing was done at 67 °C (10 cycles) and 69 °C (20 cycles). Annealing temperatures were calculated according to NEB Tm calculator. Extension was done at 72 °C for 5 minutes and 29 seconds. Q5 High GC Enhancer was used for the amplification of the backbone. Conditions for the amplification via PCR are summarized in Chapter 10.8.2. Successful amplification of the backbone was verified with preparative gel electrophoresis as described in Chapter 10.7 (see Figure 78). After subsequent gel purification as described in Chapter 10.4, a concentration of 19.6 ng/μl was obtained.

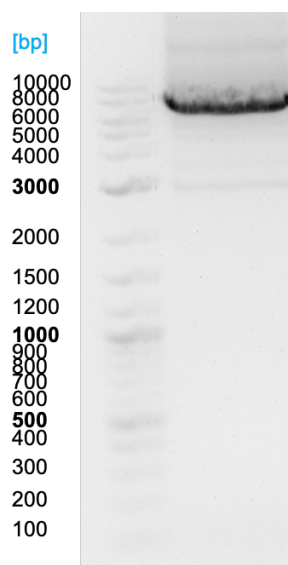


Figure 78: Gel electrophoresis of PCR reaction for the generation of backbone2. There is a band visible at approximately 7000 bp, as expected (7307 bp). Some unspecific binding of the primer pair was observed, but resulting bands are much weaker than the main band at 7000 bp.

11.5.10 Successful Assembly of pKA1_alkj::aspter by NEBuilder® HiFi DNA

Assembly

The insert (1028 bp) for assembly of pKA1_alkj::aspter, was amplified by PCR, using pGASTON_aspter (provided by Prof. Uwe T. Bornscheuer from the University of Greifswald, Germany) as a template.

Originally, the following primer pair was used:

plysu010: 5'-gagatataccatggcaagcaTGGATAAAG-3'

plysu009: 5'-caactcagctctgcagtcaaTGATGATG-3'

However, after several rounds of unsuccessful assemblies, the primers were adjusted to have 30 bp and 31 bp overlapping overhangs for DNA assembly instead of 20 bp yielding the target insert *aspter* with 1049 bp. The following primers were used:

plysu017: 5'-ctttaagaaggagatataccatggcaagcaTGGATAAAG-3'

plysu016: 5'-gtggcagcagccaactcagctctgcagtcaaTGATGATG-3'

Annealing was done at 58 °C (10 cycles) and 60 °C (20 cycles). Annealing temperatures were calculated according to NEB Tm calculator. Extension was done for 1 minute. Conditions for the amplification via PCR are summarized in Chapter 10.8.2. Successful amplification of the target insert was verified with preparative gel electrophoresis as described in Chapter 10.7 (see Figure 79) and after excision of the corresponding band, purified as described in Chapter 10.8.3 for further use in the assembly.

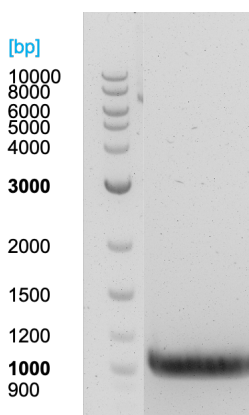


Figure 79: Gel electrophoresis of PCR reaction for the generation of the target insert *aspter*. There is a band visible at approximately 1000 bp, as expected (1049 bp).

The assembly of backbone2 with target insert *aspter* was conducted as described in Chapter 10.8.4. However, it was used a molar ratio 1:5 backbone to insert instead of 1:10. The following reaction mix was prepared and incubated at 50 °C in the thermocycler (Biometra TAdvanced Twin Analytik Jena) for 3 hours:

Table 40: Assembly Reaction Mix

Assembly 3_3 pKA1_alkj:: <i>aspter</i>	Size	Amount [ng]	Concentration [ng/μl]	Volume [μl]
Backbone2	7307	100	19.6	5.10
<i>aspter</i>	1049	71.78	75	0.96
Nuclease-free water	-	-	-	3.94
NEBuilder HiFi DNA assembly master mix	-	-	-	10

After transformation in chemically competent *E. coli* Top cells (see Chapter 10.3), five transformants were obtained. Colony PCR (see Chapter 10.6) using following primers and subsequent gel electrophoresis (see Chapter 10.7) verified correct assembly in clones 1-5 (see Figure 80):

plysu012: 5'-gggtgcagagctagagttg-3'

plysu011: 5'-gggttatgctagttattgctcag-3'

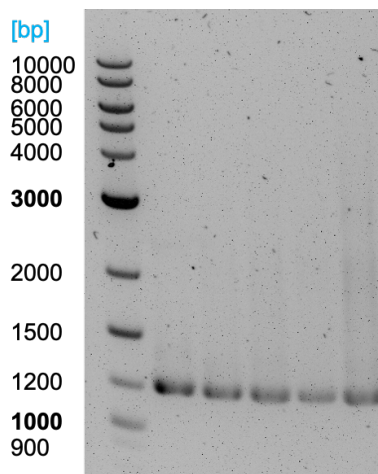


Figure 80: Gel electrophoresis of Colony PCR reaction to verify target insert *aspter*. There is a band visible at approximately 1200 bp, as expected (1217 bp) in clone 1-5.

An overnight culture of clone 2 was prepared for subsequent plasmid isolation (see Chapter 10.4) yielding a concentration of 200.5 ng/ μ l. The correct assembly of the target insert *aspter* as well as the presence of *alkj* were confirmed by sequencing using following primers:

plysu012: 5'-gggtgcagagctagagttg-3'

t7terbis: 5'-aaccctcaagaccg-3'

plysu018: 5'-gaagcagcccagtagtaggttgag-3'

plysu019: 5'-gatccttacatgcagacagctatc-3'

11.6 Validation of Vector Functionality by Protein Production Analysis and Biotransformation (Mini-Pathway)

Assembled constructs were transformed in chemically competent *E. coli* BL21 (DE3) cells as described in Chapter 10.3. *E. coli* strains were cultivated according to standard cultivation conditions by autoinduction (as described in Chapter 10.9.2), and protein content analysed by Bradford Assay and SDS-PAGE (as described in Chapters 10.10 and 10.11). The CFE and RCs were prepared as described in Chapters 10.9.3 and 10.9.4. Standard reaction conditions for biotransformations using the CFE or RCs are described in Chapters 10.12.1 and 10.12.2. The reaction progress was monitored via calibrated GC as described in Chapter 10.12.3.

11.6.1 Co-Expression Study of *AlkJ* and *PDC_{Ap}*

Enzyme Expression by Autoinduction

Assembly A4_c2 (pKA1_alkj::pdc_{Ap}) was transformed and enzyme co-production analysed via SDS-PAGE (see Figure 29 in Chapter 7.5.1).

11.6.2 Co-Expression Study of *AlkJ* and *PDC_{Ap}_mutant* and Mini-Pathway Validation

Enzyme Expression by Autoinduction

Assembly A6_c2 (pKA1_alkj::pdc_{Ap}_mutant) was transformed and enzyme co-production analysed via SDS-PAGE (see Figure 29 in Chapter 7.5.1). The cofactors MgSO₄ and ThDP were added to a final conc. of 2.5 mM and 0.1 mM respectively to the cell suspension prior to lysis by sonication.

Mini-Pathway Validation

The mini-pathway employing the enzymes *AlkJ* and *PDC_{Ap}_mutant* was tested by the conversion of 8 mM benzyl alcohol **1a** to benzaldehyde **1b** and subsequent reaction with 10 mM sodium pyruvate to phenylacetylcarbinol **1g** under the addition of 2.5 mM MgSO₄ and 0.1 mM ThDP in RCs at 30 °C, 250 rpm. Conversion to **1b**, and subsequently, 30 % conversion to **1g** was observed after 24 h (see Figure 31 in Chapter 7.5.1). The reaction employing a biomass concentration of OD₅₉₀ = 30 was conducted in 50 mM potassium phosphate buffer (pH 6.5) under the addition of 1 % (w/v) glucose.

Moreover, to verify that the functionality of the enzyme *PDC_{Ap}_mutant*, a biotransformation was performed using the CFE to test the conversion of 8 mM benzaldehyde **1b** with 10 mM sodium pyruvate to phenylacetylcarbinol **1g** under the addition of 2.5 mM MgSO₄ and 0.1 mM ThDP in 50 mM potassium phosphate buffer (pH 6.5) at 30 °C, 250 rpm. Total protein content was set to 30 mg/ml. 73 % conversion to **1g** was observed already after 1 h (see Figure 81).

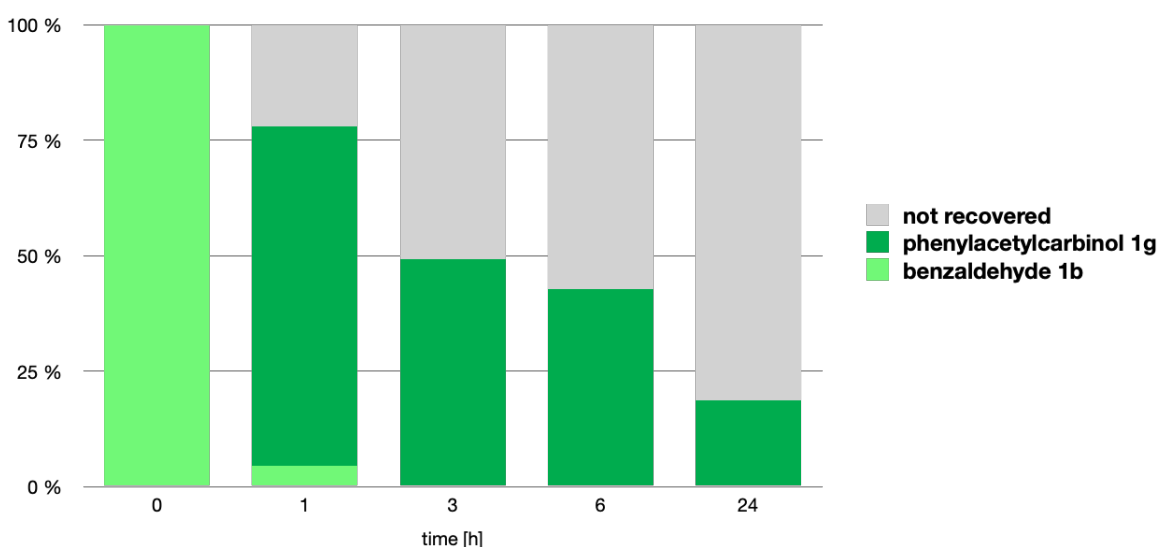


Figure 81: Conversion of benzaldehyde **1b** with sodium pyruvate to phenylacetylcarbinol **1g** by *PDC_{Ap}_mutant* (expressed from A6_c2 (pKA1_alkj::pdc_{Ap}_mutant)). Samples were analysed by calibrated GC/FID. The relative concentration of components over time is shown.

11.6.3 Co-Expression Study of *AlkJ* and *VfIH6/AspFum/AspTer* and Mini-Pathway Validation

Enzyme Expression by Autoinduction

Assemblies A1_5_c1 (pKA1_alkj::vflh6), A2_4_c1 (pKA1_alkj::aspfum) and A3_3_c2 (pKA1_alkj::aspter) were transformed and enzyme co-production analysed via SDS-PAGE (see Figure 32 in Chapter 7.5.2). The cofactor PLP was added to a final conc. of 0.1 mM to the cell suspensions prior to lysis by sonication.

Mini-Pathway Validation

The mini-pathway employing the enzymes *AlkJ* and *VfIH6/AspFum/AspTer* was tested by the conversion of 8 mM benzyl alcohol **1a** to benzaldehyde **1b** and subsequent reaction with 25 equivalents L-alanine (200 mM) to benzylamine **1d** under the addition of 0.1 mM PLP in RCs at 25 °C, 250 rpm. Conversion to **1b**, and subsequently, 76 % conversion to **1d** was observed after 24 h (see Figure 34 in Chapter 7.5.2).

Substrate Acceptance Screening

To expand the substrate scope, the mini-pathway was tested employing the enzymes *AlkJ* and *VfIH6* by the conversion of 8 mM alcohols **1-3a** to the corresponding aldehyde **1-3b** and subsequent reaction with

10 equivalents L-alanine (200 mM) to the corresponding amine **1-3d** under the addition of 0.1 mM PLP in RCs at 25 °C, 250 rpm. Conversion to the aldehydes, and subsequently, 26 %, 54 % and 64 % conversion to the amines (**1d**, **2d** and **3d** respectively) was observed after 24 h (see Figures 35 and 36 in Chapter 7.5.2).

11.6.4 Co-Expression Study of *AlkJ* and *AspRedAm*

Enzyme Expression by Autoinduction

Assembly A5_c1 (pKA1_alkj::aspredam) was transformed and enzyme co-production analysed via SDS-PAGE (see Figure 37 in Chapter 7.5.3).

11.6.5 Co-Expression Study of *AlkJ* and *PIR13/PIR23* and Mini-Pathway Validation

Enzyme Expression by Autoinduction

Assembly A7_c1 (pKA1_alkj::pir13) and A8_c1 (pKA1_alkj::pir23) were transformed and enzyme co-production analysed via SDS-PAGE (see Figure 39 in Chapter 7.5.3).

Mini-Pathway Validation

The mini-pathway employing the enzymes *AlkJ* and *PIR13/PIR23* was tested by the conversion of 8 mM benzyl alcohol **1a** to benzaldehyde **1b** and subsequent reaction with 2 equivalents aniline **7** (16 mM) to N-benzylaniline **1e** in RCs at 30 °C, 250 rpm. With the enzymes *AlkJ* and *PIR23*, conversion to **1b**, and subsequently, reductive amination yielding 73 % **1e** was observed after 26 h (see Figure 51 in Chapter 7.5.3).

11.7 Expression of all Pathway Enzymes in a Single Host Cell and Validation by Biotransformation (Maxi-Pathway)

Constructs were co-transformed in chemically competent *E. coli* BL21 (DE3) cells as described in Chapter 10.3. Plasmid uptake was validated by Colony PCR and subsequent gel electrophoresis (as described in Chapters 10.6 and 10.7). *E. coli* strains were cultivated according to standard cultivation conditions by autoinduction (as described in Chapter 10.9.2), and protein content analysed by Bradford Assay and SDS-PAGE (as described in Chapters 10.10 and 10.11). The CFE and RCs were prepared as described in Chapters 10.9.3 and 10.9.4. Standard reaction conditions for biotransformations using RCs are described in Chapter 10.12.2. The reaction progress was monitored via calibrated GC as described in Chapter 10.12.3.

11.7.1 Co-Production of *AlkJ*, *PDC_{AP}_mutant*, *CAR_{Ni}* and *PPtase_{Ec}* and Maxi-Pathway Validation

Validation of Plasmid Uptake by Colony PCR

After co-transformation of pKA1_alkj::pdc_{AP}_mutant (A6_c2) and pETDuet1_pptase_{Ec}::car_{Ni}, approximately 70 transformants were obtained. Colony PCR of three clones, using following primers and subsequent gel electrophoresis verified the presence of the target inserts pdc_{AP}_mutant in pKA1_alkj::pdc_{AP}_mutant and car_{Ni} in pETDuet1_pptase_{Ec}::car_{Ni} (see Figure 82):

plysu012: 5'-gggtgcagagctagagttg-3'

plysu011: 5'-gggttatgctagttattgctcag-3'

tom37: 5'-gagaaagaggagaaataactaatgtcgtactaccatcacca-3'

tom38: 5'-gctttttatattcttaagcttacagcagttgcagcagtt-3'

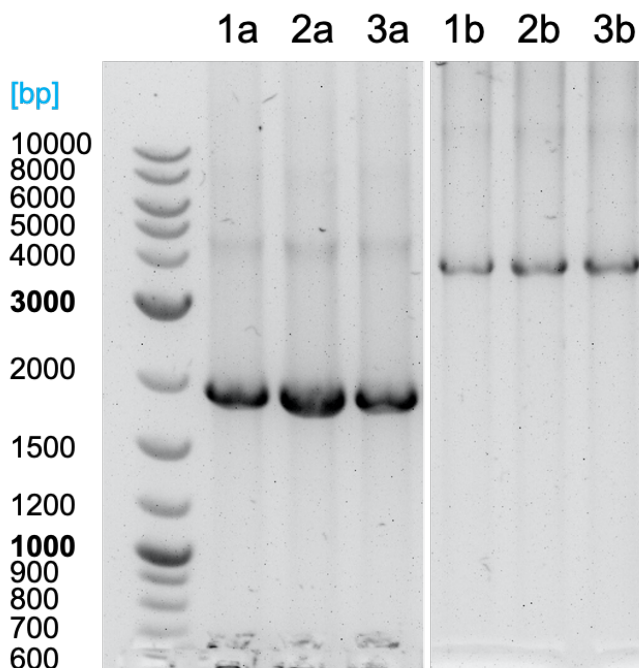


Figure 82: Gel electrophoresis of Colony PCR reaction to verify target inserts *pdc_{AP}_mutant* and *car_{Ni}*. There is a band visible at approximately 1900 bp (1a, 2a and 3a), as expected (1937 bp) and at approximately 3500 bp (1b, 2b and 3b) as expected (3664 bp).

Enzyme Expression by Autoinduction

Enzyme co-production and analysis via SDS-PAGE is described in Chapter 7.6.1.

Maxi-Pathway Validation

The maxi-pathway employing the enzymes *AlkJ*, *PDC_{AP}_mutant* and *CAR_{Ni}* was tested starting either with 8 mM benzyl alcohol **1a**, benzoic acid **1c** or with a 50:50 mixture of both. The conversion to benzaldehyde **1b** and subsequent reaction with 10 mM sodium pyruvate to phenylacetylcarbinol **1g** under the addition of 2.5 mM MgSO₄ and 0.1 mM ThDP in RCs was performed at 30 °C, 250 rpm. Conversion to **1b**, and subsequently, 16 % conversion to **1g** was observed after 24 h (see Figure 44 in Chapter 7.6.1). A biomass concentration of OD₅₉₀ = 30 and a volume of 1 ml were used.

Mixed Culture Approach

There was conducted an experiment combining RCs containing *AlkJ* and *PDC_{AP}_mutant* and RCs containing *CAR_{Ni}* respectively in a mixed culture approach. Therefore, *E. coli* BL21 (DE3) containing pKA1_alkj::pdc_{AP}_mutant (A6_c2) and *E. coli* BL21 (DE3) containing pETDuet1_pptase_{EC}::car_{Ni} were cultured separately. Optimized enzyme production was performed following the protocol for cultivation in autoinduction media. The maxi-pathway was tested starting either with 8 mM benzyl alcohol **1a**, benzoic acid **1c** or with a 50:50 mixture of both. The conversion to benzaldehyde **1b** and subsequent reaction with 10 mM sodium pyruvate to phenylacetylcarbinol **1g** under the addition of 2.5 mM MgSO₄ and 0.1 mM ThDP was performed at 30 °C, 250 rpm. RCs containing *AlkJ* and *PDC_{AP}_mutant* were normalized to a biomass concentration of OD₅₉₀ = 30 and RCs containing *CAR_{Ni}* were normalized to a biomass concentration of OD₅₉₀ = 15. Conversion to **1b**, and subsequently, 14 % conversion to phenylacetylcarbinol **1g** was observed after 24 h (see Figure 83).

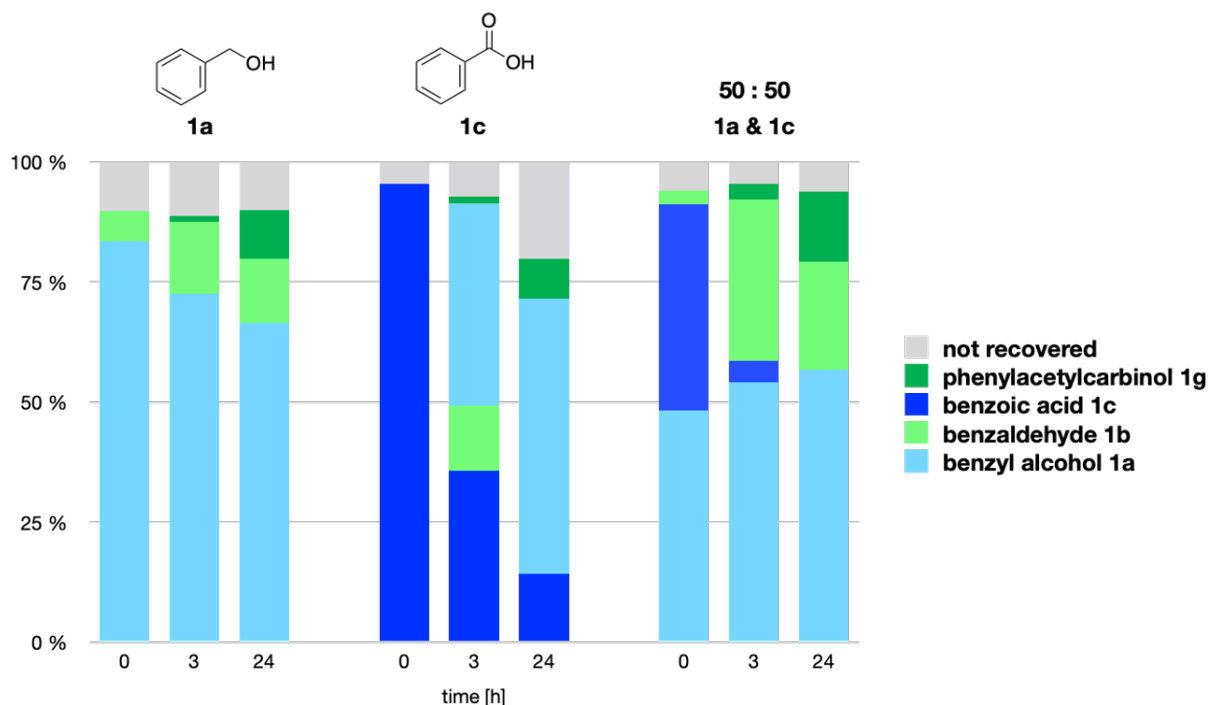


Figure 83: Conversion of benzyl alcohol 1a or benzoic acid 1c to benzaldehyde 1b by *AlkJ* or *CAR_{Ni}* respectively and subsequent reaction with sodium pyruvate to phenylacetylcarbinol 1g by *PDC_{Ap}_mutant* in a mixed culture approach. Mean values of biological duplicates were analysed by calibrated GC/FID. The relative concentration of components over time is shown.

11.7.2 Co-Production of *AlkJ*, *VflH6/AspFum/AspTer*, *CAR_{Ni}* and *Pptase_{Ec}* and Maxi-Pathway Validation

Validation of Plasmid Uptake by Colony PCR

After co-transformation of pKA1_alkj::vflh6/aspfum/aspter (A1_5_c1, A2_4_c1, A3_3_c2) and pETDuet1_pptase_{Ec}::car_{Ni}, approximately 100 transformants were obtained respectively. Colony PCR of two clones respectively, using following primers and subsequent gel electrophoresis verified the presence of the target inserts vflh6/aspfum/aspter in pKA1_alkj:: vflh6/aspfum/aspter and car_{Ni} in pETDuet1_pptase_{Ec}::car_{Ni} (see Figure 84):

plysu012: 5'-gggtgcagagctagagttg-3'

plysu011: 5'-gggttatgctagttattgctcag-3'

tom37: 5'-gagaaagaggagaaataactaatgctgtactaccatcacca-3'

tom38: 5'-gcttttatattctctaagcttacagcagttgcagcagtt-3'

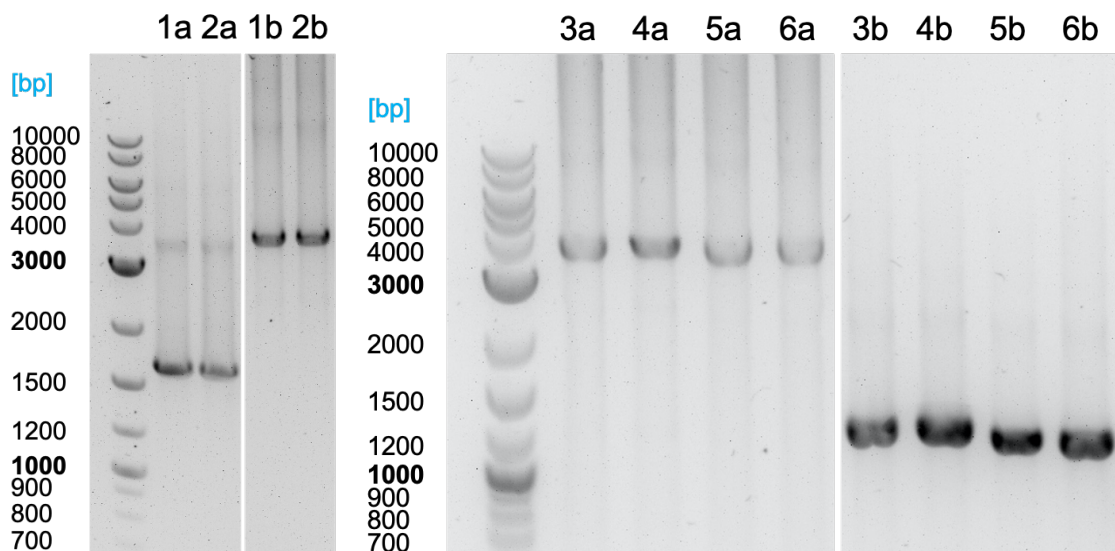


Figure 84: Gel electrophoresis of Colony PCR reaction to verify target inserts *vflh6/aspfum/asppter* and *car_{Ni}*. There is a band visible for *vflh6* at approximately 1600 bp (1a and 2a), as expected (1665 bp) and there are bands visible for *aspfum* and *asppter* at approximately 1200 bp (3a – 6a) as expected (1277 bp and 1214 bp respectively). A band for insert *car_{Ni}* at approximately 3500 bp is visible in all clones (1b – 6b) as expected (3664 bp).

Enzyme Expression by Autoinduction

Enzyme co-production and analysis via SDS-PAGE is described in Chapter 7.6.2. The cofactor PLP was added to a final concentration of 1 mM to the cell suspension prior to lysis by sonication.

Maxi-Pathway Validation

The maxi-pathway employing the enzymes *AlkJ*, *VfIH6/AspFum/AspTer* and *CAR_{Ni}* was tested starting either with 8 mM benzyl alcohol **1a**, benzoic acid **1c** or with a 50:50 mixture of both. The conversion to benzaldehyde **1b** and subsequent reaction with with 10 equivalents (80 mM) L-alanine to benzylamine **1d** under the addition of 0.1 mM PLP in RCs was performed at 25 °C, 250 rpm. With the enzymes *AlkJ*, *VfIH6* and *CAR_{Ni}*, conversion to **1b** and subsequently, 76 % conversion to **1d** was observed after 23 h (see Figure 47 in Chapter 7.6.2).

Substrate Acceptance Screening

To expand the substrate scope, the maxi-pathway was tested employing the enzymes *AlkJ* and *VfIH6* and *CAR_{Ni}* starting either with 8 mM alcohol **2a** and **3a**, acid **2c** and **3c** or with a 50:50 mixture of both in RCs at 25 °C, 250 rpm. Conversion to the aldehydes **2d** and **3b**, and subsequently, 57 % and 78 % conversion to the amines (**2d** and **3d** respectively) was observed after 23 h (see figure 48 in chapter 7.6.2).

11.7.3 Co-Production of *AlkJ*, *PIR23*, *CAR_{Ni}* and *Pptase_{EC}* and Maxi-Pathway Validation

Validation of Plasmid Uptake by Colony PCR

After co-transformation of pKA1_alkj::pir23 (A8_c1) and pETDuet1_pptase_{EC}::car_{Ni}, approximately 70 colonies were obtained. Colony PCR of two clones, using following primers and subsequent gel electrophoresis verified the presence of the target inserts *pir23* in pKA1_alkj::pir23 and *car_{Ni}* in pETDuet1_pptase_{EC}::car_{Ni} (see Figure 85):

plysu012: 5'-gggtgcagagctagagttg-3'

plysu011: 5'-gggttatgctagttattgctcag-3'

tom37: 5'-gagaaagaggagaaataactaatgtcgtactaccatcacca-3'

tom38: 5'-gctttttatattctctaagcttacagcagttgcagcagtt-3'

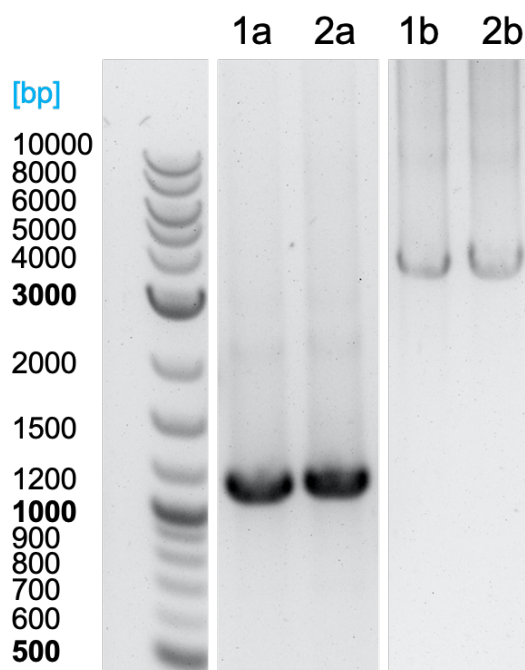


Figure 85: Gel electrophoresis of Colony PCR reaction to verify target inserts *pir23* and *car_{Ni}*. There are bands visible for *pir23* at approximately 1200 bp (1a and 2a), as expected (1198 bp) and there are bands visible for insert *car_{Ni}* at approximately 3500 bp (1b and 2b) as expected (3664 bp).

Enzyme Expression by Autoinduction

Enzyme co-production and analysis via SDS-PAGE is described in Chapter 7.6.3.

Maxi-Pathway Validation

The maxi-pathway employing the enzymes *AlkJ*, *PIR23* and *CAR_{Ni}* was tested starting either with 8 mM benzyl alcohol **1a**, benzoic acid **1c** or with a 50:50 mixture of both. The conversion to benzaldehyde **1b** and subsequent reaction with with 2 equivalents aniline **7** (16 mM) to N-benzylaniline **1e** in RCs was performed at 30 °C, 250 rpm. Conversion to **1b**, and subsequently, 40 % conversion to **1e** was observed after 25 h (see Figure 51 in Chapter 7.6.3).

Substrate Acceptance Screening

Attempts to expand the substrate scope are described in Chapter 7.6.3.

12 Appendix

12.1 Gene Sequences

In the following, vectors used in this thesis with their antibiotic resistance and gene sequences are summarized. The start codon is highlighted in green, the stop codon in red and a possible 6 x His tag in orange.

Table 41: Vectors used in this Thesis and Corresponding Antibiotic Resistance

Vector	Antibiotic Resistance
pKA1	chloramphenicol
pETDuet1	ampicillin
pET22b(+)	ampicillin
pET24a	kanamycin
pGASTON	ampicillin
pET28a	kanamycin
pET28b	kanamycin

Carboxylic Acid Reductase *CAR_{Ni}* and Phosphopantetheinyl Transferase *Pptase_{Ec}*

The genes were obtained in plasmid pETDuet1_*pptase_{Ec}::car_{Ni}*. The enzyme *CAR_{Ni}* carries a N-terminal 6 x His tag.

car_{Ni}

```
ATGTCGTA  
ACTACCATCACCATCACCATCACGATTACGACATCCCAACGACCGAAAACCTGTATTTTCAGGGCGCCAT  
GGCTGATATCGGATCCGAATTCATGGCAGTCGACAGCCCAGACGAACGCCTGCAAAGACGCATCGCCCAATTGTT  
CGCAGAGGACGAGCAGGTGAAGGCGGCTCGCCCGCTGGAAGCCGTGAGCGCGGCTGTTTCTGCTCCGGGTATGC  
GCCTGGCGCAGATCGCAGCGACGGTCATGGCCGGCTATGCCGACCGTCCTGCAGCCGGTCAACGCGCATTTCGAGC  
TGAACACTGATGACGCCACCGGTCGCACCAGCTTGCCTGCTGCCGCGTTTTGAAACCATCACCTATCGTGAGCT  
GTGGCAACGCGTGGGCGAGGTGGCGGCTGCGTGGCATCATGACCCGAAAACCGTTGCGTGCGGGCGATTTTCG  
TGGCACTGCTGGGTTTACCAGCATTGATTATGCGACGCTGGACCTGGCCGACATCCATCTGGGTGCTGTGACCGT  
GCCGCTGCAGGCCAGCGCAGCAGTGTCCCAACTGATTGCGATCCTGACGAAACCTCCCCTCGTTGCTGGCGTCT  
ACCCCGGAGCACCTGGACGCAGCGGTTGAATGTCTGCTGGCGGGTACCACCCCGAGCGCCTGGTCTGTTTGAT  
TATACCCCGAAGATGACGATCAACGCGCAGCGTTTGAAGAGCGCGCTCGCCGCTGCTGGCTGATGCGGGTAGCCT  
GGTTATCGTTGAAACCTGGACGCGGTCCGTGCACGTGGCCGTGACCTGCCAGCGGCACCGCTGTTTCGTTCCCGGA  
CACTGACGATGATCCACTGGCGCTGCTGATTTACACCAGCGGCAGCACCAGTACGCCGAAGGGCGCGATGTACAC  
CAATCGCTTGGCGGCGACCATGTGGCAAGGTAACAGCATGCTGCAAGGTAACCTCCAGCGTGTGGCATCAATTT  
GAATTACATGCCGATGAGCCATATTGCGGGTCGTATTAGCCTGTTCCGGTGTGCTGGCTCGTGGCGGTACGGCCTAT  
TTCGAGCGAAGTCCGATATGAGCACCTGTTTGAAGATATCGGTCTGGTCCGTCGACCGAGATCTTCTTCGTT  
CGCGTGTGTTGATATGGTGTTCAGCGTTATCAGTCGGAACCTGGACCGTCGTAGCGTCGAGGTGCGGACCTGG  
ACACGCTGGATCGCGAGGTCAAAGCCGACCTGCGCCAGAATTATCTGGGCGGTCGCTTCTGGTCCCGTGGTGG  
GCTCCGCTCCGCTGGCAGCGGAGATGAAAACCTTTATGGAGAGCGTCTTGGATCTGCCGCTGCACGATGGCTATG  
GTAGCACGGAAGCGGGTGCCTCGTCTTGGTGGATAACCAAATTCAGCGTCTCCAGTGTGACTATAAACTGG  
TGGATGTGCCGGAACCTGGGCTATTTTCGTACCGATCGCCCGCATCCGCGTGGTGAGCTGCTGCTGAAGGCGGAAA  
CTACCATCCCGGTTACTACAAGCGTCCGGAGGTTACGGCAGAAATCTTTGATGAAGATGGTTTCTACAAGACGG  
GTGACATCGTTGCGGAGCTGGAACACGATCGTTTGGTTTACGTTGACCGTCGCAACAACGTGCTGAAACTGTCTCA
```

AGGTGAGTTCGTCACCTGGAAGCTGTGTTTGAAGCAGCCCGCTGATTCGTCAGATCTTCATCTAC
GGTAGCTCTGAACGCAGCTACTTGCTGGCCGTTATCGTTCCGACCGACGACGCATTGCGTGGCCGCGACTGCA
ACCCTGAAGAGCGCATTGGCCGAGAGCATCCAACGTATTGCAAAAGACGCGAACCTGCAACCATACGAGATCCCG
CGTGATTTCTGATCGAAACCGAACCGTTCACCATTGCGAATGGTCTGCTGAGCGGCATTGCAAAGCTGCTGCGTC
CGAATCTGAAAGAGCGTTACGGTGCCAGTTGGAGCAGATGTACACGGACTTGCGCAGCGGTGACGGCGGACGAA
TTGCTGGCGCTGCGTCGTGAGGCGGCAGACCTGCCGGTACTGAAACCGTTAGCCGTGCGGCCAAAGCGATGCT
GGGTGTTGCCAGCGCGGATATGCGTCCGGATGCGCACTTACCGACTTGGGCGGTGACAGCCTGAGCGCGCTGA
GCTTCTCTAATCTGCTGCACGAAATCTTTGGCGTGGAGGTGCCGGTTGGCGTCGTGGTGGACCCCTGCAAATGAATT
GCGTGATCTGGCTAATTACATCGAGGCCGAACGCAATAGCGGTGCGAAACGTCCGACCTTACCAGCGTGCATGG
CGGTGGCTCGGAGATTGCTGCGGCGGATCTGACGCTGGATAAGTTTATTGATGCTCGTACGCTGGCAGCCGCTGA
CAGCATTCCGCACGCACCGGTGCCAGCGCAGACGGTCTGCTGACGGGTGCCAACGGTTACCTGGGTGCTTTCT
GTGCCTGGAGTGGCTGGAGCGTCTGGACAAAACGGGCGGTACCCTGATCTGTGTTGTGCGTGGCTCGGATGCAG
CAGCCGCACGCAAACGTTTGGACAGCGCCTTCGACTCGGGTGACCCGGGTCTGTTGGAGCATTATCAGCAGCTGG
CGGCACGCACCCTGGAGTTCTGGCGGGTGATATTGGCGATCCGAATCTGGGCCTGGACGATGCGACCTGGCAG
CGTCTGGCGGAGACTGTCGATTTGATTGTCCACCCGGCAGCGTTGGTTAACCATGTTCTGCCGTACACCCAAGTGT
TCGGCCCGAACGTTGTAGGTACGGCCGAAATTGTCGGTCTGGCAATCACTGCGCGTCGCAAGCCGGTACAGTACC
TGAGCACCGTTGGCGTGGCCGATCAGGTTGACCCGGCAGAGTATCAAGAGGATTCTGACGTTCTGAGATGAGC
GCGGTTGCGTGTCCGTGAGAGCTATGCGAACGGTTACGGCAACAGCAAGTGGGCGGGTGAAGTTTGTGCGG
TGAGGCTCACGATTTGTCGGGCTTCCGGTGCAGTTTTCCGTTCTGACATGATTCTGGCCACAGCCGTTATGCG
GGTCAGCTGAATGTTAGGATGTGTTTACGCGCCTGATTCTGAGCTTGGTTCGCGACCGGTATCGCGCCGTACAGCT
TCTACCGTACGGACGCCGACGGTAACCGCCAGCGTGCCATTACGACGGCCTGCCGGCAGACTTCACGGCTGCGG
CGATTACCGCGCTGGGTATTCAAGCGACGGAAGGCTTTCGTACCTATGATGTGCTGAACCCGTACGACGACGGTA
TCAGCCTGGACGAGTTCGTGGATTGGCTGGTGGAGAGCGGCCACCCGATTACGCGTATTACGGACTATAGCGATT
GGTTTACCGCTTCAAACCGCCATTGTCGCGTCCCGGAAAAACAGCGTCAGGCGTCCGTCCTGCCGCTGCTGG
ATGCATATCGTAATCCGTGCCAGCAGTCCGCGGTGCTATTCTGCCTGCCAAAGAGTTTCAAGCGGCGGTGCAAAC
CGCAAAGATTGGCCCGAGCAAGACATCCCGCACCTGTCTGCACCGCTGATCGACAAATACGTTAGCGATTTGGA
ACTGCTGCAACTGCTGTAA

pptase_{Ec}

ATGGTTCGATATGAAAACCTACGCATACCTCCCTCCCCTTTGCCGGACATACGCTGCATTTTGTGAGTTCGATCCGGC
GAATTTTTGTGAGCAGGATTTACTCTGGCTGCCGCACTACGCACAACCTGCAACACGCTGGACGTAAACGTAAAACA
GAGCATTTAGCCGACGGATCGCTGCTGTTTATGCTTTGCGGGAATATGGCTATAAATGTGTGCCCGCAATCGGC
GAGCTACGCCAACCTGTCTGGCCTGCGGAGGTATACGGCAGTATTAGCCACTGTGGGACTACGGCATTAGCCGTG
GTATCTCGTCAACCGATTGGCATTGATATAGAAGAAATTTTTCTGTACAAACCGCAAGAGAATTGACAGACAACA
TTATTACACGAGCGAACACGAGCGACTCGCAGACTGCGGTTTAGCCTTTCTCTGGCGCTGACTGGCATTTC
CGCAAAGAGAGCGCATTAAAGGCAAGTGAGATCCAAACTGATGCAGTTTTCTGGACTATCAGATAATTAGCTG
GAATAAACAGCAGGTATCATTATCGTGAGAATGAGATGTTTGTGCTGTGCACTGGCAGATAAAAGAAAAGATAGT
CATAACGCTGTGCCAACACGATTA

Alcohol Dehydrogenase *AlkJ*

The gene was obtained in plasmid pKA1_alkj.

ATGTACGACTATATAATCGTTGGTGCTGGATCTGCAGGATGTGTGCTTGCTAATCGTCTTTGCGCCGACCCCTCTAA
AAGAGTTTGTACTTGAAGCTGGGCCGCGAGATACGAATCCGCTAATTCATATGCCGTTAGGTATTGCTTTGCTTT
CAAATAGTAAAAAGTTGAATTGGGCTTTTCAAACCTGCGCCACAGCAAATCTCAACGGCCGAGCCTTTTCTGGCC
ACGAGGAAAAACGTTAGGTGGTTCAAGCTCAATCAACGCAATGGTCTATATCCGAGGGCATGAAGACGATTACCA
CGCATGGGAGCAGGCCGCGCCGCTACTGGGGTTGGTACCGGGCTCTTGAGTTGTTCAAAGGCTTGAATGCA
ACCAGCGATTGATAAGTCCGAGCACCATGGGGTTGACGGAGAATTAGCTGTTAGTGATTTAAAATATATCAATCC
GCTTAGCAAAGCATTTCGTGCAAGCCGGCATGGAGGCCAATTAATTTCAACGGAGATTTCAACGGCGAGTACCA
GGACGGCGTAGGGTTCTATCAAGTAACCCAAAAAATGGACAACGCTGGAGCTCGGCGCGTGATTCTTGCACGG
TGTACTTTCCAGACCAAATCTAGACATCATTACTGATGCGCATGCATCAAAAATTCTTTTGAAGACCGTAAGGCGG
TTGGTGTTCCTATATAAAGAAAAATATGCACCATCAAGTCAAGACAACGAGTGGTGGTGAAGTACTTCTTAGTCT
TGGCGCAGTCGGCACGCCTCACCTTCTAATGCTTTCTGGTGTGGGGCTGCAGCCGAGCTTAAGGAACATGGTGT
TCTTAGTCCATGATCTTCTGAGGTGGGAAAAATCTTCAAGATCATTGGACATCACATTGATGTGCGCAGCAA
ATTGAGAGAGCCGATAGGTGTTGCTCTTTCTTTCATCCCTCGTGGTGTCTCGGGTTGTTTTCATATGTGTTAAG
CGCGAGGGGTTTCTACTAGTAACGTGGCAGAGTCGGGTGGTTTTGTAAAAAGTTCTCCTGATCGTGATCGGCC
AATTTGCAGTTTCATTTCTTCCAACCTATCTTAAAGATCACGGTCGAAAAATAGCGGGTGGTTATGGTTATACGCT
ACATATATGTGATCTTTTGCCTAAGAGCCGAGGCAGAATTGGCCTAAAAAGCGCCAATCCATTACAGCCGCTTTA
ATTGACCCGAACCTATCTTAGCGATCATGAAGATATTAACCATGATTGCGGGTATTAAGATAGGGCGCGCTATTT
TGCAGGCCCATCGATGGCGAAGCATTTTAAGCATGAAGTAGTACCGGGCCAGGCTGTTAAAACCTGATGATGAAA
TAATCGAAGATATTCGTAGGCGAGCTGAGACTATATACCATCCGGTAGGTAAGTACTTGTAGGATGGGTAAAGATCCAG
CGTCAGTTGTTGATCCGTGCCTGAAGATCCGTGGGTGGCAAATATTAGAGTCGTTGATGCGTCAATTATGCCGCA
CTTGGTCGCGGTAACACAAACGCTCCAACCTATTATGATTGCAGAAAATGCGGCAGAAATAATTATGCGGAATCTT
GATGTGGAAGCATTAGAGGCTAGCGCTGAGTTTGTCTCGCGAGGGTGCAGAGCTAGAGTTGGCCATGATAGCTGT
CTGCATGTAA

Alcohol Dehydrogenase *AlkJ-short*

The genes were obtained in plasmid pKA1_alkj-short.

ATGTACGACTATATAATCGTTGGTGCTGGATCTGCAGGATGTGTGCTTGCTAATCGTCTTTGCGCCGACCCCTCTAA
AAGAGTTTGTACTTGAAGCTGGGCCGCGAGATACGAATCCGCTAATTCATATGCCGTTAGGTATTGCTTTGCTTT
CAAATAGTAAAAAGTTGAATTGGGCTTTTCAAACCTGCGCCACAGCAAATCTCAACGGCCGAGCCTTTTCTGGCC
ACGAGGAAAAACGTTAGGTGGTTCAAGCTCAATCAACGCAATGGTCTATATCCGAGGGCATGAAGACGATTACCA
CGCATGGGAGCAGGCCGCGCCGCTACTGGGGTTGGTACCGGGCTCTTGAGTTGTTCAAAGGCTTGAATGCA
ACCAGCGATTGATAAGTCCGAGCACCATGGGGTTGACGGAGAATTAGCTGTTAGTGATTTAAAATATATCAATCC
GCTTAGCAAAGCATTTCGTGCAAGCCGGCATGGAGGCCAATTAATTTCAACGGAGATTTCAACGGCGAGTACCA
GGACGGCGTAGGGTTCTATCAAGTAACCCAAAAAATGGACAACGCTGGAGCTCGGCGCGTGATTCTTGCACGG
TGTACTTTCCAGACCAAATCTAGACATCATTACTGATGCGCATGCATCAAAAATTCTTTTGAAGACCGTAAGGCGG
TTGGTGTTCCTATATAAAGAAAAATATGCACCATCAAGTCAAGACAACGAGTGGTGGTGAAGTACTTCTTAGTCT
TGGCGCAGTCGGCACGCCTCACCTTCTAATGCTTTCTGGTGTGGGGCTGCAGCCGAGCTTAAGGAACATGGTGT
TCTTAGTCCATGATCTTCTGAGGTGGGAAAAATCTTCAAGATCATTGGACATCACATTGATGTGCGCAGCAA
ATTGAGAGAGCCGATAGGTGTTGCTCTTTCTTTCATCCCTCGTGGTGTCTCGGGTTGTTTTCATATGTGTTAAG
CGCGAGGGGTTTCTACTAGTAACGTGGCAGAGTCGGGTGGTTTTGTAAAAAGTTCTCCTGATCGTGATCGGCC
AATTTGCAGTTTCATTTCTTCCAACCTATCTTAAAGATCACGGTCGAAAAATAGCGGGTGGTTATGGTTATACGCT
ACATATATGTGATCTTTTGCCTAAGAGCCGAGGCAGAATTGGCCTAAAAAGCGCCAATCCATTACAGCCGCTTTA
ATTGACCCGAACCTATCTTAGCGATCATGAAGATATTAACCATGATTGCGGGTATTAAGATAGGGCGCGCTATTT
TGCAGGCCCATCGATGGCGAAGCATTTTAAGCATGAAGTAGTACCGGGCCAGGCTGTTAAAACCTGATGATGAAA
TAATCGAAGATATTCGTAGGCGAGCTGAGACTATATACCATCCGGTAGGTAAGTACTTGTAGGATGGGTAAAGATCCAG
CGTCAGTTGTTGATCCGTGCCTGAAGATCCGTGGGTGGCAAATATTAGAGTCGTTGATGCGTCAATTATGCCGCA
CTTGGTCGCGGTAACACAAACGCTCCAACCTATTATGATTGCAGAAAATGCGGCAGAAATAATTATGCGGAATCTT
GATGTGGAAGCATTAGAGGCTAGCGCTGAGTTTGTCTCGCGAGGGTGCAGAGCTAGAGTTGGCCATGATAGCTGT
GATGTGGAAGCATTAGAGGCTAGCGCTGAGTTTGTCTCGCGAGGGTGCAGAGCTAGAGTTGGCATGA

Pyruvate Decarboxylase *PDC_{Ap}*

The gene was obtained in plasmid pET22b(+)*_pdc_{Ap}* and subcloned into pKA1_alkj (see Chapter 11.5.2). The enzyme carries a C-terminal 6 x His tag.

```
ATGACCTATACTGTTGGCATGTATCTTGCAGAACGCCTTGTACAGATCGGGCTGAAGCATCACTTCGCCGTGGCGG
GCGACTACAATCTCGTTCTTCTGGATCAGTTGCTCCTCAACAAGGACATGAAACAGATCTATTGCTGCAATGAGTT
GAACTGTGGCTTCAGCGCGGAAGGCTACGCCGTTCTAACGGGGCTGCGGCAGCGGTTGTCACCTTCAGCGTTGG
CGCCATTTCCGCCATGAACGCCCTCGGCGGCGCCTATGCCGAAAACCTGCCGTTATCCTGATTTCCGGCGCGCCC
AACAGCAATGATCAGGGCACAGGTCATATCCTGCATCACACAATCGGCAAGACGGATTACAGCTACCAGCTTGAA
ATGGCCCGTCAGGTCACCTGTGCCGCCGAAAGCATTACCGACGCTCACTCCGCCCGGCCAAGATTGACCACGTCA
TTCGCACGGCGCTGCGCGAGCGTAAGCCGGCCTATCTGGACATCGCGTGCAACATTGCCTCCGAGCCCTGCGTGC
GGCCTGGCCCTGTCAGCAGCCTGCTGTCCGAGCCTGAAATCGACCACACGAGCCTGAAGGCCGAGTGGACGCCA
CGTTGCCTTGCTGGAAAAATCGGCCAGCCCCGTCATGCTGCTGGGCAGCAAGCTGCGGGCCGCCAACGCACTGG
CCGCAACCGAAACGCTGGCAGACAAGCTGCAATGCGCGGTGACCATCATGGCGGCCGCGAAAGGCTTTTTCCCG
AAGACCACGCGGGTTTCCGCGCCTGTAAGGGGCGAAGTCTCGAACCCCGCGTGCAGGAACTGGTGGAGACC
TCCGACGCACTGCTGTGCATCGCCCCGTATTCAACGACTATTCAACAGTCGGCTGGTCGGCATGGCCCAAGGGCC
CCAATGTGATTCTGGCTGAGCCCGACCGCGTAACGGTCGATGGCCGCGCCTATGACGGCTTTACCCTGCGCGCCTT
CCTGCAGGCTCTGGCGGAAAAAGCCCCGCGCGCCCGGCCTCCGCACAGAAAAGCAGCGTCCCGACGTGCTCGCT
CACCGCGACATCCGATGAAGCCGGTCTGACGAATGACGAAATCGTCCGTCATATCAACGCCCTGCTGACATCAAC
ACGACGCTGGTGGCAGAAACCGGCGATTGATGGTTCAATGCCATGCGCATGACCCTGCCGCGCGGTGCGCGCGT
GGAAGTGGAAATGCAGTGGGGCCATATCGGCTGGTCCGTGCCCTCCGCCTTCGGCAATGCCATGGGCTCGCAGGA
CCGCCAGCATGTGGTGTAGGCGATGGCTCCTCCAGCTTACCGCGCAGGAAGTGGCTCAGATGGTGCCTA
CGAACTGCCCCTCATTATCTTTCTGATCAACAACCGTGGCTATGTCATTGAAATCGCCATTCATGACGGCCCGTACA
ACTATATCAAGAACTGGGATTACGCCGGCCTGATGGAAGTCTCAACGCCGAGAAAGGCCATGGACTTGGCCTGA
AAGCCACCACCCGAAGGAACTGACAGAAGCCATCGCCAGGGCAAAAGCCAATACCCGCGGCCCGACGCTGATC
GAATGCCAGATCGACCGCACGGACTGCACGGATATGCTGGTTCAATGGGGCCGCAAGGTTGCCTCAACCAACGCG
CGCAAGACCACTCTGGCCCTCGAGACCACCACCACCACCCTGA
```

Pyruvate Decarboxylase *PDC_{Ap}_mutant*

The gene was obtained in plasmid pET22b(+)*_pdc_{Ap}_mutant* and subcloned into pKA1_alkj (see Chapter 11.5.3). Because the sequence of the gene has not been published yet, it cannot be disclosed in this thesis.

Transaminase *VfIH6*

The gene was obtained in plasmid pET24a_ *vflh6* and subcloned into pKA1_ *alkj* (see Chapter 11.5.4). The enzyme carries a C-terminal 6 x His tag.

ATGAACAAACCGCAAAGCTGGGAAGCCCCGGGCCGAGACCTATTCGCTCTATGGTTTCACCGACATGCCTTCGCTGC
ATCAGCGCGGCACGGTCGTCTGACCCATGGCGAGGGACCCTATATCGTCGATGTGAATGGCCGGCGTTATCTGG
ACGCCAACTCGGGCCTGTGGAACATGGTCGCGGGCTTTGACCACAAGGGGCTGATCGACGCCGCAAGGCCAA
TACGAGCGTTTTCCCGTTATCACGCCTTTTTCGGCCGATGTCGATCAGACGGTAATGCTGTCCGAAAAGCTGG
TCGAGGTGTCGCCCTTTGATTCGGGCCGGGTGTTCTATACAAACCTCGGGTCCGAGGCGAATGACACCATGGTCA
AGATGCTATGGTTCCTGCATGCAGCCGAGGGCAAACCGCAAAGCGCAAGATCCTGACCCGCTGGAACGCCTATC
ACGGCGTGACCGCCGTTTCGGCCAGCATGACCGGCAAGCCCTATAATTCGGTCTTTGGCCTGCCGCTGCCGGGCTT
TGTGCATCTGACCTGCCCCGATTACTGGCGCTATGGCGAAGAGGGCGAAACCGAAGAGCAGTTCGTCGCCCCGCT
CGCCCGGAGCTGGAGGAAACGATCCAGCGCGAGGGCGCCGACACCATCGCCGTTTCTTTGCCGAACCGGTGA
TGGGCGCGGGCGGCGTGATCCCCCGCCAAGGGGTATTTCCAGGCGATCCTGCCAATCCTGCGCAAATATGACA
TCCCCGTCATCTCGACGAGGTGATCTGCGGTTTCGGACGCACCGGTAACACCTGGGGCTGCGTGACCTATGACT
TTACACCCGATGCAATCATCTCGTCCAAGAATCTTACAGCGGGCTTTTTCCCATGGGGGCGGTGATCCTTGCCCC
GGAACCTTCCAAACGGCTGGAACCGCAATCGAGGCGATCGAGGAATCCCCATGGCTTACCGCCTCGGGCCA
TCCGGTCGGCTGTGCTATTGCGCTGAAAGCAATCGACGTGGTGTGATGAATGAAGGGCTGGCTGAGAACGTCCGCC
GCCTTGCCCCCGTTTCGAGGAAAGGCTGAAACATATCGCCGAGCGCCGAACATCGGTGAATATCGCGGCATCG
GCTTCATGTGGGCGCTGGAGGCTGTCAAGGACAAGGCAAGCAAGACGCCGTTTCGACGGCAACCTGTCGGTCAGC
GAGCGTATCGCAATACCTGCACCGATCTGGGGCTGATTTGCCGGCCGTTGGTCAGTCCGTCGTCCTTTGTCCGC
CCTTTATCCTGACCGAGGCGCAGATGGATGAGATGTTGATAAACTCGAAAAGCCCTTGATAAGGTCTTTGCCGA
GGTTGCCCTGACGGATCCGAATTCGAGCTCCGTCGACAAGCTTTCGGGCCGCACTCGAGCACCACCACCACCACCAC
TGA

Transaminase *AspFum*

The gene was obtained in plasmid pET22b(+)_ *aspfum* and subcloned into pKA1_ *alkj* (see Chapter 11.5.5). The enzyme carries a C-terminal 6 x His tag.

ATGGCATCTATGGATAAAGTTTTAGTGGTACTACGCGCGCCAGAACTGCTGGAACGTAGTGATAATCCGTTCA
GCAAAGGTATTGCCTATGTTGAAGGCAAACCTGGTGCTGCCGAGTGATGCACGCATCCCCTGCTGGATGAAGGTT
TTATGCATAGTGATCTGACCTACGATGTTATTAGCGTGTGGGATGGCCGTTTCTTTCGCCTGGATGATCACCTGCA
GCGCATCCTGGAAAGCTGCGATAAAATGCGTCTGAAATTTCCGCTGGCACTGAGCTCTGTTAAAAACATTCTGGCA
GAAATGGTGGCGAAAAGCGGCATTCGTGATGCGTTCGTGGAAGTTATTGTTACCCGTGGTCTGACCGGTGTTGCT
GGTCTAAACCGGAAGATCTGTATAACAATAACATTTACCTGCTGGTTCTGCCGTATATCTGGGTGATGGCGCCGG
AAAATCAGCTGCATGGCGGTGAAGCCATTATTACCCGTACCGTTTCGTCGCACCCCGCCGGGTGCATTTGATCCGAC
CATTAAAAACCTGCAGTGGGGTGATCTGACCAAAGGCCTGTTGAAGCCATGGATCGTGGTGCAACCTATCCGTTCT
CTGACGGATGGCGATACCAATCTGACGGAAGGCTCTGGTTTCAATATCGTTCTGGTGAAAAACGGCATTATCTACA
CCCCGATCGTGGTGTCTGCGCGGCATTACGCGTAAATCTGTTATCGATGTGGCGCGGCCAACAGTATTGATAT
CCGTCTGGAAGTGGTTCCGGTGGAAACAGGCGTATCATAGCGATGAAATTTTTATGTGTACCACGGCCGGCGGTAT
TATGCCGATCACCTGCTGGATGGTCAGCCGTTAATGATGGTCAAGTGGGCCCGATTACCAAGAAAATTTGGGA
TGGCTATTGGGAAATGCACTATAACCCGGCGTACAGCTTCCCGGTGGATTACGGCTCTGGTTCAGGATCCCATCAT
CATCATCATCATTGA

Transaminase *AspTer*

The gene was obtained in plasmid pGASTON_*aspter* and subcloned into pKA1_*alkj* (see Chapter 11.5.10). The enzyme carries a C-terminal 6 x His tag.

ATGGCAAGCATGGATAAAGTTTTTGGCGTTATGCAGCACGTCAGGCAATTCTGGAAAGCACCGAAACCACCAAT
CCGTTTGCAAAGGTATTGCATGGGTTGAAGGTGAACTGGTCCGCTGGCAGAAGCACGTATCCGCTGCTGGAT
CAGGGTTTTATGCATAGCGATCTGACCTATGATGTTCCGAGCGTTTGGGATGGTCGTTTTTTTCGCTCGGATGATCA
TATTACCCGTCTGGAAGCCAGCTGTACCAAAGTGCCTGCTGCGTCTGCCGCTGCCTCGTGATCAGGTTAAACAAATT
CTGGTTGAAATGGTTGCCAAAAGCGGTATTCTGATGCATTTGTGGAAGTATTGTTACCCGTGGTCTGAAAGGT
GTTCTGGCACCCGTCGGAAGATATCGTGAATAATCTGTATATGTTTGTGCAGCCGTATGTTGGGTTATGGAAC
CGGATATGCAGCGTGTGGTGGTAGCGCAGTTGTTGCACGTACCGTTGCTCGTGTCCGCCTGGTGCAATTGATCC
GACCGTTAAAAATCTGCAGTGGGGTGTATCTGGTTCGTGGTATGTTTGAAGCAGCAGATCGTGGTGAACCTATCC
GTTTCTGACCGATGGTGTATGCACATCTGACCGAAGGTAGCGGTTTAAACATTGTGCTGGTGAAGATGGTGTCTG
TATACACCGGATCGTGGTGTCTGCAGGGTGTACACGTAAGCGTGATTAATGCAGCAGAAGCCTTTGGTATT
GAAGTGCCTGTTGAATTTGTTCCGGTTGAACTGGCATATCGCTGTGATGAAATTTTATGTGTACCACCGCAGGCG
GTATTATGCCGATTACCACCCTGGATGGTATGCCGGTTAATGGTGGTCAGATTGGTCCGATTACCAAAAAAATTTG
GGATGGCTATTGGCAATGCATTATGATGCAGCCTATAGCTTTGAAATTGATTATAATGAACGCAATTCAGGATCC
CATCATCATCATCATCATTGA

Reductive Aminase *AspRedAm*

The gene was obtained in plasmid pET28a_*aspredam* and subcloned into pKA1_*alkj* (see Chapter 11.5.6). The enzyme carries a N-terminal 6 x His tag.

ATGGGCAGCAGCCATCATCATCATCACAGCAGCGGCCTGGTGCCGCGCGGCAGCCATATGTCCAAGCACATC
GGTATCTTCGGTCTGGGTGCAATGGGTACCGCACTGGCTGCGAAATACCTGGAGCATGGTTACAAAACCTCTGTTT
GGAACCGTACTACCGCGAAAGCGATCCCGCTGGTTGAGCAGGGTGCTAAGCTGGCGTCTACCATCAGCGAAGGT
GTTAACGCGAACGACCTGATCATTATCTGCCTGCTGAACAACAGGTTGTTGAAGATGCGCTGCGTGACGCGCTG
CAAACCTGCCGTCTAAAACCATCGTTAACCTGACTAACGGTACTCCGAACCAGGCGCGTAAACTGGCAGACTTCG
TTACCTCTCACGGTGCACGTTACATCCACGGTGGTATCATGGCGGTGCCGACCATGATTGGCTCTCCGCACGCAGT
GCTGCTGTAATCTGGTGAATCCCTGGAAGTGTTCAGTCTATTGAATCTCACCTGTCTCTGCTGGGTATGAGCAAGT
ATCTGGGCACTGACGCGGGCTCTGCGAGCCTGCATGATCTGGCACTGCTGTCTGGCATGTACGGTCTGTTCTCTGG
TTTCTGACGCGGTGGCTCTGATTAATCTGGTCAAGACACCTCCACCACTGCAACTGGTCTGCTGCCGCTGCTG
ACTCCGTGGCTGAGCGCAATGACCGTTACCTGAGCTCTATCGCGAAACAGATCGACGACGGTATTACGCGACC
CAGGGTTCTAACCTGGGCATGCAGCTGGCTGGTGTGAAAACATCATCCGTGCGGGTGAAGAACAGCGTGTCTCT
TCTCAGATGATCCTGCCGATCAAAGCACTGATTGAACAGGCGTTGGTGAAGGTCATGGTGGCGAAGACCTGTCC
GCGCTGATCGAATACTTCAAGGTGGGTAACAAACGTTGACTAA

Imine Reductase *PIR13*

The gene was obtained in plasmid pET28b_*pir13* and subcloned into pKA1_*alkj* (see Chapter 11.5.7). The enzyme carries a N-terminal 6 x His tag.

```
ATGGGCAGCAGCCATCATCATCATCACAGCAGCGGCCTGGTGCCGCGCGGCAGCCATATGACCGAACATGGT
AAAACACCGGTTACCGTTTTAGGTCTGGGTGCAATGGGCACCGCACTGGTTGAAGCACTGCTGGCAGCAGGTCAT
CCGGTGACCGCATGGAATCGTACCGCAAGCCGTGCAGAAGGTGTTGCAGCAAAGGTGCAAGCGTTGCAAGCAC
CGTTAGCGAAGCACTGGCAGCAAATAAAACCGTTATTGCATGTCTGCTGGATTATGATAGCGTTCATGAAGTTCTG
GATCCGGTTGCAAGCGGTCTGGAAGGTCGTCAGCTGATTAATCTGACCAATGGCACCCCTGGTCAGGCACGTGAA
ATGAGCGCATGGGCTGAAGAACTGGGTGCAGAATATCTGGATGGTGGTATTATGGCAGTTCGCGCTATGATTGGT
ACACCGGTGCATTTATCTTTATAGCGGTAGCGGCACCGTTTTGGCCAGGCACGTACAGCACTGGATACCTTTG
GTGGTGTTAATTATCTGGGTGCCGATCCTGGTCTGGCACCGCTGCATGATATTGCACTGCTGAGCGGTATGTATGG
TAACTTTATTGGTGTTATTCAGGCCTTTGCGCTGGTTGGTAGTGCCGGTGTTAAAGCACGTGAATTTGCTCCGCTGC
TGCGTGGTTGGATGGATGCAATGAGCGTTTTCTGGAACGCACCGCAGAAGTATTGATGATGGTGATTATGAAC
GTGGTGTGGTGAGCAATATTGGTATGCAGGCAGCAGCATTTCCGAATCTGGCAAAGCAGCAGAAGAACAGGGT
ATTCAGCAGAGCTGCTGGCTCCTCTGCAGCCGCTGATGGATAAACGTGTTGCCGAGGTCATGGTGCCGAAGAT
CTGGTGGGTGTTATCGAACTGCTGAAAAATGA
```

Imine Reductase *PIR23*

The gene was obtained in plasmid pET28b_*pir23* and subcloned into pKA1_*alkj* (see Chapter 11.5.8). The enzyme carries a N-terminal 6 x His tag.

```
ATGGGCAGCAGCCATCATCATCATCACAGCAGCGGCCTGGTGCCGCGCGGCAGCCATATGAAACCGGGTATT
AGCGTTTTAGGCACCGGTCGTATGGGTAGCGCACTGGTTGGTGCATTTCTGAAACAGGGTTATAATGTTGCAGTTT
GGAATCGCACCAAAGCAAATGTGCACCGCTGGCAGCACTGGGTGCACGTGTTGCAACCACCGTTCGTGATGCAG
TTGCAGATGCCGAAGTTGTTGTTGTTAATGTGAATGATTATGTGACCAGCGAAGCACTGCTGCGTCAGGATGATGT
TACCAAAGGTCTGCGTGGTAAACTGATTGTTAGCTGACCAGCGGTAGTCCGCGTCAGGCACGTGAAATGGCAGC
ATGGGCACGTGAGCATGAACTGCAGTATCTGGATGGTGCAATTATGGGCACCCCGAACTTTATTGGTGAACCTGG
TGGCACCAATTCTGTATAGCGGTCCGGGTGCACTGTTTGAAAAATACAAACCGGTTCTGCTGGTTTTAGGTGGTAAT
AGCCTGCATGTTGGTAGTGATGTTGGTCATGCAAGTGCCTGGATAGTGCCTGCTGAGCTTTCTGTGGGGTAGC
ATGTTTGGTGTCTGCAGGCAGTTAGCGTTTGTGAAGCCGAAGGTCTGCCGCTGGGTGCATATATGGAATATGTTT
AGGCAACCAAACCGATGGTTGATGGTGCAAGTACCGATTTGTTAAACGTATTGAGCCGGTCGTTTTGCCGGTGA
TGAAAAAACCTGGCAACCGTTGAAGCACATCATGGTGCCTGCTCATCTGATTGAACTGTGTGAAGAACATGG
TATTCATCATGCAGTTCGCGCAGCATTTGGCCAGCTGTTTCAGGCAGCCCTGCAAGCAGGTCATGCACAGGATGAT
TTTGCAGTTCTGAACAAGTTCATGAAATAA
```

12.2 List of Primers

Primer pairs which are highlighted in grey did not yield the desired construct and therefore, should be neglected.

Table 42: Primers used in this Thesis

Mutagenesis		
Construct	Primer	T _a [°C]
pKA1_alkj_mutag	plysu001: CATGATAGCTGTCTGCATG	61
& pPOP_mutag	plysu002: gCCAACCTCTAGCTCTGCAC	61
Cloning		
Construct	Primer	T _a [°C]
pKA1_alkj::pdc _{Ap}	Insert	
pKA1_alkj::pdc _{Ap} _mutant	plysu006: ggctgctaacCGATCCCGCGAAATTAATAC	61
pKA1_alkj::vflh6	plysu005: caactcagctTCCTTTCCGGCTTTGTTAG	71
pKA1_alkj::aspfum	Backbone	
pKA1_alkj::aspredam	plysu003: cgcgggatcgGTTAGCAGCCGGATCCTTAC	65
pKA1_alkj::pir13	plysu004: cccgaaaggaAGCTGAGTTGGCTGCTGC	72
pKA1_alkj::pir23	Backbone new	
	plysu014: gtattaatttcgcgggatcgGTTAGCAGCCGGATCCTTAC	65
	plysu015: gctaacaaagcccgaagg	64
pKA1_alkj::aspter	Insert	
	plysu010: gagatataaccATGGCAAGCATGGATAAAG	67
	plysu009: caactcagctCTGCAGTCAATGATGATG	58*
	Insert new	
	plysu017: ctttaagaaggagatataaccATGGCAAGCATGGATAAAG	60
	plysu016: gtggcagcagccaactcagctCTGCAGTCAATGATGATG	58
	Backbone	
	plysu007:	
	tgcttgccatGGTATATCTCCTTCTTAAAGTTAAACAAAATTATTTCTAGAG	67
	plysu008: ttgactgcagAGCTGAGTTGGCTGCTGC	69

*accidentally, an annealing temperature of 69 °C was used

Sequencing and Colony PCR		
Construct	Primer	T _a [°C]
pKA1_alkj	t7terbis: AACCCCTCAAGACCCG	
pPOP	t7probis: TCCCGCGAAATTAATACG	
pET22b(+)_pdc _{Ap}	t7term: TGCTAGTTATTGCTCAGCGG	
pET22b(+)_pdc _{Ap} _mutant		
pET24a_vflh6		
pET22b(+)_aspfum		
pET28a_aspredam		
pET28b_pir13		
pET28b_pir23		
pGASTON_aspter	pBADrev: GATTTAATCTGTATCAGG	

pETDuet1_aptase _{EC} ::car _{Ni}	tom1: ATGTCGTACTACCATCACCATCAC	
	tom2: GCAAGGTAACCTCCAGCGT	
	tom3: GCAAAAGACGCGAACCTGC	
	tom4: GTTGGTTAACCATGTTCTGCCG	
	tom37: GAGAAAGAGGAGAAATACTAATGTCGTACTACCATCACCA	50
	tom38: GCTTTTTATATTCTCTAAGCTTACAGCAGTTGCAGCAGTT	50

pKA1_alkj::pdc _{Ap}	GOI	
pKA1_alkj::pdc _{Ap} _mutant	plysu012: GGGTGCAGAGCTAGAGTTG	55
pKA1_alkj::vflh6	plysu011: GGGTTATGCTAGTTATTGCTCAG	55
pKA1_alkj::aspfum	t7terbis: AACCCCTCAAGACCCG	
pKA1_alkj::aspredam	alkJ	
pKA1_alkj::pir13	plysu018: GAAGCAGCCCAGTAGTAGGTTGAG	
pKA1_alkj::pir23	plysu019: GATCCTTACATGCAGACAGCTATC	

13 References

1. R.A. Sheldon and D. Brady, *The limits to biocatalysis: pushing the envelope*. Chemical Communications, **2018**, 54, 6088-6104.
2. I.R. Shaikh, *Organocatalysis: key trends in green synthetic chemistry, challenges, scope towards heterogenization, and importance from research and industrial point of view*. Journal of Catalysis, **2014**, 2014.
3. P.T. Anastas and R.H. Crabtree, *Green Catalysis: Biocatalysis*. **2013**, John Wiley & Sons.
4. P. Anastas and N. Eghbali, *Green chemistry: principles and practice*. Chemical Society Reviews, **2010**, 39, 301-312.
5. P.E.V. Paul, V. Sangeetha, and R.G. Deepika, *Emerging Trends in the Industrial Production of Chemical Products by Microorganisms, in Recent Developments in Applied Microbiology and Biochemistry*. **2019**, Elsevier, 107-125.
6. J.P. Adams, M.J. Brown, A. Diaz-Rodriguez, R.C. Lloyd, and G.D. Roiban, *Biocatalysis: A pharma perspective*. Advanced Synthesis & Catalysis, **2019**, 361, 2421-2432.
7. F. Rudroff, *Whole-cell based synthetic enzyme cascades—light and shadow of a promising technology*. Current opinion in chemical biology, **2019**, 49, 84-90.
8. U. Bornscheuer, G. Huisman, R. Kazlauskas, S. Lutz, J. Moore, and K. Robins, *Engineering the third wave of biocatalysis*. Nature, **2012**, 485, 185-194.
9. C. Zeymer and D. Hilvert, *Directed evolution of protein catalysts*. Annual review of biochemistry, **2018**, 87, 131-157.
10. E. Ricca, B. Brucher, and J.H. Schrittwieser, *Multi-enzymatic cascade reactions: overview and perspectives*. Advanced Synthesis & Catalysis, **2011**, 353, 2239-2262.
11. S. Wu and Z. Li, *Whole-cell cascade biotransformations for one-pot multistep organic synthesis*. ChemCatChem, **2018**, 10, 2164-2178.
12. F. Garzón-Posse, L. Becerra-Figueroa, J. Hernández-Arias, and D. Gamba-Sánchez, *Whole cells as biocatalysts in organic transformations*. Molecules, **2018**, 23, 1265.
13. J. Muschiol, C. Peters, N. Oberleitner, M.D. Mihovilovic, U.T. Bornscheuer, and F. Rudroff, *Cascade catalysis—strategies and challenges en route to preparative synthetic biology*. Chemical Communications, **2015**, 51, 5798-5811.
14. C.C. de Carvalho, *Whole cell biocatalysts: essential workers from Nature to the industry*. Microbial biotechnology, **2017**, 10, 250-263.
15. F. Lopez-Gallego and C. Schmidt-Dannert, *Multi-enzymatic synthesis*. Current opinion in chemical biology, **2010**, 14, 174-183.
16. S.P. France, L.J. Hepworth, N.J. Turner, and S.L. Flitsch, *Constructing biocatalytic cascades: in vitro and in vivo approaches to de novo multi-enzyme pathways*. ACS Catalysis, **2017**, 7, 710-724.
17. H.P. Sørensen and K.K. Mortensen, *Soluble expression of recombinant proteins in the cytoplasm of Escherichia coli*. Microbial cell factories, **2005**, 4, 1.
18. M. Ashwini, S.B. Murugan, S. Balamurugan, and R. Sathishkumar, *Advances in molecular cloning*. Molecular Biology, **2016**, 50, 1-6.
19. D.G. Gibson, L. Young, R.-Y. Chuang, J.C. Venter, C.A. Hutchison, and H.O. Smith, *Enzymatic assembly of DNA molecules up to several hundred kilobases*. Nature methods, **2009**, 6, 343-345.
20. Z. Liu, Y. Liang, E.L. Ang, and H. Zhao, *A New Era of Genome Integration Simply Cut and Paste!* ACS synthetic biology, **2017**, 6, 601-609.
21. T. Bayer, S. Milker, T. Wiesinger, F. Rudroff, and M.D. Mihovilovic, *Designer microorganisms for optimized redox cascade reactions—challenges and future perspectives*. Advanced Synthesis & Catalysis, **2015**, 357, 1587-1618.
22. R.P. Shetty, D. Endy, and T.F. Knight, *Engineering BioBrick vectors from BioBrick parts*. Journal of biological engineering, **2008**, 2, 5.
23. P. Xu, A. Vansiri, N. Bhan, and M.A. Koffas, *ePathBrick: a synthetic biology platform for engineering metabolic pathways in E. coli*. ACS synthetic biology, **2012**, 1, 256-266.

24. T. Ellis, T. Adie, and G.S. Baldwin, *DNA assembly for synthetic biology: from parts to pathways and beyond*. Integrative Biology, **2011**, *3*, 109-118.
25. N. Oberleitner, A. Ressmann, K. Bica, P. Gärtner, M. Fraaije, U. Bornscheuer, F. Rudroff, and M. Mihovilovic, *From waste to value—direct utilization of limonene from orange peel in a biocatalytic cascade reaction towards chiral carvolactone*. Green Chemistry, **2017**, *19*, 367-371.
26. J. Kulig, T. Sehl, U. Mackfeld, W. Wiechert, M. Pohl, and D. Rother, *An Enzymatic 2-Step Cofactor and Co-Product Recycling Cascade towards a Chiral 1, 2-Diol. Part I: Cascade Design*. Advanced synthesis & catalysis, **2019**, *361*, 2607-2615.
27. B. Lin and Y. Tao, *Whole-cell biocatalysts by design*. Microbial Cell Factories, **2017**, *16*, 106.
28. S. Klätte and V.F. Wendisch, *Redox self-sufficient whole cell biotransformation for amination of alcohols*. Bioorganic & medicinal chemistry, **2014**, *22*, 5578-5585.
29. S. Klätte and V.F. Wendisch, *Role of L-alanine for redox self-sufficient amination of alcohols*. Microbial Cell Factories, **2015**, *14*, 9.
30. J. Sun, J.G. Jeffryes, C.S. Henry, S.D. Bruner, and A.D. Hanson, *Metabolite damage and repair in metabolic engineering design*. Metabolic engineering, **2017**, *44*, 150-159.
31. C. Lerma-Ortiz, J.G. Jeffryes, A.J. Cooper, T.D. Niehaus, A.M. Thamm, O. Frelin, T. Aunins, O. Fiehn, V. de Crécy-Lagard, and C.S. Henry, *'Nothing of chemistry disappears in biology': the Top 30 damage-prone endogenous metabolites*. Biochemical Society Transactions, **2016**, *44*, 961-971.
32. A.M. Kunjapur, Y. Tarasova, and K.L. Prather, *Synthesis and accumulation of aromatic aldehydes in an engineered strain of Escherichia coli*. Journal of the American Chemical Society, **2014**, *136*, 11644-11654.
33. T. Bayer, S. Milker, T. Wiesinger, M. Winkler, M.D. Mihovilovic, and F. Rudroff, *In vivo synthesis of polyhydroxylated compounds from a "hidden reservoir" of toxic aldehyde species*. ChemCatChem, **2017**, *9*, 2919-2923.
34. M. Petrovova, J. Tkadlec, L. Dvoracek, E. Streitova, and I. Licha, *NAD (P) H-hydrate dehydratase-a metabolic repair enzyme and its role in Bacillus subtilis stress adaptation*. PloS one, **2014**, *9*, e112590.
35. M. Grninger, K. Zeth, and D. Oesterhelt, *Dodecins: a family of lumichrome binding proteins*. Journal of molecular biology, **2006**, *357*, 842-857.
36. C.A. Hutchison, R.-Y. Chuang, V.N. Noskov, N. Assad-Garcia, T.J. Deerinck, M.H. Ellisman, J. Gill, K. Kannan, B.J. Karas, and L. Ma, *Design and synthesis of a minimal bacterial genome*. Science, **2016**, *351*.
37. P. Both, H. Busch, P.P. Kelly, F.G. Mutti, N.J. Turner, and S.L. Flitsch, *Whole-Cell Biocatalysts for Stereoselective C–H Amination Reactions*. Angewandte Chemie International Edition, **2016**, *55*, 1511-1513.
38. T. Wiesinger, T. Bayer, S. Milker, M.D. Mihovilovic, and F. Rudroff, *Cell Factory Design and Optimization for the Stereoselective Synthesis of Polyhydroxylated Compounds*. ChemBioChem, **2018**, *19*, 361-368.
39. R.J. Conrado, G.C. Wu, J.T. Boock, H. Xu, S.Y. Chen, T. Lebar, J. Turnšek, N. Tomšič, M. Avbelj, and R. Gaber, *DNA-guided assembly of biosynthetic pathways promotes improved catalytic efficiency*. Nucleic acids research, **2012**, *40*, 1879-1889.
40. Y.J. Zhou, N.A. Buijs, Z. Zhu, D.O. Gómez, A. Boonsombuti, V. Siewers, and J. Nielsen, *Harnessing yeast peroxisomes for biosynthesis of fatty-acid-derived biofuels and chemicals with relieved side-pathway competition*. Journal of the American Chemical Society, **2016**, *138*, 15368-15377.
41. G.M. Rodriguez and S. Atsumi, *Isobutyraldehyde production from Escherichia coli by removing aldehyde reductase activity*. Microbial cell factories, **2012**, *11*, 90.
42. J.L. Avalos, G.R. Fink, and G. Stephanopoulos, *Compartmentalization of metabolic pathways in yeast mitochondria improves the production of branched-chain alcohols*. Nature biotechnology, **2013**, *31*, 335-341.
43. T. Bayer, *Design, application, and optimization of synthetic enzyme cascades in Escherichia coli*, Technical University Vienna, Austria, **2017**.

44. A.M. Kunjapur and K.L. Prather, *Microbial engineering for aldehyde synthesis*. Appl. Environ. Microbiol., **2015**, *81*, 1892-1901.
45. K.E. Scholz, D. Okrob, B. Kopka, A. Grünberger, M. Pohl, K.-E. Jaeger, and U. Krauss, *Synthesis of chiral cyanohydrins by recombinant Escherichia coli cells in a micro-aqueous reaction system*. Applied and environmental microbiology, **2012**, *78*, 5025-5027.
46. F. Guo and P. Berglund, *Transaminase biocatalysis: optimization and application*. Green Chemistry, **2017**, *19*, 333-360.
47. M. Müller, G.A. Sprenger, and M. Pohl, *CC bond formation using ThDP-dependent lyases*. Current opinion in chemical biology, **2013**, *17*, 261-270.
48. L. Kirmair and A. Skerra, *Biochemical analysis of recombinant AlkJ from Pseudomonas putida reveals a membrane-associated, flavin adenine dinucleotide-dependent dehydrogenase suitable for the biosynthetic production of aliphatic aldehydes*. Applied and environmental microbiology, **2014**, *80*, 2468-2477.
49. K. Napora-Wijata, K. Robins, A. Osorio-Lozada, and M. Winkler, *Whole-Cell Carboxylate Reduction for the Synthesis of 3-Hydroxytyrosol*. ChemCatChem, **2014**, *6*, 1089-1095.
50. K. Napora-Wijata, G.A. Strohmeier, and M. Winkler, *Biocatalytic reduction of carboxylic acids*. Biotechnology journal, **2014**, *9*, 822-843.
51. M. Wei, Z. Li, T. Li, B. Wu, Y. Liu, J. Qu, X. Li, L. Li, L. Cai, and P.G. Wang, *Transforming flask reaction into cell-based synthesis: production of polyhydroxylated molecules via engineered Escherichia coli*. Acs Catalysis, **2015**, *5*, 4060-4065.
52. G. Brahmachari, *Design for carbon-carbon bond forming reactions under ambient conditions*. RSC advances, **2016**, *6*, 64676-64725.
53. M. Breuer and B. Hauer, *Carbon-carbon coupling in biotransformation*. Current opinion in biotechnology, **2003**, *14*, 570-576.
54. V. Shukla and P. Kulkarni, *L-Phenylacetylcarbinol (L-PAC): biosynthesis and industrial applications*. World Journal of Microbiology and Biotechnology, **2000**, *16*, 499-506.
55. D. Gocke, T. Graf, H. Brosi, I. Frindi-Wosch, L. Walter, M. Müller, and M. Pohl, *Comparative characterisation of thiamin diphosphate-dependent decarboxylases*. Journal of Molecular Catalysis B: Enzymatic, **2009**, *61*, 30-35.
56. D. Meyer, L. Walter, G. Kolter, M. Pohl, M. Müller, and K. Tittmann, *Conversion of pyruvate decarboxylase into an enantioselective carboligase with biosynthetic potential*. Journal of the American Chemical Society, **2011**, *133*, 3609-3616.
57. D. Rother, G. Kolter, T. Gerhards, C.L. Berthold, E. Gauchenova, M. Knoll, J. Pleiss, M. Müller, G. Schneider, and M. Pohl, *S-selective mixed carboligation by structure-based design of the pyruvate decarboxylase from Acetobacter pasteurianus*. ChemCatChem, **2011**, *3*, 1587-1596.
58. H.C. Hales, D. Rother, M. Müller, R. Westphal, J.M. Ward, J. Pleiss, C. Vogel, and M. Pohl, *Engineering stereoselectivity of ThDP-dependent enzymes*. The FEBS journal, **2013**, *280*, 6374-6394.
59. D. Ghislieri and N.J. Turner, *Biocatalytic approaches to the synthesis of enantiomerically pure chiral amines*. Topics in Catalysis, **2014**, *57*, 284-300.
60. H. Kohls, F. Steffen-Munsberg, and M. Höhne, *Recent achievements in developing the biocatalytic toolbox for chiral amine synthesis*. Current opinion in chemical biology, **2014**, *19*, 180-192.
61. M.S. Malik, E.-S. Park, and J.-S. Shin, *Features and technical applications of ω -transaminases*. Applied microbiology and biotechnology, **2012**, *94*, 1163-1171.
62. E. O'Reilly and N.J. Turner, *Enzymatic cascades for the regio- and stereoselective synthesis of chiral amines*. Perspectives in Science, **2015**, *4*, 55-61.
63. M. Höhne and U.T. Bornscheuer, *Biocatalytic routes to optically active amines*. ChemCatChem, **2009**, *1*, 42-51.
64. M. Fuchs, J.E. Farnberger, and W. Kroutil, *The industrial age of biocatalytic transamination*. European journal of organic chemistry, **2015**, *32*, 6965.

65. D. Koszelewski, K. Tauber, K. Faber, and W. Kroutil, *ω -Transaminases for the synthesis of non-racemic α -chiral primary amines*. Trends in biotechnology, **2010**, *28*, 324-332.
66. R.C. Simon, N. Richter, E. Busto, and W. Kroutil, *Recent developments of cascade reactions involving ω -transaminases*. ACS catalysis, **2014**, *4*, 129-143.
67. J. Mangas-Sanchez, S.P. France, S.L. Montgomery, G.A. Aleku, H. Man, M. Sharma, J.I. Ramsden, G. Grogan, and N.J. Turner, *Imine reductases (IREDs)*. Current opinion in chemical biology, **2017**, *37*, 19-25.
68. G.A. Aleku, S.P. France, H. Man, J. Mangas-Sanchez, S.L. Montgomery, M. Sharma, F. Leipold, S. Hussain, G. Grogan, and N.J. Turner, *A reductive aminase from Aspergillus oryzae*. Nature chemistry, **2017**, *9*, 961.
69. M. Sharma, J. Mangas-Sanchez, S.P. France, G.A. Aleku, S.L. Montgomery, J.I. Ramsden, N.J. Turner, and G. Grogan, *A mechanism for reductive amination catalyzed by fungal reductive aminases*. ACS Catalysis, **2018**, *8*, 11534-11541.
70. E. Cabiscol Català, J. Tamarit Sumalla, and J. Ros Salvador, *Oxidative stress in bacteria and protein damage by reactive oxygen species*. International Microbiology, **2000**, *3*, 3-8.
71. K.M.S. Pillai, *Exploring biosynthetic pathways for aromatic ester production*, Arizona State University, USA, **2016**.
72. J.-S. Shin, H. Yun, J.-W. Jang, I. Park, and B.-G. Kim, *Purification, characterization, and molecular cloning of a novel amine: pyruvate transaminase from Vibrio fluvialis JS17*. Applied microbiology and biotechnology, **2003**, *61*, 463-471.
73. M. Genz, O. Melse, S. Schmidt, C. Vickers, M. Dörr, T. Van Den Bergh, H.J. Joosten, and U.T. Bornscheuer, *Engineering the amine transaminase from Vibrio fluvialis towards branched-chain substrates*. ChemCatChem, **2016**, *8*, 3199-3202.
74. K.S. Midelfort, R. Kumar, S. Han, M.J. Karmilowicz, K. McConnell, D.K. Gehlhaar, A. Mistry, J.S. Chang, M. Anderson, and A. Villalobos, *Redesigning and characterizing the substrate specificity and activity of Vibrio fluvialis aminotransferase for the synthesis of imagabalin*. Protein Engineering, Design & Selection, **2013**, *26*, 25-33.
75. L. Skalden, M. Thomsen, M. Höhne, U.T. Bornscheuer, and W. Hinrichs, *Structural and biochemical characterization of the dual substrate recognition of the (R)-selective amine transaminase from Aspergillus fumigatus*. The FEBS journal, **2015**, *282*, 407-415.
76. K. Fesko, K. Steiner, R. Breinbauer, H. Schwab, M. Schürmann, and G.A. Strohmeier, *Investigation of one-enzyme systems in the ω -transaminase-catalyzed synthesis of chiral amines*. Journal of Molecular Catalysis B: Enzymatic, **2013**, *96*, 103-110.
77. P. Schaaf, *Chemoenzymatic one-pot reaction sequence for the production of chiral alcohols and amines*, Technical University Vienna, Austria, **2017**.
78. J.I. Ramsden, R.S. Heath, S.R. Derrington, S.L. Montgomery, J. Mangas-Sanchez, K.R. Mulholland, and N.J. Turner, *Biocatalytic N-alkylation of amines using either primary alcohols or carboxylic acids via reductive aminase cascades*. Journal of the American Chemical Society, **2019**, *141*, 1201-1206.
79. S.L. Montgomery, A. Pushpanath, R.S. Heath, J.R. Marshall, U. Klemstein, J.L. Galman, D. Woodlock, S. Bisagni, C.J. Taylor, and J. Mangas-Sanchez, *Characterization of imine reductases in reductive amination for the exploration of structure-activity relationships*. Science advances, **2020**, *6*, eaay9320.
80. F.W. Studier, *Protein production by auto-induction in high-density shaking cultures*. Protein expression and purification, **2005**, *41*, 207-234.
81. K. Sakaguchi, T. Miyakawa, S. Takeuchi, K. Nakagawa, and E. Hayase, *Interaction of benzaldehyde to the membrane protein of Escherichia coli*. Agricultural and Biological Chemistry, **1979**, *43*, 1775-1777.
82. T. Miyakawa, J.-L. Zundel, and K. Sakaguchi, *Selective inhibitory effect of benzaldehyde on the growth of simian virus 40-transformed cells*. Biochemical and biophysical research communications, **1979**, *87*, 1024-1030.

83. W. Finnigan, A. Thomas, H. Cromar, B. Gough, R. Snajdrova, J.P. Adams, J.A. Littlechild, and N.J. Harmer, *Characterization of carboxylic acid reductases as enzymes in the toolbox for synthetic chemistry*. ChemCatChem, **2017**, 9, 1005-1017.
84. M. Fakruddin, R. Mohammad Mazumdar, K.S. Bin Mannan, A. Chowdhury, and M. Hossain, *Critical factors affecting the success of cloning, expression, and mass production of enzymes by recombinant E. coli*. International Scholarly Research Notices, **2013**, 2013.
85. D.S.-W. Ow, D.-Y. Lee, H.-H. Tung, and S. Lin-Chao, *Plasmid regulation and systems-level effects on Escherichia coli metabolism*, in *Systems Biology and Biotechnology of Escherichia coli*. **2009**, Springer, 273-294.
86. B. Lin and Y. Tao, *Whole-cell biocatalysts by design*. Microbial Cell Factories, **2017**, 16, 1-12.